TU Delft

Delft University of Technology

Elastic Instabilities in Polymer-Solution Flow Through Porous Media

Kawale, Durgesh

DOI
10.4233/uuid:275dbc0a-db3d-4b53-90ee-6fe25de24f7e

Publication date
2017

Document Version
Final published version

Citation (APA)
Kawale, D. (2017). *Elastic Instabilities in Polymer-Solution Flow Through Porous Media*. [Dissertation (TU Delft), Delft University of Technology]. https://doi.org/10.4233/uuid:275dbc0a-db3d-4b53-90ee-6fe25de24f7e

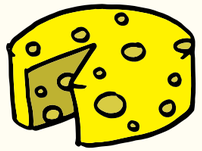
Important note
To cite this publication, please use the final published version (if applicable).
Please check the document version above.

Copyright
Other than for strictly personal use, it is not permitted to download, forward or distribute the text or part of it, without the consent of the author(s) and/or copyright holder(s), unless the work is under an open content license such as Creative Commons.

Takedown policy
Please contact us and provide details if you believe this document breaches copyrights.
We will remove access to the work immediately and investigate your claim.

This work is downloaded from Delft University of Technology.
For technical reasons the number of authors shown on this cover page is limited to a maximum of 10.

Certain types of cheese contain holes within them that are interconnected. If one tries to push a liquid through such a cheese, the liquid will flow through the interconnected holes. Similarly, certain crude oil-bearing geological porous media also contain interconnected pores.



Polymers are type of molecules that contain a long chain of repeating sub-units. Injecting polymer-solutions through an oil-bearing geological porous media can improve crude oil recovery. This thesis shows that elastic instabilities exist during the flow of polymer solutions through porous media. Using single-DNA experiments, the molecular-scale processes were related to the pore-scale processes in interconnected pores.

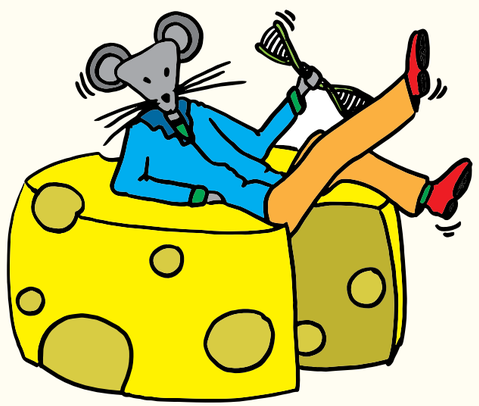


ISBN: 978-94-92516-74-9

Elastic Instabilities in Polymer-Solution Flow Through Porous Media Durgesh Kawale 2017

Elastic Instabilities in Polymer-Solution Flow Through Porous Media

Durgesh Kawale



Invitation

It's my pleasure to invite you to attend the public defense of my doctoral thesis

Elastic Instabilities in Polymer-Solution Flow Through Porous Media



Wednesday, September 6th 2017 at 15:00 HRS in the Senaatszaal of the Aula, Delft University of Technology, Mekelweg 5, Delft.

You are most welcome to attend the reception that will follow the defense at PSOR café, CiTG.

Durgesh Kawale

Propositions

accompanying the dissertation

ELASTIC INSTABILITIES IN POLYMER-SOLUTION FLOW THROUGH POROUS MEDIA

by

Durgesh KAWALE

1. Time-dependent elastic instability cause the apparent shear thickening behaviour of polyacrylamide polymers in porous media. (Chapter 3, 4)
2. Direct visualization of polymer chains using single molecule experiments is a far convincing method to settle debates on the structure-performance relationship and the mechanism of the apparent shear-thickening behaviour than bulk methods such as birefringence, viscosity measurement, etc. (Chapter 2, 5)
3. The pore-scale elastic instabilities for a realistic microfluidic porous medium should simply be some combination of the flow patterns in the microfluidic porous media containing staggered and aligned pillars. (Chapter 3)
4. In spite of varying inter- and intra-molecular physio-chemical interactions, a fluorescent DNA chain can serve as a molecular tracer for studying polyacrylamide polymer flow dynamics. (Chapter 5)
5. Multidisciplinary scientific progress in oil & gas field is hampered by excessive use of jargon.
6. Elastic turbulence is essentially a type of elastic instability and is often used wrongly for describing polymeric flow through porous media.
7. Ignoring dynamic pressure-drop fluctuations during core-flood experiments has saved researchers over past several decades a ton of explanation. Such ignorance prevented discovery of elastic instabilities during polymer flow in porous media in the 80s and the 90s.
8. Calling EOR polymers as viscosifying agents limits openness to studying the viscoelastic contribution to polymer rheology in porous media.
9. For-profit publishers are defrauding the public.
10. In applied sciences, multidisciplinary collaborative work often leads to breakthroughs.

These propositions are regarded as opposable and defendable, and have been approved as such by the promotor prof. dr. ir. M. T. Kreutzer.

Stellingen

behorende bij het proefschrift

ELASTIC INSTABILITIES IN POLYMER-SOLUTION FLOW THROUGH POROUS MEDIA

door

Durgesh KAWALE

1. Tijdsafhankelijke elastische instabiliteit veroorzaakt dilatantie bij polyacrylamine polymeren in poreuze media. (Hoofdstuk 3, 4)
2. Directe visualisatie van polymeerketens door middel van metingen van individuele moleculen is een veel betere methode om inzicht te krijgen in de relatie tussen structuur en prestaties en dilatantie dan bulkmethoden zoals het meten van dubbelbreking of viscositeit. (Hoofdstuk 2, 5)
3. Elastische instabiliteiten op porieschaal, voor een realistische microfluïdisch poreus medium, zouden eenvoudigweg een combinatie moeten zijn van de stromingspatronen in een microfluïdisch poreus medium dat bestaat uit verspreide en opgelijnde staafjes. (Hoofdstuk 3)
4. In weerwil van inter- en intramoleculaire fysisch-chemische interacties kan een fluorescente DNA keten dienst doen als moleculaire merkstof om de dynamiek van stroming van polyacrylaminde polymeren te bestuderen. (Hoofdstuk 5)
5. Multidisciplinaire wetenschappelijke vooruitgang op het gebied van olie en gas wordt belemmerd door buitensporig gebruik van vaktermen.
6. Elastische turbulentie is in wezen een soort elastische instabiliteit en wordt vaak onjuist gebruikt voor het omschrijven van de polymere stroom door poreuze media.
7. Het negeren van dynamische drukvalverschillen tijdens kern-doorstroomingsexperimenten heeft onderzoekers over de afgelopen decennia gered van een heleboel uitleg. Dergelijke onwetendheid heeft de ontdekking van elastische instabiliteit tijdens polymeer-stroom in poreuze media in de jaren 80 en 90 verhindert.
8. Door polymeren voor verbeterde olie winningsmethodes verdikkingsmiddelen te noemen weerhoudt dit het onderzoek naar de visco-elasticiteit contributie van polymeer reologie in poreuze media.
9. Uitgevers met winstoogmerk bedriegen het publiek.
10. In toegepaste wetenschappen leidt multidisciplinaire samenwerkingen vaak tot nieuwe inzichten.

Deze stellingen worden opponeerbaar en verdedigbaar geacht en zijn als zodanig goedgekeurd door de promotor prof. dr. ir. M. T. Kreutzer.

Elastic Instabilities in Polymer-Solution Flow through Porous Media

ELASTIC INSTABILITIES IN POLYMER-SOLUTION FLOW THROUGH POROUS MEDIA

Proefschrift

ter verkrijging van de graad van doctor
aan de Technische Universiteit Delft,
op gezag van de Rector Magnificus prof. ir. K.C.A.M. Luyben,
voorzitter van het College voor Promoties,
in het openbaar te verdedigen op woensdag 6 september 2017 om 15:00 uur

door

Durgesh KAWALE

Master of Science in Chemical Engineering,
Technische Universiteit Delft, Delft, Nederland,
geboren te Mumbai, India.

Dit proefschrift is goedgekeurd door de

promotor: prof. dr. ir. M. T. Kreutzer
promotor: prof. dr. W. R. Rossen

Samenstelling promotiecommissie:

Rector Magnificus,	voorzitter
Prof. dr. ir. M. T. Kreutzer,	Technische Universiteit Delft
Prof. dr. W. R. Rossen,	Technische Universiteit Delft
Onafhankelijke leden:	
Prof. dr. S. J. Picken	Technische Universiteit Delft
Prof. dr. ir. J. D. Jansen	Technische Universiteit Delft
Dr. S. Berg	Shell International Exploration & Production
Prof. dr. F. Picchioni	Rijksuniversiteit Groningen
Overige leden:	
Dr. P. E. Boukany	Technische Universiteit Delft
Prof. dr. J. Bruining	Technische Universiteit Delft, reservelid

This work was financially supported by the Dutch Polymer Institute (DPI), project number #736n.

Keywords: polymer rheology, porous media, elastic instabilities, microfluidics, enhanced oil recovery.

Printed by: Gildeprint, the Netherlands.

Front & Back: Cover design by Susanne Groot and Durgesh Kawale.

Copyright © 2017 by Durgesh Kawale

ISBN 978-94-92516-74-9

An electronic version of this dissertation is available at
http://repository.tudelft.nl/.

In loving memory of my grandmother

CONTENTS

1 Introduction **1**
- 1.1 Polymer solution rheology . . . 3
- 1.2 Polymer apparent viscosity in porous media . . . 4
- 1.3 Research objectives . . . 6
- 1.4 Thesis outline . . . 6
- References . . . 7

2 Polymer chain dynamics during simple and complex flows **11**
- 2.1 Introduction . . . 12
- 2.2 DNA flow in microfluidics . . . 13
- 2.3 Dimensionless groups . . . 13
- 2.4 DNA as a model polymer for visualization . . . 17
- 2.5 Relaxation of stretched DNA: Zimm and Reptation theory meet experiments . . . 18
- 2.6 Dynamics of individual DNA molecules in fluid flow . . . 21
  - 2.6.1 Extensional flow: Coil-stretch transition meets experiment . . . 21
  - 2.6.2 Dynamics of DNA in shear flow . . . 24
  - 2.6.3 Dynamics of DNA in contraction flow . . . 26
  - 2.6.4 Coil-stretch transition at high Wi in random flow and flow around obstacles . . . 27
- 2.7 Stretching of DNA molecules on micropatterned surfaces . . . 29
- 2.8 Conclusions . . . 30
- References . . . 31

3 Elastic instabilities in different pore shapes **39**
- 3.1 Introduction . . . 39
- 3.2 Experimental Details . . . 42
  - 3.2.1 Polymer solution . . . 42
  - 3.2.2 Microfluidic devices . . . 44
- 3.3 Results and discussion . . . 46
  - 3.3.1 Effect of pore-shape . . . 48
- 3.4 Conclusions . . . 53
- References . . . 53

4 Elastic instabilities with varying ionic strength **59**
- 4.1 Introduction . . . 59
- 4.2 Experimental Details . . . 60
- 4.3 Results and discussion . . . 61
  - 4.3.1 Maximum dead-zone area . . . 62
  - 4.3.2 $Wi - Re$ and $Ma - El$ flow pattern map . . . 63

4.4 Conclusions . . . 64
References . . . 64

5 Polymer chain dynamics during elastic instabilities in porous media 67
5.1 Introduction . . . 67
5.2 Experimental details . . . 70
5.2.1 Microfluidic device and pressure measurements . . . 70
5.2.2 Polymer solutions . . . 72
5.2.3 Flow visualization . . . 73
5.2.4 DNA visualization . . . 73
5.3 Results and discussion . . . 76
5.3.1 Apparent viscosity and streamline visualization . . . 76
5.3.2 DNA conformations . . . 78
5.4 Conclusions . . . 82
References . . . 83

6 Conclusions and outlook 91
6.1 Conclusions . . . 91
6.1.1 Polymer chain dynamics during simple and complex flows . . . 92
6.1.2 Elastic instabilities during polymer solution flow through porous media . . . 92
6.1.3 Polymer chain dynamics during elastic instabilities in porous media . . . 93
6.2 Outlook . . . 94
6.2.1 2D porous media *versus* 3D porous media . . . 94
6.2.2 Effect of oil on elastic instabilities . . . 94
6.2.3 Apparent viscosity model with elastic instabilities . . . 95
6.2.4 Investigate effect of HPAM architecture . . . 96
6.2.5 Relate HPAM molecular conformation to macroscopic behaviour . . . 96
References . . . 97

Summary 99

Samenvatting 101

Acknowledgements 105

A Appendix A 111

B Appendix B 119

Curriculum Vitæ 127

List of Publications 129

1

INTRODUCTION

As the world population continues to rise, the need for energy demand also increases. Crude oil plays a crucial role in meeting current and future energy needs of the world. The existing recovery factor[1] from mature oil fields is around 30 %.[1–3] Therefore, it is in the interest of oil companies to focus on maximizing the recovery factor.

Crude oil is located in underground sedimentary basins known as reservoirs. Within the reservoir, oil occupies the pore space surrounding the rock grains. Recovery of crude oil from this pore space can be classified into three categories. First, primary-stage recovery, the crude oil can be recovered by controlling the release of initial reservoir pressure through the production well. The second, secondary-stage recovery, involves maintaining the pressure-gradient between the reservoir and the production well by injecting water (also known as initial water flooding) from a separate injection well. In both, the primary- and secondary-stage recovery, this pressure-gradient serves as the driving force. The recovery from water-flooding in the secondary-stage is limited due to the water-front-channeling through the reservoir and breaking through into the production well. Once the water front breaks through in the production well, any further improvement in recovery with injection of water decreases. Water-front-channeling can occur either via viscous or capillary fingering. Both these fingering phenomena depend on the viscosity ratio of displacing fluid (such as water) to the displaced fluid (oil in this case) and on the capillary number.

The third category, Enhanced Oil Recovery (EOR), relates to injecting a fluid in to an oil reservoir that can increase recovery over the secondary stage, or over the recovery

[1] The total crude oil volume recovered as a percent of total crude oil originally in place from oil fields that are at the end of their economic production life

1

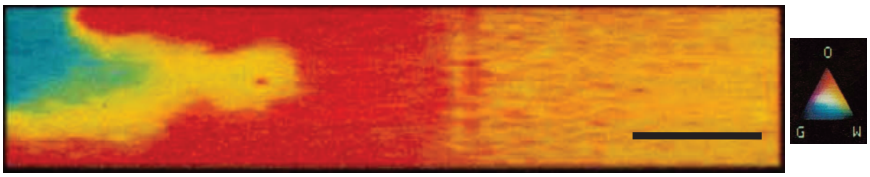


Figure 1.1: Computerized X-Ray tomography image showing core-scale viscous fingering of a tertiary miscible CO_2 flood in Berea without surfactant. CO_2 viscosity is 6×10^{-5} Pa s and oil viscosity is 8.75×10^{-4} Pa s. Flow direction is left to right and the legend colour key is O: Oil, W: Water, G: CO_2. Scale bar is 10 cm. Figure is adapted from Wellington *et al.* [4].

achievable by maintaining reservoir pressure. The type of fluid and the injection strategy depends on the density and viscosity of the crude oil. A few examples of various EOR processes for lighter crude oil include polymer flooding,[2] water-alternating-gas injection,[5] miscible gas injection,[6] flow diversion by polymer gels and surfactants.[7, 8] Examples of EOR processes for viscous (or heavy) oil include steam injection and *in situ* combustion by air injection.[9]

EOR processes can improve oil recovery via multiple effects. After water flooding, some oil droplets inside the pore space are trapped due to capillary forces. The efficiency related to the fraction of oil that is recovered from the reservoir volume where the injected fluid has flowed is termed as microscopic displacement efficiency. Typically, microscopic displacement efficiency from a water flood is ~ 70 %.[3] On the other hand, a water flood might not sweep across the entire volume of a reservoir. As the water front displaces the oil bank, the water-oil displacement front becomes unstable, leading to fingers of water phase. Capillary number is an important parameter which is a non-dimensional parameter that relates the viscous forces to the capillary forces. Figure 1.1 shows the viscous fingering process visualized at a core-scale using X-Ray computed tomography.[4] Viscous fingering at a pore-scale is show in figure 1.2 at a fixed capillary number. In this figure, we can see the displacing fluid (in dark colour) channeling (from left side) through the porous medium towards the outlet (on the right side of the each image). Viscous/capillary fingering causes the water phase to break through to the production well. More subsequent water injection then channels through these viscous fingers. Therefore, the reservoir oil that is not swept due to a water flood will be mobilized very slowly. The efficiency defined by the fraction of reservoir volume swept by a fluid-flood process is known as macroscopic sweep efficiency. Sweep efficiency tends to be significantly less than the microscopic displacement efficiency; thus, improving it is often desired from EOR processes.

Polymer flooding is a commercially viable EOR process for increasing sweep[2] and

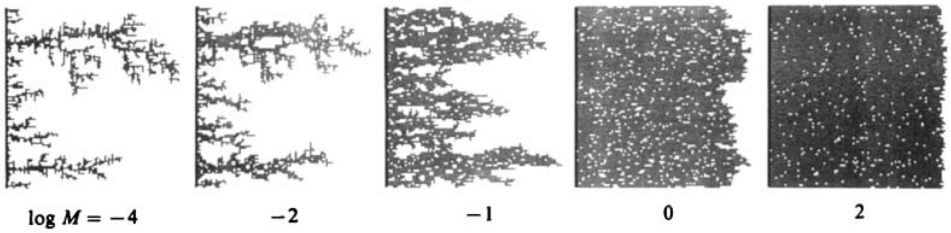


Figure 1.2: Simulation results showing pore-scale viscous fingering of a non-wetting fluid displacing a wetting fluid through a two-dimensional porous medium consisting of interconnected capillaries. $M = \eta_2/\eta_1$ is the viscosity ratio, where η_2 is viscosity of the displacing fluid and η_1 is viscosity of the displaced fluid. The capillary number is set to unity. Mean pore radius is 0.23 mm. Figure adapted from Lenormand *et al.* [15].

displacement efficiency,[10, 11] which includes injecting high-viscosity polymer solutions into the reservoir. These polymers are typically high-molecular-weight, water-soluble substances such as hydrolyzed polyacrylamides,[12, 13] Xanthan gum[12, 13] and Schizophyllan.[14] Contrary to a water flood, a polymer flood does not lead to viscous fingering.[15] Consequently, the sweep efficiency of a polymer flood is higher than a water flood.[2] In order to optimize the polymer-flooding process, it is crucial to understand the mechanisms that increase the polymer viscosity as polymer solutions flow through the reservoir rock. As the polymer solution flows through the pore space within the reservoir rock, it experiences a combination of shear and extensional flow fields. Owing to the non-Newtonian response to these complex flow fields, polymer-solution flow through porous media has elastic and shear effects. In order to characterize the contribution of elastic and shear effects during flow of polymer solutions through porous media, a macroscopic parameter, the polymer apparent viscosity, is used. In the next section we briefly describe the non-Newtonian rheology of polymer solutions followed by a description on polymer apparent viscosity in porous media. Then we establish the research objectives and present an outline of the current thesis.

1.1. POLYMER SOLUTION RHEOLOGY

Polymer solutions often exhibit viscoelasticity; that is, they exhibit a viscous response as well as an elastic response due to deformation. In this thesis we are concerned with the polymer solutions that exhibit viscoelasticity. A viscous response is the ability of a fluid to dissipate energy during flow. As an example, we consider a fluid separated by two parallel plates such that the bottom plate is stationary and the top plate is moving with a velocity, v. In this case, the force per unit area, σ necessary to maintain flow is proportional to the velocity gradient, (also known as shear-rate, $\dot{\gamma}$). The constant of

proportionality is known as viscosity -

$$\eta = \frac{\sigma}{\dot{\gamma}} \tag{1.1}$$

If the steady-shear viscosity decreases as the shear rate increases, then the polymer solution is known as a shear-thinning fluid; whereas if the steady-shear viscosity is shear rate independent then the polymer solution is known as a Boger fluid. A shear-thinning fluid can be described by various models such as the power-law and the Carreau-Yasuda model.

The elastic response indicates the ability of polymer solutions to recover the stress once it is removed and is typically characterized by a polymer relaxation time. At a molecular scale, the relaxation time is a time-scale that a deformed polymer chain need to return to equilibrium. Further details on characterization of polymer solution rheology can be found in several textbooks.[16, 17]

1.2. POLYMER APPARENT VISCOSITY IN POROUS MEDIA

Polymer apparent viscosity is a crucial parameter used during designing of an optimal polymer flood process.[2] The apparent viscosity η_{app} in porous media of length L_{PM} is the macroscopic averaged apparent shear viscosity as obtained from Darcy's law relating the pressure drop with superficial velocity v_{darcy} in the reservoir as -

$$\eta_{\text{app}} = \frac{k}{v_{\text{darcy}}} \frac{\Delta P}{L_{\text{PM}}} \tag{1.2}$$

where k is permeability and ΔP is the pressure-drop across the porous media. Relating such an apparent viscosity to polymer solution rheology has been challenging.[2] Figure 1.3 shows a schematic of polymer apparent viscosity as a function of the apparent shear-rate in porous media. We can see three key regions, the Newtonian behaviour at low shear-rate (below the first critical shear rate) followed by the pseudoplastic behaviour (between first and the second critical shear-rate) and the dilatant behaviour (beyond the second critical shear-rate). Several existing models have been able to predict the Newtonian and the pseudoplastic behaviour.[18–23] Predicting the dilatant behaviour has been challenging as the exact mechanism causing the dilatant behaviour has been a subject of debate.[19, 21, 24] Several effects occur simultaneously as the polymer solutions flow through a porous medium such as (1) coupling between viscoelasticity of polymer-solutions with the converging-diverging nature of flow through porous media,[18, 25, 26] (2) polymer adsorption and retention inside the pores[27–29] and (3)

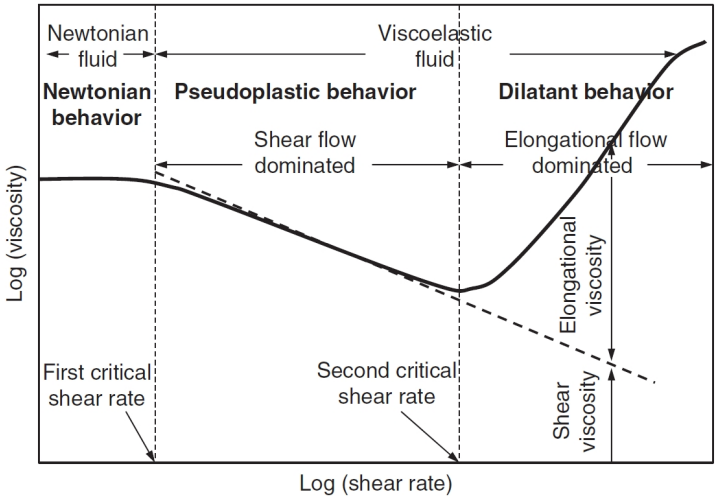


Figure 1.3: Schematic of polymer apparent viscosity versus apparent shear-rate in porous media.[31]

blockage at the rock surface by micro-gels.[30]

The dilatant behaviour causes an increase in flow resistance. This increase in flow resistance occurs at Weissenberg number, $Wi > 1$, (where $Wi = \tau\dot{\gamma}$, τ is polymer relaxation time and $\dot{\gamma}$ is shear-rate). Such an increase in the apparent viscosity has been linked to the polymer elasticity. The increase in flow resistance of polymer solutions in porous media has also been attributed to elastic flow instabilities at negligible inertial effects. [32–36] Elastic flow instabilities are essentially a state of non-homogeneous flow fields and these inhomogeneous flow patterns depend on the geometry and polymer solution rheology.[37, 38] For instance, at $Re \ll 1$ and $Wi \sim 1$, or $Wi \gg 1$ the flow of polymer solution exhibits (1) the well-known toroidal-cell instability in a Couette cell (analogous to the Newtonian-fluid flow in same geometry at $Re \gg 1$), [39] (2) a corner-vortex in entry-channel flows,[39, 40] (3) shear banding/wall slip in shear flow[41] or (4) asymmetricity or temporally fluctuating instability in stagnation-point flows.[42, 43] In highly elastic solutions, the elastic instability in a Couette cell above $Wi \sim 20$ transitions into a state of chaotically oscillating vortices known as *Disordered Oscillations*.[44] Another type of elastic instability, *elastic turbulence*, which closely resembles disordered oscillations, appeared to be occurring for highly elastic solutions in parallel-plate geometry[45], serpentine geometry[46] and many more geometries/non-Newtonian systems.[47, 48] However, the exact mechanism via which the polymer elasticity contributes to the apparent viscosity is debatable. In this thesis, the focus is on identifying and characterizing the pseudoplastic and dilatant behaviour mechanism at a pore-scale and at molecular-scale.

1

1.3. RESEARCH OBJECTIVES

Polymer apparent viscosity is a macroscopic averaged property that includes the shear and elastic effects during flow of polymer solutions through porous media.[2, 49] Specifically, the polymer solution viscoelasticity and the complex pore shape inside a porous medium affects the polymer apparent viscosity. In order to improve the understanding of the nature of flow of polymer solutions through porous media, the following sub-objectives are identified:

1. Relate the macroscopic flow-field to the molecular conformation of polymer chains.
2. Characterize the flow field of viscoelastic polymer solutions through porous media.
3. Investigate the effect of increasing the ionic strength on the flow-field.
4. Characterize the molecular conformation of polymer chains during flow of polymer solutions through porous media.

1.4. THESIS OUTLINE

In this section, we briefly describe the approach adopted to achieve the sub-objectives in the different chapters. The first chapter is the introduction to the scope of this thesis, and the sixth chapter is the conclusion of this thesis. Chapters two through five are collection of papers, and accordingly are largely self-reliant.

In chapter 2, we review the relevant fundamentals of polymer physics with an emphasis on relating the molecular conformation with the macroscopic flow behaviour to achieve sub-objective 1. This chapter also introduces the single-DNA experiments that we have used to characterize the molecular conformation of polymer solutions as they flow through porous media. In chapter 3, we address sub-objective 2 by visualizing the flow field and simultaneously measuring pressure drop in microfluidic devices containing square and cylindrical pillars in staggered and aligned layouts. In chapter 4, we address sub-objective 3 by varying the ionic strength of polymer solutions, and using the experimental protocol developed in chapter 3. Finally, in chapter 5, we address sub-objective 4, by directly visualization of polymer chains by using single-DNA experiments during flow through porous media. In particular, we focus on visualizing polymer conformation in the flow field as characterized in chapter 3.

Note from the author: This text includes published/under-review papers in peer-reviewed journals and scientific conferences. Consequently, the reader may find similar texts and sentences in some parts of the thesis.

REFERENCES

[1] I. Sandrea and R. Sandrea, *Global oil reserves-1: Recovery factors leave vast target for eor technologies,* Oil and Gas Journal **105**, 44 (2007).

[2] L. W. Lake, R. Johns, W. Rossen, and G. Pope, *Fundamentals of enhanced oil recovery* (Society of Petroleum Engineers, 2014).

[3] A. Muggeridge, A. Cockin, K. Webb, H. Frampton, I. Collins, T. Moulds, and P. Salino, *Recovery rates, enhanced oil recovery and technological limits,* Phil. Trans. R. Soc. A **372**, 20120320 (2014).

[4] S. L. Wellington, H. J. Vinegar, *et al.*, *X-ray computerized tomography,* Journal of Petroleum Technology **39**, 885 (1987).

[5] J. R. Christensen, E. H. Stenby, A. Skauge, *et al.*, *Review of wag field experience,* in *International Petroleum Conference and Exhibition of Mexico* (Society of Petroleum Engineers, 1998).

[6] P. McGuire, A. Moritz Jr, *et al.*, *Compositional simulation and performance analysis of the prudhoe bay miscible gas project,* SPE reservoir engineering **7**, 329 (1992).

[7] A. Moradi-Araghi, *A review of thermally stable gels for fluid diversion in petroleum production,* Journal of Petroleum Science and Engineering **26**, 1 (2000).

[8] F. Chang, Q. Qu, W. Frenier, *et al.*, *A novel self-diverting-acid developed for matrix stimulation of carbonate reservoirs,* in *SPE International Symposium on Oilfield Chemistry* (Society of Petroleum Engineers, 2001).

[9] R. M. Butler, *Thermal recovery of oil and bitumen* (Old Tappan, NJ (United States); Prentice Hall Inc., 1991).

[10] D. Wang, J. Cheng, Q. Yang, G. Wenchao, L. Qun, F. Chen, *et al.*, *Viscous-elastic polymer can increase microscale displacement efficiency in cores,* in *SPE annual technical conference and exhibition* (Society of Petroleum Engineers, 2000).

[11] A. Clarke, A. M. Howe, J. Mitchell, J. Staniland, L. Hawkes, and K. Leeper, *Mechanism of anomalously increased oil displacement with aqueous viscoelastic polymer solutions,* Soft matter **11**, 3536 (2015).

[12] A. Abidin, T. Puspasari, and W. Nugroho, *Polymers for enhanced oil recovery technology,* Procedia Chemistry **4**, 11 (2012).

[13] D. Wever, F. Picchioni, and A. Broekhuis, *Polymers for enhanced oil recovery: a paradigm for structure–property relationship in aqueous solution,* Progress in Polymer Science **36**, 1558 (2011).

[14] B. Leonhardt, F. Visser, E. Lessner, B. Wenzke, and J. Schmidt, *From flask to field–the long road to development of a new polymer,* in *IOR 2011-16th European Symposium on Improved Oil Recovery* (2011).

[15] R. Lenormand, E. Touboul, and C. Zarcone, *Numerical models and experiments on immiscible displacements in porous media,* Journal of Fluid Mechanics **189**, 165–187 (1988).

[16] R. B. Bird, ed., *Dynamics of polymeric liquids*, 2nd ed. (Wiley, New York, 1987) p. 2.

[17] C. W. Macosko, ed., *Rheology: principles, measurements, and applications* (VCH, New York, 1994) p. 550.

[18] G. Chauveteau, M. Moan, and A. Magueur, *Thickening behaviour of dilute polymer solutions in non-inertial elongational flows,* Journal of non-newtonian fluid mechanics **16**, 315 (1984).

[19] K. S. Sorbie, *Polymer-improved oil recovery* (Springer Science & Business Media, 2013).

[20] W. Cannella, C. Huh, R. Seright, *et al.*, *Prediction of xanthan rheology in porous media,* in *SPE annual technical conference and exhibition* (Society of Petroleum Engineers, 1988).

[21] M. Delshad, D. Kim, O. Magbagbeola, C. Huh, G. Pope, and F. Tarahhom, *Mechanistic interpretation and utilization of viscoelastic behavior of polymer solutions for improved polymer-flood efficiency,* in *SPE/DOE Symposium on Improved Oil Recovery* (2008).

[22] F. Durst, R. Haas, and B. Kaczmar, *Flows of dilute hydrolyzed polyacrylamide solutions in porous media under various solvent conditions,* Journal of Applied Polymer Science **26**, 3125 (1981).

[23] F. Durst, R. Haas, and W. Interthal, *The nature of flows through porous media,* Journal of Non-Newtonian Fluid Mechanics **22**, 169 (1987).

[24] A. Stavland, H. Jonsbraten, A. Lohne, A. Moen, and N. Giske, *Polymer flooding-flow properties in porous media versus rheological parameters,* in *SPE EUROPEC/EAGE Annual Conference and Exhibition* (2010).

[25] J. Heemskerk, R. Rosmalen, R. Janssen-van, R. Holtslag, D. Teeuw, *et al.*, *Quantification of viscoelastic effects of polyacrylamide solutions,* in *SPE Enhanced Oil Recovery Symposium* (Society of Petroleum Engineers, 1984).

[26] D. G. Hatzignatiou, U. L. Norris, and A. Stavland, *Core-scale simulation of polymer flow through porous media,* Journal of Petroleum Science and Engineering **108**, 137 (2013).

[27] M. Singleton, K. Sorbie, R. Shields, *et al.*, *Further development of the pore scale mechanism of relative permeability modification by partially hydrolysed polyacrylamide,* in *SPE/DOE Improved Oil Recovery Symposium* (Society of Petroleum Engineers, 2002).

[28] P. L. Zitha, G. Chauveteau, and L. Léger, *Unsteady-state flow of flexible polymers in porous media,* Journal of colloid and interface science **234**, 269 (2001).

[29] A. Omari, M. Moan, and G. Chauveteau, *Wall effects in the flow of flexible polymer solutions through small pores,* Rheologica Acta **28**, 520 (1989).

[30] R. S. Seright, J. M. Seheult, T. Talashek, *et al.*, *Injectivity characteristics of eor polymers,* in *SPE annual technical conference and exhibition* (Society of Petroleum Engineers, 2008).

[31] J. Sheng, *Modern Chemical Enhanced Oil Recovery: Theory and Practice* (Gulf Professional Publishing, 2010).

[32] J. Deiber and W. Schowalter, *Flow through tubes with sinusoidal axial variations in diameter,* AIChE Journal **25**, 638 (1979).

[33] B. Khomami and L. D. Moreno, *Stability of viscoelastic flow around periodic arrays of cylinders,* Rheologica acta **36**, 367 (1997).

[34] F. J. Galindo-Rosales, L. Campo-Deaño, F. Pinho, E. Van Bokhorst, P. Hamersma, M. Oliveira, and M. Alves, *Microfluidic systems for the analysis of viscoelastic fluid flow phenomena in porous media,* Microfluidics and nanofluidics **12**, 485 (2012).

[35] A. M. Howe, A. Clarke, and D. Giernalczyk, *Flow of concentrated viscoelastic polymer solutions in porous media: effect of mw and concentration on elastic turbulence onset in various geometries,* Soft matter **11**, 6419 (2015).

[36] A. Machado, H. Bodiguel, J. Beaumont, G. Clisson, and A. Colin, *Extra dissipation and flow uniformization due to elastic instabilities of shear-thinning polymer solutions in model porous media,* Biomicrofluidics **10**, 043507 (2016).

[37] E. S. Shaqfeh, *Purely elastic instabilities in viscometric flows,* Annual Review of Fluid Mechanics **28**, 129 (1996).

[38] S.-Q. Wang, S. Ravindranath, and P. E. Boukany, *Homogeneous shear, wall slip, and shear banding of entangled polymeric liquids in simple-shear rheometry: A roadmap of nonlinear rheology,* Macromolecules **44**, 183 (2011), http://dx.doi.org/10.1021/ma101223q .

[39] R. G. Larson, *Instabilities in viscoelastic flows,* Rheologica Acta **31**, 213 (1992).

[40] R. G. Larson, E. S. Shaqfeh, and S. J. Muller, *A purely elastic instability in taylor–couette flow,* Journal of Fluid Mechanics **218**, 573 (1990).

[41] P. E. Boukany, S.-Q. Wang, S. Ravindranath, and L. J. Lee, *Shear banding in entangled polymers in the micron scale gap: a confocal-rheoscopic study,* Soft Matter **11**, 8058 (2015).

[42] P. E. Arratia, C. C. Thomas, J. Diorio, and J. P. Gollub, *Elastic instabilities of polymer solutions in cross-channel flow,* Physical Review Letters **96**, 144502 (2006).

[43] S. Haward and G. McKinley, *Instabilities in stagnation point flows of polymer solutions,* Physics of Fluids (1994-present) **25**, 083104 (2013).

[44] A. Groisman and V. Steinberg, *Mechanism of elastic instability in couette flow of polymer solutions: experiment,* Physics of Fluids (1994-present) **10**, 2451 (1998).

[45] A. Groisman and V. Steinberg, *Elastic turbulence in a polymer solution flow,* Nature **405**, 53 (2000).

[46] A. Groisman and V. Steinberg, *Efficient mixing at low reynolds numbers using polymer additives,* Nature **410**, 905 (2001).

[47] A. Groisman and V. Steinberg, *Elastic turbulence in curvilinear flows of polymer solutions,* New Journal of Physics **6**, 29 (2004).

[48] J. Beaumont, N. Louvet, T. Divoux, M.-A. Fardin, H. Bodiguel, S. Lerouge, S. Manneville, and A. Colin, *Turbulent flows in highly elastic wormlike micelles,* Soft Matter **9**, 735 (2013).

[49] F. A. Dullien, *Porous media: fluid transport and pore structure*, Vol. 2 (Academic press San Diego, 1992).

2

POLYMER CHAIN DYNAMICS DURING SIMPLE AND COMPLEX FLOWS

Thanks to direct observation and manipulation of DNA in microfluidic devices, we are now able to elucidate the relationship between the polymer microstructure and its rheological properties, as well as to design new single-molecule platforms for biophysics and biomedicine. This allows exploration of many new mechanisms and phenomena, which were previously unachievable with conventional methods such as bulk rheometry tests. For instance, the field of polymer rheology is at a turning point to relate the complex molecular conformations to the nonlinear viscoelasticity of polymeric fluids (such as coil-stretch transition, shear thinning, and stress overshoot in startup shear). In addition, nanofluidic devices provided a starting point for manipulating single DNA molecules by applying basic principles of polymer physics, which is highly relevant to numerous processes in biosciences. In this chapter, we review recent progress regarding the flow and deformation of DNA in microfluidic systems from both fundamental and application perspectives. We particularly focus on advances in the understanding of polymer rheology and identify the emerging research trends and challenges.

Parts of this chapter have been published in L. Rems, **D. Kawale**, L. J. Lee, P. E. Boukany, *Flow of DNA in micro/nanofluidics: From fundamentals to applications*, Biomicrofluidics **10**, 043403 (2016).

2.1. INTRODUCTION

Understanding the deformation and flow of (bio)polymers, such as DNA, is a critical challenge in life sciences as well as in polymer science and engineering.[1] Beyond the DNA's biological relevance as the carrier of the genetic information in all forms of life, DNA can also be employed as a model polymer for experiments relevant to fundamental studies on polymer physics. Compared with synthetic model polymers, DNA has several advantages, including ease of fluorescent labeling and narrow size distribution at a given number of DNA base pairs (bp $\sim$ 0.34 nm). In addition, DNA can be prepared in a variety of sizes ranging from just few base pairs to hundreds of thousands of base pairs via gene synthesis and genetic engineering techniques.[2, 3] Fluorescently labeled DNA with a typically used contour length L of several tens of micrometers can be visualized under a common fluorescence microscope while still being classified as a (semi-)flexible chain under physiological conditions, since the DNA's persistence length P is only about 50 nm.[4] Furthermore, micro/nanofluidics is nowadays an established technology, which offers unique features to explore and examine biological and complex fluids under controlled and reproducible conditions.[5, 6] Different fluidic geometries with spatial scales from nanometers to centimeters can be fabricated by soft lithography and etching techniques.[7–9] Combination of micro/nanofluidics and DNA visualization has allowed scientists to test polymer theories directly against experiments at the single-molecule level, which presents an important step for advancements in both polymer rheology and genomic sciences.

In contrast to Newtonian fluids, polymeric fluids exhibit complex flow behavior such as shear thinning, rod climbing, transient stress-overshoot during shear, and flow instabilities, which are related to flow-induced changes in polymer molecular conformation at very high deformation rate. However, the exact molecular picture behind many of these complex flow responses is not well-understood and is still under debate.[10, 11] This limits the design, control, and optimization of the technological processes related to polymer products.[12] In order to overcome the technological limitations, it is essential to develop new methods that can link the macroscopic flow responses with the molecular conformation of polymer molecules in the flow.

Traditionally, polymer rheologists focused on measuring the macroscopic flow responses using "bulk" experimental methods including rotational rheometry, light scattering, and birefringence.[13, 14] In such bulk measurements, the rheological properties of polymers are averaged over an ensemble of many molecules. In the past two decades, the approach of analyzing the rheological response has been changed by utilizing newly developed tools such as microfluidics-based rheometers[15] coupled with

advanced single-molecule techniques.[16, 17] In particular, direct observation of individual DNA molecules during flow in microfluidic channels provided a fresh insight into the nature of the rheological responses of polymeric fluids by describing flow properties on the single-molecule level.[2, 2, 18, 19] For instance, single-molecule experiments have directly shown the details of how coiled DNA molecules become significantly stretched when the hydrodynamic flow rate is sufficiently fast, which revealed a complex transition from the equilibrium (coiled) to the non-equilibrium (un-coiled) conformation.[20, 21]

This review gives an overview of the use of microfluidic systems to visualize, study and manipulate DNA molecules. We focus on how the field of polymer rheology has benefitted from flow studies of DNA inside microfluidic systems by relating the complex conformation of DNA molecules to their flow responses.

2.2. DNA FLOW IN MICROFLUIDICS

Different types of flow fields such as shear, extension, and compression can co-exist during polymer-processing operations. Understanding the physics of such viscoelastic flows can be extremely challenging, because of the competition between various forces such as inertia, viscosity, and elasticity of polymeric materials. The development of microfluidics stimulated an interest to investigate the rheological response of polymeric fluids in microfluidic devices, because the latter offer an easy control over inertial and elastic forces in experiments.

In sections 2.3 - 2.7, we first introduce the dimensionless groups, that are later used in the thesis to characterize the dominant forces governing a given flow behavior (Section 2.3). We then continue with a brief discussion on the general use of DNA molecules for visualization of polymer conformations within the flow field (Section 2.4). Finally, we describe in greater detail how a stained DNA molecule has been used as a model polymer to study the relaxation of stretched (deformed) polymers, and polymer molecular conformations in extensional, shear, and other industrially relevant flows at high Weissenberg number (Sections 2.5 - 2.7). These studies have been helpful in understanding the rheological properties of polymer solutions by validating basic polymer theories at the single-molecule level.

2.3. DIMENSIONLESS GROUPS

Dimensional analysis is a powerful tool to identify the dominant forces in complex flows of polymeric materials.[22] Four dimensionless groups are highly relevant to rheological studies of polymers: the Reynolds number (Re), the Weissenberg number (Wi), the Deb-

orah number (*De*), and the elasticity number (*El*). Additionally, the viscoelastic Mach number (*Ma*) is also relevant in the rest of this thesis.

The definition of the Reynolds number is given as $Re = \rho v l/\eta$, where ρ is the fluid density, v is the average velocity, l is a characteristic length scale, and η is the fluid viscosity. The Weissenberg number is defined for shear flow as $Wi = \dot{\gamma}\tau$, for channel flow as $Wi = (v/l)\tau$, and for extensional flow as $Wi = \dot{\varepsilon}\tau$, where $\dot{\gamma}$ is the shear strain rate, $\dot{\varepsilon}$ is the extensional strain rate, and τ is the longest relaxation time.

The Deborah number was originally defined as $De = \tau / t_{\text{obs}}$, where t_{obs} is the observation time during transient deformation.[23, 24] There has been a lot of confusion about the intended usage of *Wi* and *De* numbers in order to generalize the findings from a particular rheological problem. In some literature, different definitions of *De* have been proposed, by altering the time of observation to either the process time or the residence time in a given flow field. Therefore, *De* has been also defined as the ratio of the sample's characteristic relaxation time to the characteristic flow rate, i.e., $De = \dot{\varepsilon}\tau$ or $De = (v/l)\tau$. To avoid confusion in this review, we will consider the original definition of *De*.[24] According to the original definition, the observation time can be infinite, resulting in $De \sim 0$ in steady flows (such as steady simple shear and extension). Hence, we will retain *Wi* to characterize the ratio between the polymer relaxation time and convective time scales.[25]

The Elastic number presents the ratio between the elastic and inertial forces and is defined as $El = Wi/Re$. Elasticity number is independent of the fluid kinematics as this number is independent of fluid velocity. To summarize the guidelines on how to use these numbers, see table 2.1.

The Mach number presents the ratio of local flow velocity to the speed of viscoelastic shear wave and is defined as $Ma = \sqrt{WiRe}$. The viscoelastic shear wave, c_s is defined as $c_s = \sqrt{G/\rho} = \sqrt{\eta/(\rho\tau)}$ where G is the elastic modulus.[26]

The key advantage of microfluidic devices is that one can achieve high *Wi* at low *Re*, which allows us to reach higher-*El* flows compared to conventional fluidic devices (see table 2.1). A wide variety of flow instabilities, such as vortex formation, shear banding, wall slip, and elastic turbulence, may occur in microfluidic devices, depending on the value of these dimensionless numbers. For example, Rodd *et al.* [27] could explore new regimes in contraction flows of polymer solutions, as shown in figure 2.1. This microfluidic platform provided a unique opportunity for them to study the effect of elasticity on vortex instability in polymer solutions at high-*Wi* and low-*Re*.

Table 2.1: Relevant dimensionless number used in this review.

	Physical Interpretation	Definition	Achievable range	
			Conventional fluidic devices	Microfluidic devices
Re	$\frac{\text{Inertial force}}{\text{Viscous force}}$	$\frac{\rho v l}{\eta}$	$\sim 10^{-2} - 10^{4}$ [a]	$\sim 10^{-5} - 10$ [b]
De	$\frac{\text{Stress relaxation time}}{\text{Observation time}}$	$\frac{\tau}{t_{\text{obs}}}$	$\sim 0 - \infty$	$\sim 0 - \infty$
Wi	$\frac{\text{Elastic force}}{\text{Viscous force}}$	Shear flow: $\dot{\gamma}\tau$ Extensional flow: $\dot{\varepsilon}\tau$ Channel flow: $(v/l)\,\tau$	$\sim 10^{-7} - 10^{2}$	$\sim 10^{-4} - 10^{5}$ [b,c]
El	$\frac{\text{Elastic force}}{\text{Inertial force}}$	$\frac{Wi}{Re}$	$\sim 10^{-5} - 10^{-2}$	$\sim 10 - 10^{4}$ [b]
Ma	$\frac{\text{Local flow velocity}}{\text{Viscoelastic shear wave speed}}$	$\sqrt{WiRe}$	$\sim 10^{-5} - 10^{3}$	$\sim 10^{-5} - 10^{3}$

[a] Re can be even higher than 10^4, but the higher limit depends on how much pressure the system can handle.
[b] Assuming that a typical PDMS-based microfluidic device would be delaminated at pressure higher than 1 bar.
[c] Assuming maximum $\dot{\gamma} = 1000\,\text{s}^{-1}$ and $\tau = 100\,\text{s}$.

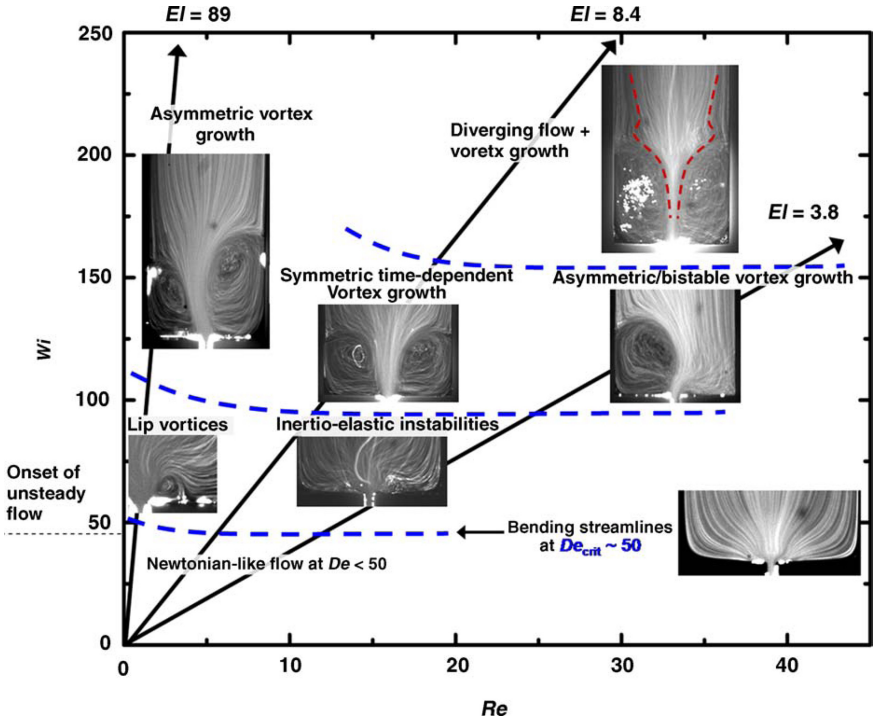


Figure 2.1: Microfluidic devices explored new regimes in Wi – Re space for polymeric fluids flowing through contraction geometries. Reproduced with permission from Rodd et al., J. Non-Newton. Fluid Mech. 129, 1 (2005). Copyright 2005 Elsevier.[27]

2.4. DNA AS A MODEL POLYMER FOR VISUALIZATION

Flows of polymer solutions were traditionally visualized and investigated by integrating (micro)fluidic geometries with optical/confocal microscopy and using velocimetry techniques. These velocimetry techniques mainly include the Particle Tracking Velocimetry (PTV), the Particle Streak Velocimetry (PSV), and the Particle Image Velocimetry (PIV), which are based on imaging the position of micro-tracer particles suspended in the polymer solution.[17, 28–30] These effective methods could determine the onset of flow instability in polymer solutions at high Wi (or high El). However, they could not provide sufficient information on the flow-induced polymer conformation.[30]

Using DNA as a molecular tracer has opened new avenues for polymer rheologists to study the polymer conformation in viscoelastic flows. DNA molecules can be stained with a fluorescent dye, such as YOYO-1 or TOTO-1,[31] which makes them visible under a fluorescence microscope when illuminated at the excitation wavelength of the dye. In the first attempts to visualize the conformation of an individual DNA molecule within the flow field, tiny amounts of fluorescently stained DNA molecules as test chains were dispersed in a solution of unstained DNA molecules (background chains). Using this approach, the stained DNA molecules and their conformations could be visualized as representative of the unstained DNA molecules. These fundamental studies of DNA dynamics were carried out in simple fluidic geometries to produce extensional or shear flow. Later on, complex geometries were also studied by introducing contraction geometries and integrating obstacles inside microfluidic devices.[32–34] Moreover, stained DNA molecules were also used as molecules probes in a solution of (unstained) synthetic polymers such as polyethylene oxide (with similar contour length L) in order to measure polymer conformations and velocity fields during flow.[35]

Recently, synthetic polymers including polyacrylamide and poly(methyl methacrylate) have also been labeled with a fluorescent dye.[36–38] However, the protocol of attaching fluorescent probes to synthetic polymers is tediously elaborate and challenging for routine applications in rheology testing laboratories. Ease of staining and manipulation is perhaps the greatest advantage of DNA over synthetic polymers. Therefore, DNA molecules are still being employed as popular fluorescent probes to study polymeric conformations within the flow field.

Nevertheless, to obtain quantitative information about the DNA chain extension in strong flows, one must be aware that the staining increases the contour length of DNA. The increase in contour length is a function of the ratio between the number of added dye molecules per DNA base pairs, and about 38 % increase in contour length has been reported for 1 YOYO-1 per 4 DNA base pairs.[39, 40] Furthermore, DNA is a negatively

charged polyelectrolyte (similar to poly(sodium styrene sulfonate) and polyacrylic acid). Therefore, its persistence length P is a function of the ionic strength in the aqueous solution. In the limit of high salt concentration (> 10 mM), DNA is a semi-flexible molecule with $P \sim 50$ nm. When reducing the salt concentration, DNA significantly stiffens. At 0.1 mM salt, the reported P of DNA is around 350 nm.[41] Consequently, most flow studies based on DNA visualization should be performed in buffer solutions containing sufficient amount of salt to decrease the stiffness of the DNA as well as to neutralize its charges.

2.5. RELAXATION OF STRETCHED DNA: ZIMM AND REPTATION THEORY MEET EXPERIMENTS

The relaxation of stretched polymers is of fundamental importance in describing the viscoelastic properties of polymeric fluids.[42] Stress relaxation measurement is generally carried out using bulk rheometry. In this test, a polymer sample is suddenly deformed by a fixed amount of deformation (called step strain), and the resulting stress decay is monitored over time when the deformation is stopped (after step shear). In this classical approach, the relaxation response of single polymers needs to be interpreted from indirect measurements averaged over an ensemble of polymer chains.

Polymer experimentalists have attempted to understand the relaxation behavior of an isolated polymer chain upon cessation of the flow (or deformation) to validate theoretical predictions using single-molecule DNA measurements. These relaxation methods have been applied to both isolated polymer chains[43] and to concentrated polymer solutions,[44] where the interaction between the test chain and the surrounding chains becomes important.

The Zimm model[45] is one of the most powerful theories of polymer dynamics, and has been successfully applied in dilute polymer solutions. This model treats the polymer chain as a string of beads connected by Hookean springs, where the beads hydrodyamically interact with the solvent. Based on this model, the relaxation time of an isolated polymer scales as $\tau \sim M^{3\nu} \sim L^{3\nu}$, where M is the molecular weight of the polymer, L is the polymer contour length, and 3ν is the scaling exponent. Within Zimm model,[45] the value of 3ν is 1.5 and 1.8 for theta and good solvents, respectively. Until the advent of using DNA as a model polymer, this scaling law was tested by indirect methods (intrinsic viscosity,[46] dynamic light scattering,[47] and birefringence[48]) giving a value ranging from 1.5 to 1.65. In order to validate the scaling law directly, Perkins *et al.* [43] stretched single isolated DNA molecules in a strong flow (at $Wi > 1$), and visualized the relaxation

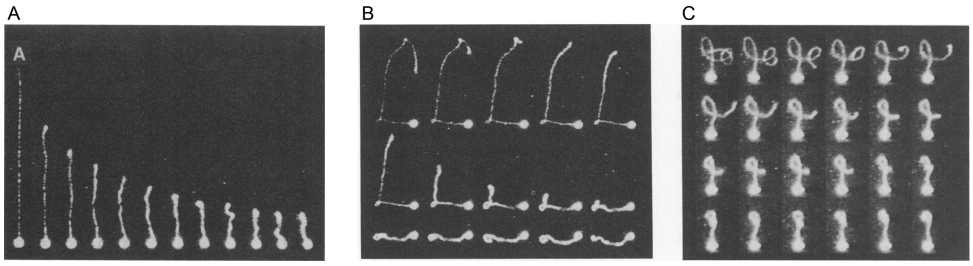


Figure 2.2: Relaxation responses of individual DNA molecules in (a) dilute and ((b) and (c)) concentrated (entangled) solutions. (a) Relaxation of a single DNA molecule, where the DNA is stretched around 40 µm in a flow and its relaxation is measured after cessation of the flow. Subsequent images are separated by 4.5 s. Reproduced with permission from Perkins et al., Science 264, 822 (1994). Copyright 1994 The American Association for the Advancement of Science.[43] ((b) and (c)) Series of images showing reptating tube-like DNA motion in a concentrated solution of DNA molecules ((a): 12 molecules/µm^3, (b): 7 molecules/µm^3). The fluorescently labeled DNA was tethered to a fluorescent microbead, which was controlled by optical tweezers. The sequence of images starts at time 0 s (top row, left) after stopping the movement of the microbead. In (b) the image sequence is shown up to 128 s (bottom row, right). Note that the topological constraints imposed by the background polymers persisted in excess of 120 s, as shown by the persistence of the small loop of DNA near the microbead. In (c) the images are separated by 1.5 s. Reproduced with permission from Perkins et al., Science 264, 819 (1994). Copyright 1994 The American Association for the Advancement of Science.[44]

process under the microscope after stopping the flow (see figure 2.2a). In their experiments, a DNA molecule was tethered by one end to a microbead, which was held still by optical tweezers, and the molecule was stretched by laterally moving the microscope stage. They found that the relaxation time scales as $\tau \sim L^{1.65}$, in qualitative agreement with predictions from the Zimm model. Although the experimental value is close to the theoretical value, it is debatable whether the DNA molecules used in their experiments can be considered as a "universal" polymer model, for which the Zimm's scaling law would be directly applicable. According to de Gennes,[49] a polymer approaches universality when the polymer is sufficiently long, such that its behavior is independent of its chemical structure. In the case of the double-stranded DNA, Tree *et al.* [50] numerically showed that universality occurs only for ultra-long chains (~ 1 megabase pairs, i.e., at least few 100 µm long), whereas typically used DNA molecules in experiments (~ 100 kilobase pairs) are somewhere in the middle of the transition to long-chain behavior. Consequently, the DNA molecules used by Perkins *et al.* [43] (4 µm–43 µm long) were probably somewhere in a transition regime of the Zimm's scaling exponent.

Later, DNA molecules have been successfully used to understand the rheological behavior of concentrated polymer solutions. Examining the molecular dynamics of concentrated polymer solutions is a challenging task, because of the high degree of interaction among polymer chains. Polymers in concentrated solutions ($C > C^*$, where C^* is the overlap concentration), are entangled with each other like cooked spaghetti. To the-

oretically address concentrated polymer solutions, de Gennes, Doi, and Edwards[18, 51] proposed an elegant concept of reptation. In this model, an entangled polymer is assumed to be confined inside an imaginary tube through which it can move in a snake-like fashion. When the polymer traverses through this imaginary tube, the tube deforms and exerts strain on the surrounding polymers. The theoretical assumptions of the tube-like motion were experimentally confirmed on the single-polymer level by Perkins *et al.* [44] The experiment was performed by visualizing a single fluorescently labelled DNA molecule (test chain) in an entangled solution of unlabeled DNA. The test chain was attached by one end to a microbead and pulled through the entangled solution by optical tweezers. As the test chain was pulled, it closely followed the path of the microbead, allowing for various conformations to be "drawn" with the test chain, such as kinks and loops (figures 2.2b and 2.2c). After releasing the stress, the test chain slowly relaxed following the drawn path in reverse. In small loops, this tube-like motion persisted for over 2 min. Using a similar protocol, Smith *et al.* [52] further corroborated the theoretical predictions from the reptation model by measuring the diffusion coefficient of entangled DNA molecules. The model predicts that the diffusion coefficient scales with L^{-2}. The experimentally determined scaling exponent of -1.8 ± 0.1 was indeed close to the theoretical.

Teixeira *et al.* [53] employed a step shear test to investigate the relaxation behavior of entangled (concentrated) DNA solutions by direct visualization of individual DNA molecules. Two distinct relaxation time scales were found. Initially, DNA solutions relaxed very fast, because chain retraction occurred almost instantaneously. Later, reptation mechanism started to take over as the slower relaxation process. In addition, they showed that the slower relaxation time scaled with concentration as $\tau_{\text{slow}} \sim C^{3.3}$ ($C > C^*$). The reported exponent is higher than predicted value by pure reptation mechanism, which might originate from the effect of constraint release and contour length fluctuations on the reptative process.

Recently, Hsiao *et al.* [54] investigated the relaxation response of individual polymers in semi-dilute solutions ($C \sim C^*$). In this experiment, the polymer solution was flowed into a microfluidic cross-slot channel at high Wi, followed by sudden cessation of the fluid flow. They also found a power-law scaling $\tau \sim (C/C^*)^{0.48}$, which was in good agreement with bulk rheological tests.

Furthermore, Li *et al.* [55] studied the effect of chain topology (linear or circular chains) on the relaxation process of single DNA molecules by cessation of elongational flow. They found that circular DNA relaxed faster and exhibited a lower scaling exponent ($3\nu \sim 1.4$) compared to linear DNA ($3\nu \sim 1.7$). They speculated that lower exponent

might be an evidence of the absence of excluded volume effects in circular DNA. It is expected that circular DNA is effectively (~ 50 %) shorter than linear DNA with same molecular weight. Therefore, excluded volume is seen to be less important in circular DNA compared with linear DNA.

With respect to the influence of the chain topology on the polymer relaxation dynamics, an upcoming area of research is the effect of DNA branching, wherein one of the challenges is to synthesize branched DNA molecules.[56, 57]

2.6. DYNAMICS OF INDIVIDUAL DNA MOLECULES IN FLUID FLOW

The field of polymer rheology is concerned with the description of the flow behavior of polymeric fluids in strong flow. In this section, we focus on single-DNA rheology, which provided direct link to bulk viscoelasticity of polymers under controlled fluidic flows such as extension, shear, and mixed flows relevant to industrial operations. Initial single-molecule measurements in fluid flow were performed mainly on dilute polymer solutions. The assumption of dilute solution is that the intermolecular interactions are negligible, and the polymer is treated as a single isolated chain. Later, fluorescently stained DNA molecules were added in a background of unstained chains enabling to test semi-dilute and concentrated polymer solutions in the flow.[41, 53] Understanding the flow behavior of concentrated polymer solutions and entangled melts is very important in numerous industrial process such as injection molding, inkjet printing, coating, and fiber-spinning, because most of polymer solutions and melts that have been employed in industry would be processed in the entangled state.[12] The subsequent paragraphs in this subsection are organized to highlight the single-DNA measurements in different flow conditions (extensional flow, shear, contraction, and random flow) from dilute, semi-dilute to entangled DNA solutions.

2.6.1. EXTENSIONAL FLOW: COIL-STRETCH TRANSITION MEETS EXPERIMENT

In 1974, de Gennes [58] predicted that a dilute polymer solution would exhibit an instantaneous coil-stretch transition in strong flows, when the flow rate exceeds a certain critical value of Wi. Later, theoretical calculation from the generalized Zimm model and numerical calculation by Larson and Magda [59] showed that the onset of polymer stretching (coil-stretch transition) occurs at a critical strain rate, $\dot{\varepsilon} \sim 0.5/\tau$, where τ is the longest relaxation time. For $\dot{\varepsilon} < \dot{\varepsilon}_c$ (that is at $Wi < 0.5$), the polymer molecules are in the

coiled state.

Chu's group combined single DNA measurements with a controlled microfluidic geometry to experimentally test the above theoretical predictions.[20, 60, 61] Perkins *et al.* [20] employed a cross-slot microfluidic cell to directly visualize the conformation of DNA molecules in extensional flows. They observed an existence of a distribution of transient molecular conformations through the coil-stretch transition at a given flow rate (or Wi). The polymer molecules could be found in five main types of conformations: dumbbell, half-dumbbell, folded, kinked, or coiled (figure 2.3a shows the optical micrograph of these conformations). At $Wi = 3.35$, the first three types of conformations including the dumbbell, half-dumbbell, and folded were dominant. In a follow-up study, Smith and Chu [60] showed that at $Wi > 10$, many more molecules became kinked or folded, with their fraction reaching an asymptotic value of about one-third. On average, folded molecules stretched the slowest, whereas kinked molecules stretched the fastest. Figures 2.3b and 2.3c display the progression of the level of extension with time in individual DNA molecules at $Wi = 2$ and $Wi = 48$, respectively. Eventually, the molecules in these different transient conformations approached an asymptotic steady-state conformation, corresponding to a nearly fully stretched straight line (> 75 % of the DNA contour length). These data confirmed that for $Wi < 0.4$, there was no stretching, and all of the molecules were coils. In addition, the ensemble average extension of the chains increased with the imposed Wi (*cf.* figures 2.3b and 2.3c). The experimentally observed transient molecular conformations could also be predicted by Brownian dynamics simulations conducted by Larson *et al.* [62] These transient conformations indicate that the coil-stretch transition proceeds in a dynamic fashion, rather than instantaneously. It further shows that polymer molecules demonstrate "individualism" in their dynamics, rather than a collective and simultaneous unwinding beyond $\dot{\varepsilon}_c$. The origins of the molecular individualism are apparently governed by the details of the random initial molecular configuration of the polymer coil.[63]

de Gennes [58] also theoretically predicted that the coil-stretch transition might be associated with a strong hysteresis in molecular conformations. The existence of the hysteresis was then experimentally confirmed by Schroeder *et al.* [61] when employing a similar cross-slot microfluidic cell to stretch very long DNA (with L from 1.3 mm–1.7 mm). They showed that within a narrow range of Wi, conformation of the molecules was either coiled or highly stretched, depending on the deformation history of the DNA.

Recently, Hsiao *et al.* [54] investigated the coil-stretch transition for semi-dilute DNA solution in elongational flow. They observed a milder coil-stretch transition for semi-dilute DNA solutions (when $C \sim C^*$) compared with dilute DNA solution. A possible ex-

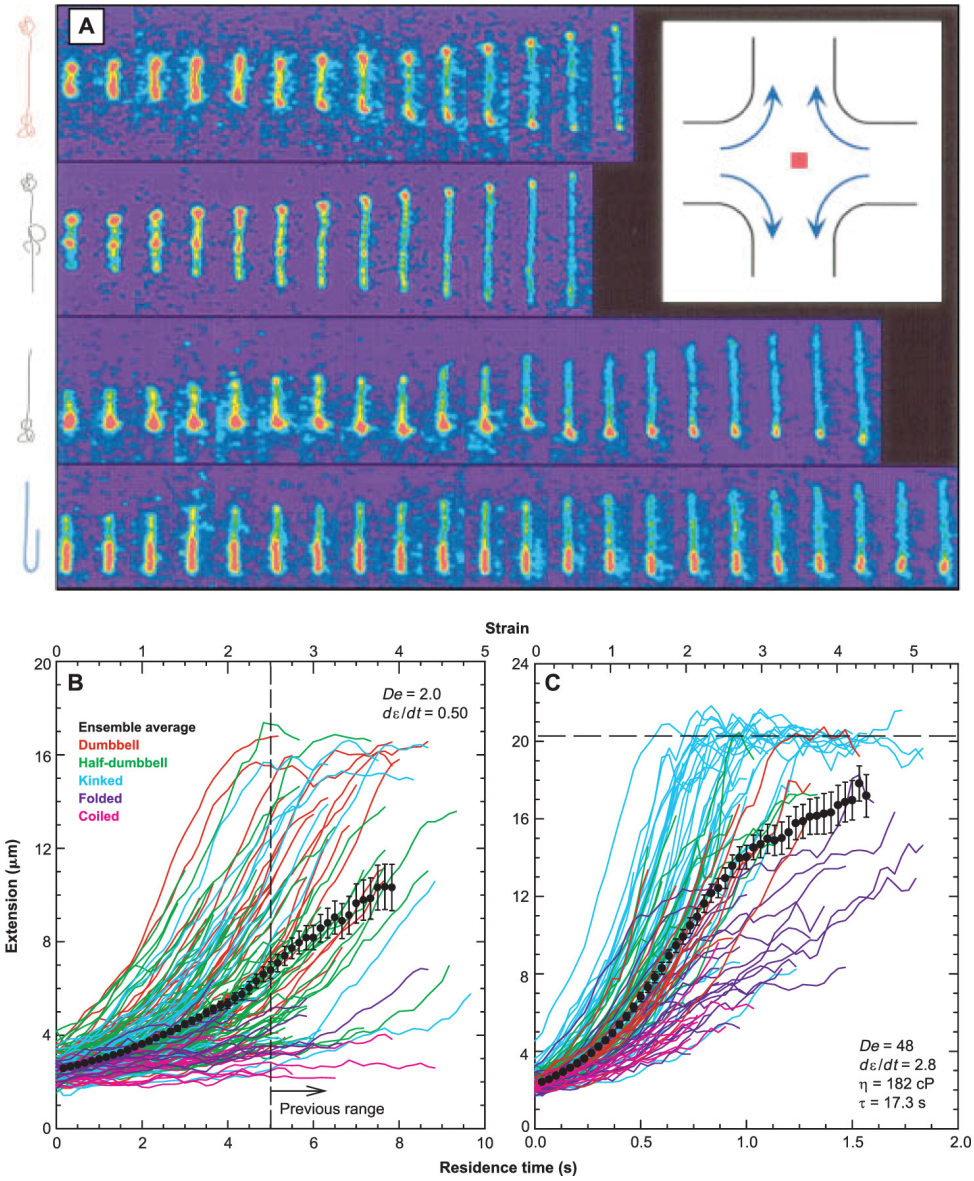


Figure 2.3: (a) The dumbbell, kinked, half-dumbbell, and folded DNA conformations in extensional flow field at $Wi = 3.4$. Images are spaced at 0.13 s. Molecular extension of the last molecule in the first row is 13.9 μm. Reproduced with permission from Perkins et al., Science 276, 2016 (1997). Copyright 1997 The American Association for the Advancement of Science.[20] ((b) and (c)) Time course of the DNA extension extracted from individual DNA molecules under the same flow conditions; (b) $Wi = 2$, (c) $Wi = 48$. The molecules were categorized with respect to their transient molecular conformations (shown in (a)), as indicated by the colors of the solid lines. The solid black points represent the ensemble average extension, which increases with Wi (*cf.* (b) and (c)). Note that we used Wi number in the figure caption to refer to De number indicated in the figure, following the discussion given in Section 2.3. Reproduced with permission from D. E. Smith and S. Chu, Science 281, 1335 (1998). Copyright 1998 The American Association for the Advancement of Science.[60]

planation is that this critical Wi might be concentration dependent, due to either inter-chain interactions among polymers or flow-induced entanglements in strong flows.

Finally, Li *et al.* [55] demonstrated that circular polymers could also display a coil-stretch transition in elongational flow. However, they have found that circular polymers need higher Wi to stretch and exhibit less diverse molecular individualism during the transient stretching process compared to linear polymers. They speculated that the delay of stretching and less diverse molecular individualism during transient extension might originate from more-compact structure of circular polymers and lower diversity of initial states available in circular chains, respectively, compared with linear chains.

2.6.2. DYNAMICS OF DNA IN SHEAR FLOW

DILUTE AND SEMI-DILUTE SOLUTIONS:

After studying the coil-stretch transition in elongational flow, Chu's group investigated the nature of coil-stretch transition in steady shear flow. Shear flow can also be considered as a superposition of a purely elongational and a purely rotational flow. de Gennes [58] had proposed that the presence of the rotational component in shear flows above $Wi > 0.5$ would drive the polymer molecules to a constantly fluctuating first-order coil-stretch transition. Smith *et al.* [64] experimentally demonstrated that the average DNA extension in steady shear flow indeed does not display a sharp coil-stretch transition. Instead, large fluctuations in polymer extension were observed that were consistent with repeating end-to-end tumbling of the molecule. The conformation of a given molecule continuously changed, and at different times, dumbbell, half-dumbbell, kinked, and folded shapes were observed, similar to those in extensional flow (figure 2.3a). The ensemble average extension of the molecules in shear flow also increased with Wi. However, the increase in the average extension with Wi was much more gradual than in extensional flow, and the highest average extension reached only about 40 %–50 % of the DNA contour length for Wi higher than ~ 40. Schroeder *et al.* [65] then demonstrated that the fluctuations in the polymer extension can be attributed to periodic cycling motion of the polymer as shown in figure 2.4. Above $Wi > 0.5$, the flow is strong enough to overcome the entropic elasticity of the coiled chain and stretch the molecule along the flow direction. As the polymer molecule extends in the direction perpendicular to the shearing flow plane, it is stretched due to hydrodynamic drag until it reaches a maximum stretch-length. A Brownian fluctuation can then cause the molecule to flip leading to a negative orientation angle θ (see figure 2.4) and the molecule starts recoiling. After the polymer tumbles, the cycle begins anew. The frequency of this cyclic motion was found to be proportional to $Wi^{0.66}$.

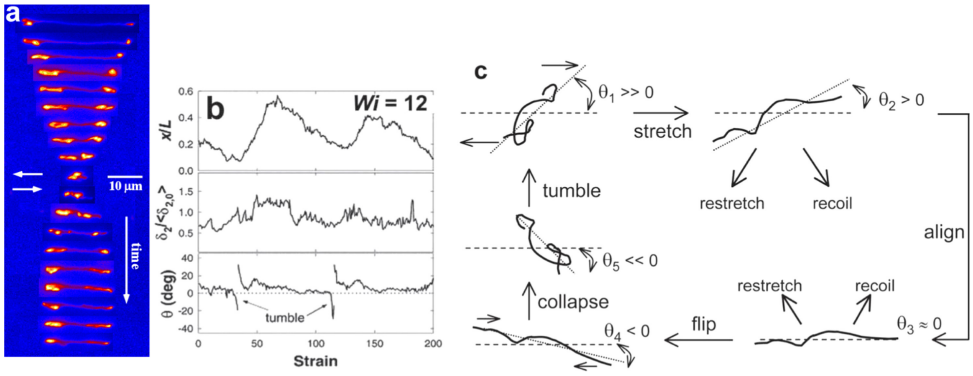


Figure 2.4: (a) DNA molecules under shear flow ($Wi = 109$) showing the end-to-end tumbling motion. Time between images is ~ 10 s. (b) Fractional polymer extension x/L, gradient-direction polymer thickness δ_2, and polymer orientation angle θ. (c) Schematic cycle of periodic polymer motion. Reproduced with permission from Schroeder et al., Phys. Rev. Lett. 95, 18301 (2005). Copyright 2005 American Physical Society.[65]

In contrast to steady shear flow, it is well known that in startup shear flow semi-dilute and concentrated polymeric fluids display a transient stress overshoot at $Wi > 1$. Hur *et al.* [66] combined single-DNA measurements with a bulk rheological test and Brownian-dynamics simulations to study the dynamics of both dilute and semi-dilute polymer solutions in startup shear flow. They observed an overshoot in the ensemble-averaged molecular extensions at high flow rates (above a critical $Wi \sim 20$) following an overshoot in shear viscosity for semi-dilute polymer solutions ($C \sim 0.5, 1.0,$ and $6.0C^*$).

SHEAR THINNING AND WALL SLIP IN CONCENTRATED SOLUTIONS:

Understanding the flow behavior of entangled linear-chain polymers has become a main goal in the development of a constitutive model in the polymer rheology. Teixeira *et al.* [53] applied steady shear, and startup shear flow to entangled DNA solutions ($C \sim 31C^*$) consisting of both fluorescent DNA chains as well as unstained background chains. This allowed to perturb both the fluorescent test chains as well as the background chains. They employed the single-molecule approach to identify the molecular conformations at different shear rates. They found that DNA molecules displayed highly individualistic behavior with a broad conformation distribution at high Wi in the shear-thinning regime ($Wi > 1$).[53] Recently, Boukany *et al.* [67] employed a confocal-rheoscope to directly image the DNA conformations in well-entangled DNA solutions ($C \sim 80$ and $160C^*$) during startup shear flow in the stress-overshoot regime ($Wi > 1$). They found that adsorbed DNA chains stretched at the surface and disentangled from other chains, which remained coiled in the bulk even at $Wi \sim 7$. This interfacial disentanglement led to strong wall slip and transient stress overshoot across the gap (~ 50 μm) at $Wi > 1$.

2.6.3. DYNAMICS OF DNA IN CONTRACTION FLOW

Polymeric flows through a contraction are highly relevant in numerous applications, such as polymer processing, extrusion, or injection molding, to name a few. In biological lab-on-a-chip applications such as DNA sequencing, one or many microfluidic contractions can exist. Therefore, understanding the molecular picture leading to macroscopic flow features, such as vortex formation and instabilities, is crucial for optimal performance of the lab-on-a-chip device.

Hemminger *et al.* [34] used calf thymus (75 kilobase pairs) DNA solutions to extensively probe flows through a 4:1 planar microfluidic contraction over a wide range of entanglements per chain, $Z = 7 - 55$ (or $16C^* < C < 160C^*$), and over a wide range of Wi ($0.7 < Wi < 21200$). Figure 2.5 shows the flow regimes on a $Wi - Re$ space, which were observed for different concentrations of the DNA. For weakly entangled solutions, the critical Wi for vortex formation was found to be $Wi_{cr} \sim 3$. They reported that most of DNA chains remained coiled in the vortex flow. A new flow regime was observed for well-entangled solutions that shows solid-like breakup (coined as jerky-shear banding). In this regime, considerable stretching of the DNA occurred in the strong local flow at the center-line of the contraction channel. However, the DNA in the weak local flow at the corner of the contraction channel underwent a quasi-periodic transition from partially coiled to fully stretched. These observations suggested that the DNA chains at the corner disentangle from chains in the center-line. Examining the new jerky-shear banding flow regime using DNA tracers enabled ruling out many microscopic hypotheses that cause flow instabilities such as flow-induced demixing, chain migrations, and chain scission.[34]

More recently, Gulati *et al.* [68] studied flows in semi-dilute and entangled ($C \sim C^*$) DNA solutions in microfluidic gradual contraction over $0.1 < Wi < 446$. No vortex was observed for non-shear thinning DNA solutions over the entire range of Wi numbers. In the case of entangled DNA solutions, the critical Wi for vortex formation in gradual contraction was reported to be $Wi_{cr} = 8.9$. In general, the Wi_{cr} for vortex formation in contraction geometry is in the order of 1–10 at any polymer concentration. The interested reader can find further information in comprehensive reviews covering both experimental and numerical efforts aimed to explore the flow through contractions.[69–71]

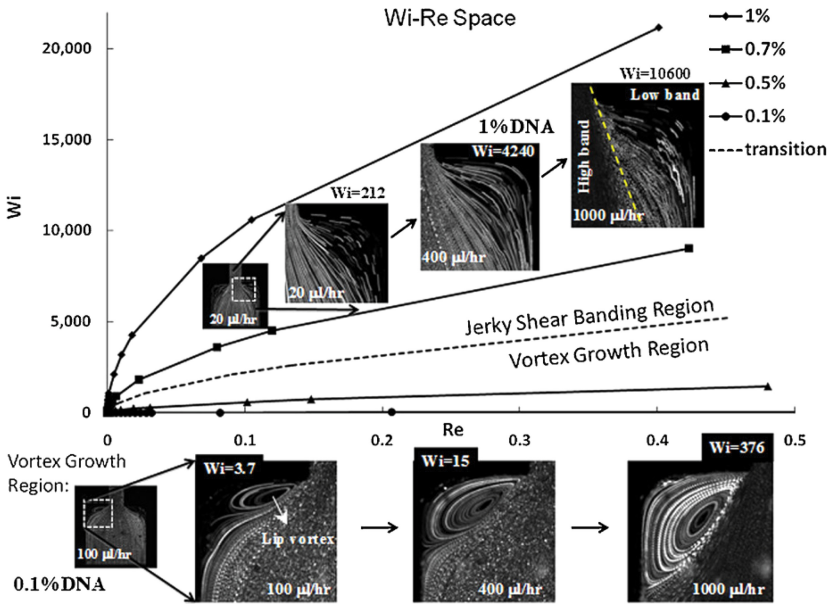


Figure 2.5: Summary of the flow behavior in *Wi*–*Re* space for four different solution concentrations of calf thymus DNA (75 kilobase pairs). Reproduced with permission from Hemminger et al., J. Non-Newton. Fluid Mech. 165, 1613 (2010). Copyright 2010 Elsevier.[34]

2.6.4. COIL-STRETCH TRANSITION AT HIGH *Wi* IN RANDOM FLOW AND FLOW AROUND OBSTACLES

Polymeric flows above Wi of $\mathcal{O}(1)$, typically exhibit a number of intriguing flow phenomena such as vortex formation and wobble, die swelling, and drag reduction in industrially relevant flows. Molecular visualization of polymer conformations in a random flow relevant to industrial applications will provide valuable information that can be used for optimization of polymer processing. The previous subsection considered flow instabilities in contraction geometries that occur at the critical Wi number of around 10. In this case, the perturbation of polymeric flow due to the contraction leads to the transition from a creeping-flow field to an unstable flow field consisting of vortices. Groisman and Steinberg [72] showed that strong instability could occur even in the case of homogenous flows of a dilute solution of high-molecular-weight polyacrylamide (PAA 18×10^6 mol, 80 ppm) between two parallel plates. This instability has all the features of developed classical turbulence, such as hysteresis, power-law scaling of the spectral density curves, albeit at low *Re*. Owing to this resemblance, this flow instability was termed as elastic turbulence. Following the seminal work of Groisman and Steinberg, elastic turbulence has been observed in polymeric flows for $Wi > 10$ in many other geometries.

Polymer stretching in elastic turbulent flows could be quantified and visualized by using DNA as a molecular probe. It was found that DNA molecules are stretched sharply in a 3D random flow at high *Wi*, via the coil-stretch transition.[73, 74] At high *Wi*, the probability distribution function of the normalized polymer length was reported to be highly skewed towards 1, that is, most of the polymer molecules were fully stretched, with the maximum probability occurring at a stretch length of 0.85.[73, 75] In contrast to this, in shear flow, the probability distribution function of the polymer length was found to be symmetric at similar value of *Wi*.[73]

Recent experiments on polymer flows through straight microfluidic channels also showed a transition to elastic turbulence,[76] provided that the flow field was initially perturbed.[77] These experimental observations on instabilities in flows without curvature are supported by nonlinear stability analysis.[78–80] By using DNA as probes, it was found that the polymer exhibits a variety of conformations during flow. In particular, stretching of up to 0.5 (normalized by contour length) length units in both parallel and perpendicular direction to the flow has been reported.[81] Since polymer conformation has been linked to elastic stresses in the fluid,[82, 83] which in turn provide the driving force for elastic turbulence,[72] the mechanism could be validated by visualizing polymer conformation in straight channels.

The significant reduction of drag by the addition of very small amounts of polymers in a turbulent fluid stimulated both engineers and rheologists, because it lies at the intersection of turbulence and rheology fields. This well-known phenomenon has found various applications in the reduction of energy loss in pipelines, ship-building industry, and oil-well fracturing.[84] Different mechanisms, such as the modification of boundary layer flow or the ability of polymers to stretch (in strong flow), have been proposed to explain this phenomenon.[85–87]

Curved boundaries can also affect the flow response of polymer solutions. For instance, it has been shown that drag on an obstacle (sphere or cylinder) can be significantly enhanced by addition of polymers. The key step to unravel the mechanism behind this phenomenon was to employ single-molecule experiments combined with microfluidic technology. François *et al.* [35] visualized DNA conformations in a microfluidic geometry with a cylindrical obstacle, which revealed strong polymer extensions near the cylinder surface (figure 2.6) coupled with velocity fluctuations indicating transition to an elastic instability.

Using similar microfluidic configuration, François *et al.* [88] subsequently studied polymer conformation and hysteresis in pressure-driven flow of polymer solutions. The motivation to use a cylinder was to study the effect of nonlinear drag forces. Combining

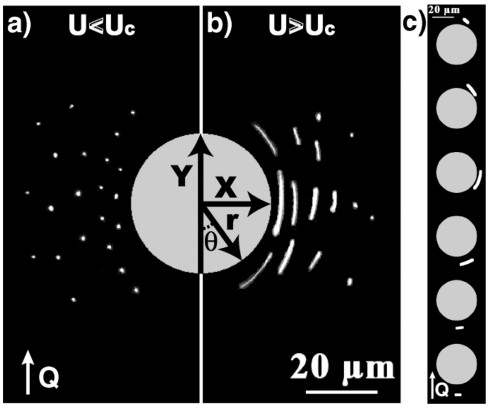


Figure 2.6: Polymer conformations near a cylinder (a) below and (b) above the critical $Wi \sim 0.3$ showing significant extensions and transition to coil-stretch. (c) DNA conformation at various locations around the cylinder. Reproduced with permission from François et al., Phys. Rev. Lett. 100, 18302 (2008). Copyright 2008 American Physical Society.[35]

an optical fiber sensor, which allowed measurements of the stresses on the cylinder due to polymer flow, together with fluorescence microscopy, they were able to link the molecular picture of polymers to the macroscopic effect of hysteresis upon stopping the flow. They reported that when the flow was stopped, the polymer molecules near the cylinder reversed their flow due to stored elastic stresses in the molecule. Several other studies on flow around obstacles and their arrays are reported for electrokinetic flows. These studies have been reviewed in detail elsewhere.[16]

2.7. STRETCHING OF DNA MOLECULES ON MICROPATTERNED SURFACES

Not only is stretching of DNA highly relevant for polymer rheology and genomic analysis, it can also be used to generate nanowire or nanotemplate arrays. DNA chains can be fully stretched across micropillars in de-wetting flow over micropatterned surfaces.[89] This is a simple and yet powerful technique (referred to as molecular combing) for stretching DNA molecules on solid substrates by forced de-wetting. This technique was originally used to visualize DNA in an elongated conformation after depositing DNA molecules on solid substrates.[90] In comparison to traditional combing techniques, long macromolecules in a solution can be immobilized into an ordered array of nanowires by de-wetting of micropatterned surfaces (figure 2.7).[91–94] Stretching of DNA is a prerequisite process to creating and depositing elongated DNA molecules on top of a micropatterned substrate. The formation of a droplet on the top of microstructured surfaces

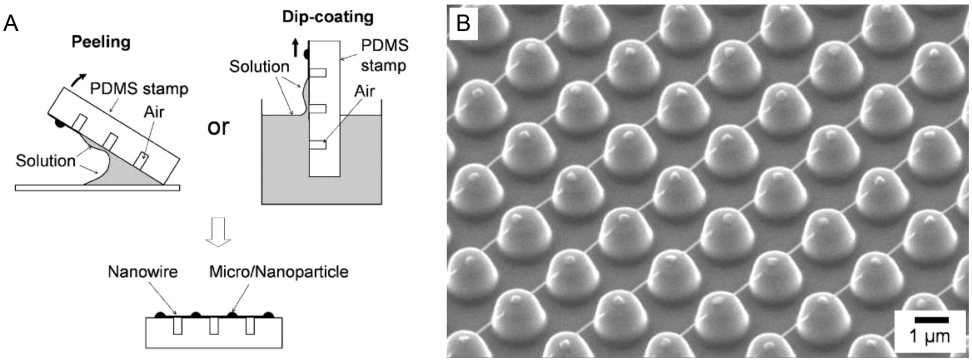


Figure 2.7: (a) Schematic illustration of DNA combing for generating a nanowire array. (b) Scanning electron microscope (SEM) images of an array of DNA nanowires. Reproduced with permission from Guan et al., Soft Matter 3, 1369 (2007). Copyright 2007 The Royal Society of Chemistry.[91]

such as micropillars during the de-wetting process produces a flow pattern allowing stretching DNA across the micropillars.[89] In addition, Guan *et al.* [95] demonstrated that DNA nanowires can be converted into nanochannels by the imprinting method. To summarize, this simple technique has a great potential for low-cost fabrication of nanofluidic systems without size limitations.

2.8. CONCLUSIONS

Microfluidic systems have been utilized to probe, manipulate and to visualize fluorescent DNA molecules for various fundamental studies concerning polymer rheology and physics. Recent progress and advances in fabrication of microfluidics have facilitated the study of polymer rheology at the single-molecule level. We have reviewed a selection of fundamental concepts in the flow of DNA inside microfluidics, which allows us to create a conceptual framework for nonlinear polymer rheology. This field is undergoing unprecedented changes, because DNA with different architecture and topology can be made and can serve as a new model for polymer scientists and engineers. We anticipate that future studies will focus on relating the polymer microstructure to bulk-flow properties in flow fields relevant to industry. In addition, new molecular-level experiments would be highly desirable in the study of the flow of well-entangled polymer solutions to improve our theoretical understanding in nonlinear flow regimes.[17] Still, nonlinear rheological responses of well-entangled polymers, such as shear banding and stress overshoot, are not understood and are under debate; therefore in-depth single-molecule studies of DNA are necessary to resolve the remaining issues in polymer rheology.[11] These examinations at the single-molecule level will allow us to create new models,

by unraveling the detailed molecular mechanisms behind various nonlinear rheology phenomena.

REFERENCES

[1] S. Dumitriu and V. I. Popa, eds., *Polymeric biomaterials* (CRC Press, Taylor & Francis Group, Boca Raton, 2013) p. 1.

[2] R. Pecora, *DNA: a model compound for solution studies of macromolecules,* Science **251**, 893 (1991).

[3] R. A. Hughes, A. E. Miklos, and A. D. Ellington, *Gene synthesis: Methods and applications,* in *Synthetic Biology, Part BComputer Aided Design and DNA Assembly*, Synthetic Biology, Part BComputer Aided Design and DNA Assembly, Vol. 498, edited by C. Voigt (Academic Press, 2011) pp. 277–309.

[4] P. J. Hagerman, *Flexibility of dna,* Annual Review of Biophysics and Biophysical Chemistry **17**, 265 (1988).

[5] G. M. Whitesides, *The origins and the future of microfluidics,* Nature **442**, 368 (2006).

[6] T. A. Waigh, *Advances in the microrheology of complex fluids,* Reports on Progress in Physics **79**, 074601 (2016).

[7] S. R. Quake, *From micro- to nanofabrication with soft materials,* Science **290**, 1536 (2000).

[8] D. Mijatovic, J. C. T. Eijkel, and A. v. d. Berg, *Technologies for nanofluidic systems: top-down vs. bottom-up–a review,* Lab on a Chip **5**, 492 (2005).

[9] D. Qin, Y. Xia, and G. M. Whitesides, *Soft lithography for micro- and nanoscale patterning,* Nature Protocols **5**, 491 (2010).

[10] Y. Lu, L. An, S.-Q. Wang, and Z.-G. Wang, *Origin of stress overshoot during startup shear of entangled polymer melts,* ACS Macro Letters **3**, 569 (2014).

[11] S.-Q. Wang, *Nonlinear rheology of entangled polymers at turning point,* Soft Matter **11**, 1454 (2015).

[12] S. G. Hatzikiriakos and K. B. Migler, *Polymer Processing Instabilities: Control and Understanding* (CRC Press, 2004) p. 484.

[13] G. G. Fuller, *Optical rheometry of complex fluids* (Oxford University Press, New York, 1995) p. 268.

[14] R. G. Larson, *The structure and rheology of complex fluids* (Oxford University Press, New York, 1999) p. 663.

[15] T. J. Ober, S. J. Haward, C. J. Pipe, J. Soulages, and G. H. McKinley, *Microfluidic extensional rheometry using a hyperbolic contraction geometry,* Rheologica Acta **52**, 529 (2013).

[16] D. J. Mai, C. Brockman, and C. M. Schroeder, *Microfluidic systems for single dna dynamics,* Soft Matter **8**, 10560 (2012).

[17] P. E. Boukany, S.-Q. Wang, S. Ravindranath, and L. J. Lee, *Shear banding in entangled polymers in the micron scale gap: a confocal-rheoscopic study,* Soft Matter **11**, 8058 (2015).

[18] de Gennes and P. G., *Reptation of a polymer chain in the presence of fixed obstacles,* The Journal of Chemical Physics **55**, 572 (1971).

[19] R. G. Larson, *Going with the flow,* Science **318**, 57 (2007).

[20] T. T. Perkins, D. E. Smith, and S. Chu, *Single polymer dynamics in an elongational flow,* Science **276**, 2016 (1997).

[21] C. M. Schroeder, E. S. G. Shaqfeh, and S. Chu, *Effect of hydrodynamic interactions on dna dynamics in extensional flow:: Simulation and single molecule experiment,* Macromolecules **37**, 9242 (2004).

[22] P. W. Bridgman, *Dimensional analysis* (Yale university press, New Haven, 1963).

[23] R. B. Bird, ed., *Dynamics of polymeric liquids*, 2nd ed. (Wiley, New York, 1987) p. 2.

[24] M. Reiner, *The deborah number,* Physics Today **17**, 62 (1964).

[25] J. M. Dealy, *Weissenberg and deborah numbers - their definition and use,* Rheol. Bull. **79**, 14 (2010).

[26] L. Rodd, J. Cooper-White, D. Boger, and G. McKinley, *Role of the elasticity number in the entry flow of dilute polymer solutions in micro-fabricated contraction geometries,* Journal of Non-Newtonian Fluid Mechanics **143**, 170 (2007).

[27] L. E. Rodd, T. P. Scott, D. V. Boger, J. J. Cooper-White, and G. H. McKinley, *The inertio-elastic planar entry flow of low-viscosity elastic fluids in micro-fabricated geometries,* Journal of Non-Newtonian Fluid Mechanics **129**, 1 (2005).

[28] P. E. Arratia, C. C. Thomas, J. Diorio, and J. P. Gollub, *Elastic instabilities of polymer solutions in cross-channel flow,* Physical Review Letters **96**, 144502 (2006).

[29] Y. T. Hu, *Steady-state shear banding in entangled polymers?* Journal of Rheology **54**, 1307 (2010).

[30] Y. Wang, D. R. Tree, and K. D. Dorfman, *Simulation of dna extension in nanochannels,* Macromolecules **44**, 6594 (2011).

[31] H. S. Rye, J. M. Dabora, M. A. Quesada, R. A. Mathies, and A. N. Glazer, *Fluorometric assay using dimeric dyes for double- and single-stranded dna and rna with picogram sensitivity,* Analytical Biochemistry **208**, 144 (1993).

[32] W. D. Volkmuth and R. H. Austin, *Dna electrophoresis in microlithographic arrays,* Nature **358**, 600 (1992).

[33] W. D. Volkmuth, T. Duke, M. C. Wu, R. H. Austin, and A. Szabo, *Dna electrodiffusion in a 2d array of posts,* Physical Review Letters **72**, 2117 (1994).

[34] O. L. Hemminger, P. E. Boukany, S.-Q. Wang, and L. J. Lee, *Flow pattern and molecular visualization of dna solutions through a 4: 1 planar micro-contraction,* Journal of Non-Newtonian Fluid Mechanics **165**, 1613 (2010).

[35] N. François, D. Lasne, Y. Amarouchene, B. Lounis, and H. Kellay, *Drag enhancement with polymers,* Physical review letters **100**, 018302 (2008).

[36] H. Aoki, K. Mori, and S. Ito, *Conformational analysis of single polymer chains in three dimensions by super-resolution fluorescence microscopy,* Soft Matter **8**, 4390 (2012).

[37] J. Tai, C. P. Lim, and Y. C. Lam, *Visualization of polymer relaxation in viscoelastic turbulent micro-channel flow,* Scientific Reports **5**, 16633 (2015).

[38] M. Keshavarz, H. Engelkamp, J. Xu, E. Braeken, M. B. J. Otten, H. Uji-i, E. Schwartz, M. Koepf, A. Vananroye, J. Vermant, R. J. M. Nolte, F. De Schryver, J. C. Maan, J. Hofkens, P. C. M. Christianen, and A. E. Rowan, *Nanoscale study of polymer dynamics,* ACS Nano **10**, 1434 (2016).

[39] K. Gunther, M. Mertig, and R. Seidel, *Mechanical and structural properties of yoyo-1 complexed dna,* Nucleic Acids Research **38**, 6526 (2010).

[40] B. Kundukad, J. Yan, and P. S. Doyle, *Effect of yoyo-1 on the mechanical properties of dna,* Soft Matter **10**, 9721 (2014).

[41] E. S. G. Shaqfeh, *The dynamics of single-molecule dna in flow,* Journal of Non-Newtonian Fluid Mechanics **130**, 1 (2005).

[42] C. W. Macosko, ed., *Rheology: principles, measurements, and applications* (VCH, New York, 1994) p. 550.

[43] T. T. Perkins, Quake, D. E. Smith, and S. Chu, *Relaxation of a single dna molecule observed by optical microscopy,* Science **264**, 822 (1994).

[44] T. T. Perkins, D. E. Smith, and S. Chu, *Direct observation of tube-like motion of a single polymer chain,* Science **264**, 819 (1994).

[45] B. H. Zimm, *Dynamics of polymer molecules in dilute solution: viscoelasticity, flow birefringence and dielectric loss,* The Journal of Chemical Physics **24**, 269 (1956).

[46] P. Debye and A. M. Bueche, *Intrinsic viscosity, diffusion, and sedimentation rate of polymers in solution,* The Journal of Chemical Physics **16**, 573 (1948).

[47] M. Adam and M. Delsanti, *Dynamical properties of polymer solutions in good solvent by rayleigh scattering experiments,* Macromolecules **10**, 1229 (1977).

[48] A. Keller and J. A. Odell, *The extensibility of macromolecules in solution; a new focus for macromolecular science,* Colloid and Polymer Science **263**, 181 (1985).

[49] de Gennes and G. P., *Scaling concepts in polymer physics* (Cornell University Press, Ithaca, N.Y, 1979) p. 324.

[50] D. R. Tree, A. Muralidhar, P. S. Doyle, and K. D. Dorfman, *Is dna a good model polymer?* Macromolecules **46**, 8369 (2013).

[51] M. Doi and S. F. Edwards, *The theory of polymer dynamics*, Vol. 73 (Oxford University Press, 1988).

[52] D. E. Smith, T. T. Perkins, and S. Chu, *Self-diffusion of an entangled dna molecule by reptation,* Physical Review Letters **75**, 4146 (1995).

[53] R. E. Teixeira, A. K. Dambal, D. H. Richter, E. S. G. Shaqfeh, and S. Chu, *The individualistic dynamics of entangled dna in solution,* Macromolecules **40**, 2461 (2007).

[54] K.-W. Hsiao, C. Sasmal, J. R. Prakash, and C. M. Schroeder, *Direct observation of dna dynamics in semidilute solutions in extensional flow,* Journal of Rheology **61**, 151 (2017), http://dx.doi.org/10.1122/1.4972236 .

[55] Y. Li, K.-W. Hsiao, C. A. Brockman, D. Y. Yates, R. M. Robertson-Anderson, J. A. Kornfield, M. J. San Francisco, C. M. Schroeder, and G. B. McKenna, *When ends meet: Circular dna stretches differently in elongational flows,* Macromolecules **48**, 5997 (2015).

[56] D. J. Mai, A. B. Marciel, C. E. Sing, and C. M. Schroeder, *Topology-controlled relaxation dynamics of single branched polymers,* ACS Macro Letters **4**, 446 (2015).

[57] A. B. Marciel, D. J. Mai, and C. M. Schroeder, *Template-directed synthesis of structurally defined branched polymers,* Macromolecules **48**, 1296 (2015).

[58] G. P. de Gennes, *Coil-stretch transition of dilute flexible polymers under ultrahigh velocity gradients,* The Journal of Chemical Physics **60**, 5030 (1974).

[59] R. G. Larson and J. J. Magda, *Coil-stretch transitions in mixed shear and extensional flows of dilute polymer solutions,* Macromolecules **22**, 3004 (1989).

[60] D. E. Smith and S. Chu, *Response of flexible polymers to a sudden elongational flow,* Science **281**, 1335 (1998).

[61] C. M. Schroeder, H. P. Babcock, E. S. G. Shaqfeh, and S. Chu, *Observation of polymer conformation hysteresis in extensional flow,* Science **301**, 1515 (2003).

[62] R. G. Larson, H. Hu, D. E. Smith, and S. Chu, *Brownian dynamics simulations of a dna molecule in an extensional flow field,* Journal of Rheology (1978-present) **43**, 267 (1999).

[63] P. G. de Gennes, *Molecular individualism,* Science **276**, 1999 (1997).

[64] D. E. Smith, H. P. Babcock, and S. Chu, *Single-polymer dynamics in steady shear flow,* Science **283**, 1724 (1999).

[65] C. M. Schroeder, R. E. Teixeira, E. S. G. Shaqfeh, and S. Chu, *Characteristic periodic motion of polymers in shear flow,* Physical Review Letters **95**, 018301 (2005).

[66] J. S. Hur, E. S. G. Shaqfeh, H. P. Babcock, D. E. Smith, and S. Chu, *Dynamics of dilute and semidilute dna solutions in the start-up of shear flow,* Journal of Rheology (1978-present) **45**, 421 (2001).

[67] P. E. Boukany, O. Hemminger, S.-Q. Wang, and L. J. Lee, *Molecular imaging of slip in entangled dna solution,* Physical review letters **105**, 027802 (2010).

[68] S. Gulati, S. J. Muller, and D. Liepmann, *Flow of dna solutions in a microfluidic gradual contraction,* Biomicrofluidics **9**, 054102 (2015).

[69] D. V. Boger, *Viscoelastic flows through contractions,* Annual Review of Fluid Mechanics **19**, 157 (1987).

[70] F. P. T. Baaijens, *Mixed finite element methods for viscoelastic flow analysis: a review,* Journal of Non-Newtonian Fluid Mechanics **79**, 361 (1998).

[71] S. A. White, A. D. Gotsis, and D. G. Baird, *Review of the entry flow problem: Experimental and numerical,* Journal of Non-Newtonian Fluid Mechanics **24**, 121 (1987).

[72] A. Groisman and V. Steinberg, *Elastic turbulence in a polymer solution flow,* Nature **405**, 53 (2000).

[73] S. Gerashchenko, C. Chevallard, and V. Steinberg, *Single-polymer dynamics: Coil-stretch transition in a random flow,* EPL (Europhysics Letters) **71**, 221 (2005).

[74] G. Boffetta, A. Celani, and S. Musacchio, *Two-dimensional turbulence of dilute polymer solutions,* Physical review letters **91**, 034501 (2003).

[75] Y. Liu and V. Steinberg, *Single polymer dynamics in a random flow,* in *Macromolecular Symposia*, Vol. 337, Wiley Online Library (Wiley Online Library, 2014) pp. 34–43.

[76] H. Bodiguel, J. Beaumont, A. Machado, L. Martinie, H. Kellay, and A. Colin, *Flow enhancement due to elastic turbulence in channel flows of shear thinning fluids,* Physical review letters **114**, 028302 (2015).

[77] L. Pan, A. Morozov, C. Wagner, and P. E. Arratia, *Nonlinear elastic instability in channel flows at low reynolds numbers,* Physical review letters **110**, 174502 (2013).

[78] B. Meulenbroek, C. Storm, V. Bertola, C. Wagner, D. Bonn, and W. van Saarloos, *Intrinsic route to melt fracture in polymer extrusion: a weakly nonlinear subcritical instability of viscoelastic poiseuille flow,* Physical review letters **90**, 024502 (2003).

[79] V. Bertola, B. Meulenbroek, C. Wagner, C. Storm, A. Morozov, W. van Saarloos, and D. Bonn, *Experimental evidence for an intrinsic route to polymer melt fracture phenomena: A nonlinear instability of viscoelastic poiseuille flow,* Physical review letters **90**, 114502 (2003).

[80] A. N. Morozov and W. van Saarloos, *Subcritical finite-amplitude solutions for plane couette flow of viscoelastic fluids,* Physical review letters **95**, 024501 (2005).

[81] D. Bonn, F. Ingremeau, Y. Amarouchene, and H. Kellay, *Large velocity fluctuations in small-reynolds-number pipe flow of polymer solutions,* Physical Review E **84**, 045301 (2011).

[82] F. Latinwo and C. M. Schroeder, *Determining elasticity from single polymer dynamics,* Soft matter **10**, 2178 (2014).

[83] C. Bustamante, Z. Bryant, and S. B. Smith, *Ten years of tension: single-molecule dna mechanics,* Nature **421**, 423 (2003).

[84] D. Bonn, Y. Amarouchène, C. Wagner, S. Douady, and O. Cadot, *Turbulent drag reduction by polymers,* Journal of Physics: Condensed Matter **17**, S1195 (2005).

[85] M. Tabor and P. G. d. Gennes, *A cascade theory of drag reduction,* EPL (Europhysics Letters) **2**, 519 (1986).

[86] K. R. Sreenivasan and C. M. White, *The onset of drag reduction by dilute polymer additives, and the maximum drag reduction asymptote,* Journal of Fluid Mechanics **409**, 149 (2000).

[87] Y. Amarouchene, D. Bonn, H. Kellay, T.-S. Lo, V. S. L'vov, and I. Procaccia, *Reynolds number dependence of drag reduction by rodlike polymers,* Physics of Fluids **20**, 065108 (2008).

[88] N. François, Y. Amarouchene, B. Lounis, and H. Kellay, *Polymer conformations and hysteretic stresses in nonstationary flows of polymer solutions,* EPL (Europhysics Letters) **86**, 34002 (2009).

[89] W.-C. Liao, X. Hu, W. Wang, and L. J. Lee, *Simulation of single dna molecule stretching and immobilization in a de-wetting two-phase flow over micropillar-patterned surface,* Biomicrofluidics **7**, 034103 (2013).

[90] X. Michalet, R. Ekong, F. Fougerousse, S. Rousseaux, C. Schurra, N. Hornigold, M. van Slegtenhorst, J. Wolfe, S. Povey, J. S. Beckmann, and A. Bensimon, *Dynamic molecular combing: stretching the whole human genome for high-resolution studies,* Science (New York, N.Y.) **277**, 1518 (1997).

[91] J. Guan, N. Ferrell, B. Yu, D. J. Hansford, and L. J. Lee, *Simultaneous fabrication of hybrid arrays of nanowires and micro/nanoparticles by dewetting on micropillars,* Soft Matter **3**, 1369 (2007).

[92] J. Guan, B. Yu, and L. J. Lee, *Forming highly ordered arrays of functionalized polymer nanowires by dewetting on micropillars,* Advanced Materials **19**, 1212 (2007).

[93] J. Guan and L. J. Lee, *Generating highly ordered dna nanostrand arrays,* Proceedings of the National Academy of Sciences of the United States of America **102**, 18321 (2005).

[94] P. J. Glazer, L. Bergen, L. Jennings, A. J. Houtepen, E. Mendes, and P. E. Boukany, *Generating aligned micellar nanowire arrays by dewetting of micropatterned surfaces,* Small **10**, 1729 (2014).

[95] J. Guan, P. E. Boukany, O. Hemminger, N.-R. Chiou, W. Zha, M. Cavanaugh, and L. J. Lee, *Large laterally ordered nanochannel arrays from dna combing and imprinting,* Advanced Materials **22**, 3997 (2010).

3

ELASTIC INSTABILITIES IN DIFFERENT PORE SHAPES

We experimentally investigate the flow of hydrolyzed polyacrylamide (HPAM) solution without salt in model porous media at high Weissenberg numbers ($Wi > 1.0$). The effect of pore shapes on flow pattern and pressure drop is explored by using periodic arrays of circular and square pillars in aligned and staggered layout. In the apparent shear-thinning regime, we observe stationary dead zones upstream of the pillars. At higher shear rates (Wi), these dead zones are periodically washed away. We present the mechanism of this elastic instability and characterize it based on the pressure-drop-fluctuation spectral density.

3.1. INTRODUCTION

The flow of complex fluids in porous media is of great importance for a diverse range of industrial applications, including filtration, chromatography, textile coating, flow in soils, and oil recovery.[1, 2] For instance, polymer solution injection increases the effectiveness of water floods.[3, 4] Natural porous media are made up of mineral grains, salts, clays, and organic matter that get consolidated over geological time scales into rocks (such as sandstone).

Parts of this chapter have been published in **D. Kawale**, E. Marques, P. L. J. Zitha, M. T. Kreutzer, W. R. Rossen, P. E. Boukany, *Elastic instabilities during the flow of hydrolyzed polyacrylamide solution in porous media: effect of pore-shape and salt*, Soft Matter, **13**, 765 (2017).

The pore space of sedimentary rock consists of randomly connected pore bodies and pore throats, which leads to complex flow patterns.[5] Converging-diverging geometries are often used to represent porous-media geometries.[6–8] However, bridging the gap between single-channel converging-diverging geometries to the topology of a realistic porous media has been challenging, because the details of the pore-scale flow pattern in the porous media are difficult to capture.

Polymer solutions exhibit both viscous and elastic response under deformation. They also display shear-thinning and elastic response at a high Weissenberg number, $Wi > 1$ ($Wi = \dot{\gamma}\tau$, where $\dot{\gamma}$ is the shear rate; τ is the relaxation time),[9] and exhibit a peculiar strain-hardening response in elongational flow.[10] During flow through porous media, polymer solutions experience shear flow near the solid walls and extensional flow away from the walls in converging-diverging flows.[7, 11–13] The flow of polymer solutions through porous media can display dramatic increase in pressure gradient (or apparent viscosity) above a critical *Wi*.[4, 6, 12, 14] The elastic nature of the polymeric fluid becomes more pronounced when it is coupled with the extensional nature of the flow field. Therefore, the increase in the slope of the pressure-drop curve is commonly referred as the dominance of elongational flow over shear[12, 15] at high *Wi*. Elongational flows were typically characterized via the extensional stresses of the polymeric fluid.[16] However, James [17] recently suggested that the shear-generated first-normal-stress difference, N_1, play a larger role in elongational flows of dilute polymer solutions.

The increase in flow resistance of polymer solutions in porous media is now attributed to elastic flow instabilities at negligible inertial effects. [8, 18–21] Elastic flow instabilities are essentially a state of non-homogeneous flow field and these inhomogeneous flow patterns depend on the geometry and polymer solution rheology.[22, 23] For instance, at $Re \ll 1$ and $Wi \sim 1$, or $Wi \gg 1$, flows of polymer solution exhibits (1) the well-known toroidal-cell instability in a Couette cell (analogous to the Newtonian-fluid flow in same geometry at $Re \gg 1$), [24] (2) a corner-vortex in entry-channel flows,[24, 25] (3) shear banding/wall slip in shear flow[26] or (4) asymmetricity or temporally fluctuating instability in stagnation-point flows.[27, 28] In highly elastic solutions, the elastic instability in a Couette cell above $Wi \sim 20$ transitions into a state of chaotically oscillating vortices known as *Disordered Oscillations*.[29] Another type of elastic instability, *elastic turbulence*, which closely resembles disordered oscillations, appeared to be occurring for highly elastic solutions in parallel-plate geometry[30], serpentine geometry[31] and many more geometries/non-Newtonian systems.[32, 33] To this date, the type of elastic instability in porous media remains to be elucidated.

Macroscopic non-Newtonian response such as elastic instabilities results from mi-

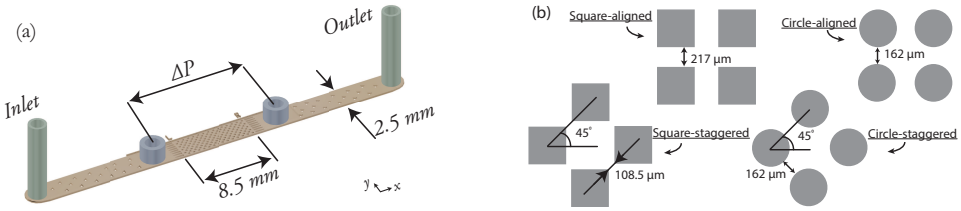


Figure 3.1: (a) Schematic showing one of our microfluidic devices. The periodic array containing cylinders and rectangular pillars (details in (b)) is located over a length of 8.5 mm in the center of the geometry.

croscopic stresses due to flow-induced changes in conformation of polymer. Thus, manipulating the length-scales at which polymer molecules are stretched is important for studying elastic instabilities. One of the key advantages of exploiting fluid flow at the micrometer length-scale (also referred as *microfluidics*) is that we can achieve high Wi at negligible Re.[34] Hu *et al.* [35] presents a detailed review on the use of the microfluidic technology to study polymer rheology. Furthermore, microfluidic devices can be fabricated using optically transparent materials, allowing for direct flow field visualization.[36] In the past decade, several researchers have exploited microfluidic technologies to investigate polymer flows in single contraction microfluidic geometry (*cf* refs.37–41) over $Wi = \mathcal{O}(0.1 - 100)$ and $Re \ll 10$.[42] Many of these studies have focussed on understanding the effect of polymer viscoelasticity on the resulting flow instabilities. Owing to the complexity of the pore space in granular porous media, fundamental studies have approached the problem by considering a single planar contraction. However, single-planar-contraction geometries were unable to account for the effect of the history of polymer deformation, inspiring microfluidic geometries that had successive contractions and expansions,[19, 43, 44] representing the 1-D analogue of a porous medium. These studies were in turn lacking inter-pore connectivity, prompting investigations into periodic arrays of cylinders, representing an idealized 2-D porous media.[18, 20, 45] Elastic instabilities have been observed in periodic arrays of cylinders via a direct flow-field visualization technique.[45, 46] These instabilities were also suggested to be a cause of the build-up of pressure drop above a certain Wi in core-floods.[19, 20, 44] In addition, the transition to instability was reported to occur at a characteristic time, which is independent of polymer concentration.[20]

A realistic porous-medium topology contains sharp edges, and a thorough understanding of how pore shape affects the nature of these flow instabilities is lacking. Our aim is to bridge this gap and present an understanding of how pore shape affects the nature of instabilities (see figure 3.1). Using microfluidic devices to fabricate our porous media allows us to measure pressure-drop and visualize the flow field simultaneously.

Table 3.1: Specifications of the microfluidic geometries used in current work. The size of pillars, that is, diameter for circle and length of square side, is (262 ± 5) µm. Channel depth in all microfluidic devices is (120 ± 2) µm.

Obstacle shape[a], Layout	Pore throat (µm)	*Nx* & *Ny*[b]	Porosity	Permeability[c] (D)
Circle, Staggered	162.0	14 & 9	0.71 ± 0.01	179.2
Circle, Aligned	162.0	20 & 6	0.71 ± 0.01	214.1
Square, Staggered	108.5	17 & 10	0.71 ± 0.01	180.0
Square, Aligned	217.0	18 & 6	0.69 ± 0.01	203.8

[a] As seen from the top of the microfluidic device.
[b] *Nx* = Number of obstacles in the *x*-direction; *Ny* = Number of obstacles in the *y*-direction.
[c] Measured based on Darcy's law using a Newtonian liquid (either DI water, ethanol or glycerol).

Thus we can directly validate the onset of elastic instability with respect to the pressure build-up. We characterize the elastic instability using spectral-density curves and explain the flow features that characterize and sustain the instability.

3.2. EXPERIMENTAL DETAILS

3.2.1. POLYMER SOLUTION

0.1 % Aqueous hydrolyzed polyacrylamide, HPAM (MW = 15×10^6 g mol^{-1}, 30% hydrolysis; Flopam 3530s, SNF Floerger, France) was used to study the effect of pore-shape by using different geometries as shown in figure 3.1b. The Mark-Houwink equation[47] for HPAM with 30 % hydrolysis is $[\eta] = 2.2 \times 10^{-2} {M_w}^{0.742}$, which gives the critical overlap concentration, $C^* \sim 0.02$ %. We expect our polymer solutions to be in the semi-dilute regime.[48]

The aqueous polymer solutions are prepared using de-ionized (DI) water. To avoid agglomeration, the granular polymer particles are slowly added in the vortex of solvent created by using a magnetic stirrer. The solvent was DI water to prepare salt-free polymer solution. After all the polymer particles are added, the air in the bottle is purged with nitrogen and the container is sealed to minimize oxidation of the polymer backbone. Once all the polymer granules are dispersed into the solution, the stirring speed is reduced to prevent shear-degradation. The polymer granules needed around 4 to 7 days to dissolve completely. The rheological properties of 0.1 % HPAM solution was characterized by using a 1°, 50 mm cone plate geometry in a commercial rheometer (MCR-302, Anton Paar GmbH). All experiments were performed at the room temperature, $T = (22 \pm 2)$ °C as shown in figure 3.2.

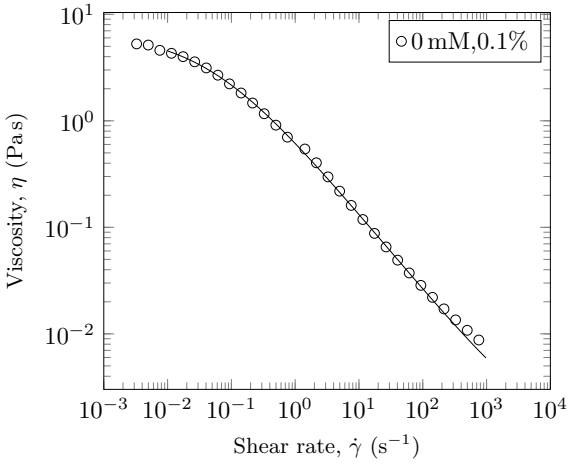


Figure 3.2: Steady-state shear viscosity of 0.1 % HPAM solutions in DI water without salt at 22 °C. The solid line is obtained by fitting the Carreau-Yasuda model shown in Eq. 5.1, and its fitting parameters are tabulated in table A.1.

Our working polymer solutions are shear-thinning, as shown in the figure 3.2. The Carreau-Yasuda model[49] shown below (eq. 3.1) is used to fit the steady-shear flow curve. We could not observe a plateau at high shear rate; therefore we set the $\eta_\infty = 10^{-3}$ Pa s, the viscosity of our solvent (DI Water) for fitting the shear rheology data. Figure 3.2 shows the measured rheology fitted to the Carreau-Yasuda model.

$$\eta - \eta_\infty = (\eta_0 - \eta_\infty)\left[1 + (\tau_{CY}\dot{\gamma})^a\right]^{\frac{n-1}{a}} \tag{3.1}$$

Here, the parameter a allows control over the width of the transition region from the zero-shear-viscosity plateau to the shear-thinning part; n is the power-law slope; and the relaxation time, $\tau_{CY} = 21.55$ s for 0.1 % HPAM in DI water. The results of CY-model fit are summarized in Appendix A.

Partially hydrolyzed polyacrylamide is a polyelectrolye because the hydrolysis process replaces the amide group ($-NH_2$) with the carboxyl group (COO−). In aqueous solutions, the charges along the polymer chain result in a repulsive polymer intra-molecular interaction. In presence of salt, the polyelectrolye charges are screened, reducing the repulsive intra-molecular interactions and the equilibrium coil size. The effect of polymer-coil-size reduction due to presence of counterions can be noticed by measuring bulk rheology of polymer solutions. Thorough analysis of HPAM in various solvents has been carried out to list the Mark-Houwink coefficients[14, 47, 50]. Ait-Kadi *et al.* [51], in particular showed that the Carreau model can be still used to obtain accurate estimates of the

relaxation time. From the Carreau-Yasuda model, we calculate the $\tau_{CY} = 21.55\,s$, whereas from SAOS measurements the relaxation time is found to be almost one order of magnitude higher, $\tau_{SAOS} = \sim 200\,s$ (See figure A.1). The order of magnitude difference between τ_{CY} and τ_{SAOS} is likely due to the high polydispersity of HPAM. The value of τ_{SAOS} that SAOS probes relates to the longest relaxation time of the longest polymer chains in our solutions. We maintained low stirring rates ($\sim 250 - 300$ rpm) as the polymer granules dissolved in solvent to prevent any shear degradation, so we expect long-chain polymer chains to remain intact before the start of every experiment. We also performed shear degradation test for 0.2 %, 17 mM NaCl solution by pre-shearing at $500\,s^{-1}$ for 120 s, and no shear degradation was observed (See figure A.3).

In a previous study on effect of the polystyrene polydispersity in various solutions, Yasuda *et al.* [52] reported that τ_{SAOS} consistently differs from τ_{CY} by factor of 1.3 to 2. From shear rheology, the relaxation time is estimated as the inverse of a certain 'critical shear rate' that marks the transition from zero-shear viscosity to shear-thinning. In figure 3.2, we can see that this transition occurs at roughly $1/\tau_{SAOS} \sim 0.005\,s^{-1}$ ($\tau_{SAOS} \sim 200\,s$, figure A.1) for the salt-free polymer solution. However, a polydisperse polymer solution will have a broad spectrum of relaxation times and the transition from zero-shear viscosity to shear-thinning will also occur over a broad range of shear rates. The Carreau-Yasuda model accounts for a broad transition from zero-shear viscosity to shear-thinning via the fitting parameter a. In the presence of a, the 'critical shear rate', $1/\tau_{CY}$ exists in between these broad transitional shear rates.

3.2.2. MICROFLUIDIC DEVICES

Standard soft lithography techniques[53, 54] are used to fabricate microfluidic devices using PDMS (Polydimethylsiloxane; Sylgard® 184, Dow Corning Corporation). The mask resolution is 20000 DPI (CAD/Art Services, Inc.); a single dot printed has a diameter of 1.27 µm. However, the smallest feature size is limited to 8 dots or ~10 µm according to CAD/Art Services. The schematic of the microfluidic geometry is shown in figure 3.1a. The center of the geometry consists of periodic array of cylinders and rectangular pillars in two layouts: aligned and staggered (see figure 3.1b). Table 3.1 summarizes the dimensions of the four microfluidic geometries used in the current research. The periodic array represents a porous medium, whereas the open channel between the periodic array and the inlet/outlet contains a few support pillars to prevent buckling of the channel.[55]

The pressure drop across the periodic array is measured by two pressure taps across the array as shown in figure 3.1a. This allowed us to isolate the contribution of the pressure drop due to the periodic array from that of the support pillars. Pressure drop was

measured by using two piezoresistive silicon pressure sensors (HSCMRNT005PGAA5, Honeywell Sensing and Control); the data was logged by an in-house-developed Labview program at 100 Hz. These pressure sensors measure gauge pressure with each having a pressure range of 0 psi–5 psi, with an accuracy of 0.25% of the full scale span. We used a pressure pump (MFCS^{TM}, Fluigent GmbH) to calibrate our sensors. The accuracy of the pressure sensors was 1 mbar for the average of a recorded time series of a static pressure difference, where the instantaneous signal fluctuated with a standard deviation of 0.1 mbar around the mean.

In order to measure the permeability, three different Newtonian liquids are employed for experiments reported in the current chapter: (1) deionized and degassed water, (2) ≥99 % absolute ethanol (Sigma Aldrich) and (3) ≥99 % Glycerol (Sigma Aldrich). The liquids are chosen such that the measured pressure drop is more than 5 % of the operating range of the pressure sensor. Flow rates in the laminar regime are chosen, as confirmed by observing streamlines. A syringe pump (PHD2000, Harvard Instruments) is used with 5 mL Hamilton Gastight Syringes to inject liquid via a PTFE tubing (ID = 0.5 mm, OD = 1.6 mm) during the experiments. For streamline visualization, the polymer solution is seeded with 1 µm dyed red aqueous fluorescent particles (542/612 nm, Catalog # R0100, Thermo Scientific^{TM}). A small concentration of ~0.1 % was sufficient to obtain discrete, but sufficiently detailed spatial density of the streamlines. The microfluidic geometry is placed on an inverted microscope (Axiovert 100M, Carl Zeiss AG). A mercury vapour short-arc lamp source in combination with optical filters was used to excite the fluorescent particles. The motion of the particles was recorded using a Phantom v9.1 high-speed camera (Vision Research Inc.).

The permeability, k, (m^2, $1\,D = 10^{-12}\,m^2$) was calculated based on Darcy's law:

$$k = \frac{\eta Q L_{pm}}{A \Delta P} \tag{3.2}$$

where, η (Pa s) is the viscosity of the Newtonian fluid, Q ($m^3\,s^{-1}$) is the flow rate, L_{pm} (m) is the length of the periodic array within the microfluidic geometry, A (m^2) is the cross-sectional area available for flow (that is, product of cross-sectional area of microfluidic device in the direction of flow multiplied by the porosity[1]), ΔP (Pa) is the pressure drop across the periodic array. The same equation is used to calculate the apparent viscosity, η_{app}. Then, η_{app} is compared with an apparent shear rate, $\dot{\gamma}_{app} = v/(L/2)$. This apparent shear rate is based on the average velocity, $v = Q/A$, across the entire microfluidic

[1] Here, we have altered the formal definition of A according to the Darcy's law. Since the Darcy's law considers porous media as a continuum, A is defined as the cross-sectional area of the porous media, without multiplying A with the porosity.

porous medium having cross-sectional area, A; Q is the volumetric flow rate and L is the length scale. In the case of circles, the L is chosen as the diameter; whereas in the case of squares, it is chosen as the length of a side. In addition, this apparent shear rate is confirmed by particle image velocimetry as shown in figure A.2. Finally the Wi is calculated as $Wi = \tau_{CY}\dot{\gamma}_{app}$.

We took particular care to ensure that no air bubbles were trapped in the microfluidic device or the pressure-tap tubing. In microfluidic chips, the channel dimension is of the order of µm. Therefore, surface forces play an important role in displacing air using polymer solution directly. We first flush the microfluidic chip with absolute ethanol until all air bubbles are removed. Gentle tapping on the chip helps to remove any persistent air bubbles. Once air is displaced from the microfluidic chip and the tubing, the pressure sensors are connected and the flow is switched to the polymer solutions via a switching valve. After switching the flow, at least 20 pore volumes of polymer solution are injected through the microfluidic device to ensure that all the ethanol is flushed. The measurement depth is $\delta z = \pm 7.4\,\mu m$ for the combination of optics in the setup.[56] The focal plane was adjusted to the middle of the channel using a 10X (N.A. = 0.5) magnification objective lens. Therefore, the streamlines visualized represent the flow dynamics in a $\pm 7.4\,\mu m$-thick region at the center of the microfluidic geometry. As our geometry has a depth of $\sim 100\,\mu m$, the streamlines do not capture the flow field near the top or bottom walls.

3.3. RESULTS AND DISCUSSION

To obtain insights into the nature of HPAM solution flow through porous media, we measured the ΔP and simultaneously visualized the flow field. At very low shear rates ($\dot{\gamma}_{app} = 7 \times 10^{-3}\,s^{-1}$, $Wi = 0.1$), streamlines show creeping flow through the porous media as shown in the figure A.4. The flow field around the stagnation point upstream of a pillar is purely extensional. As the shear rate is increased, we observe a large apparent stagnation zone upstream of the pillars. We call these apparent stagnation zones *dead zones* (DZ), and they were observed at all the probed apparent shear rates, $\dot{\gamma}_{app} = 3.63\,s^{-1}$ to $\sim 200\,s^{-1}$. The local shear rate in DZs is almost zero, and therefore we can visualize the bright spots of the fluorescent particles even when the exposure time on the imaging camera is set to as high as a few hundred milliseconds. The shape and size of DZ varies with geometry, the presence of salt and also with $\dot{\gamma}_{app}$. In the following sections, we first study the effect of pore-shape using salt-free HPAM solution. We then study the effect of salt addition to the HPAM solution using the square, staggered geometry.

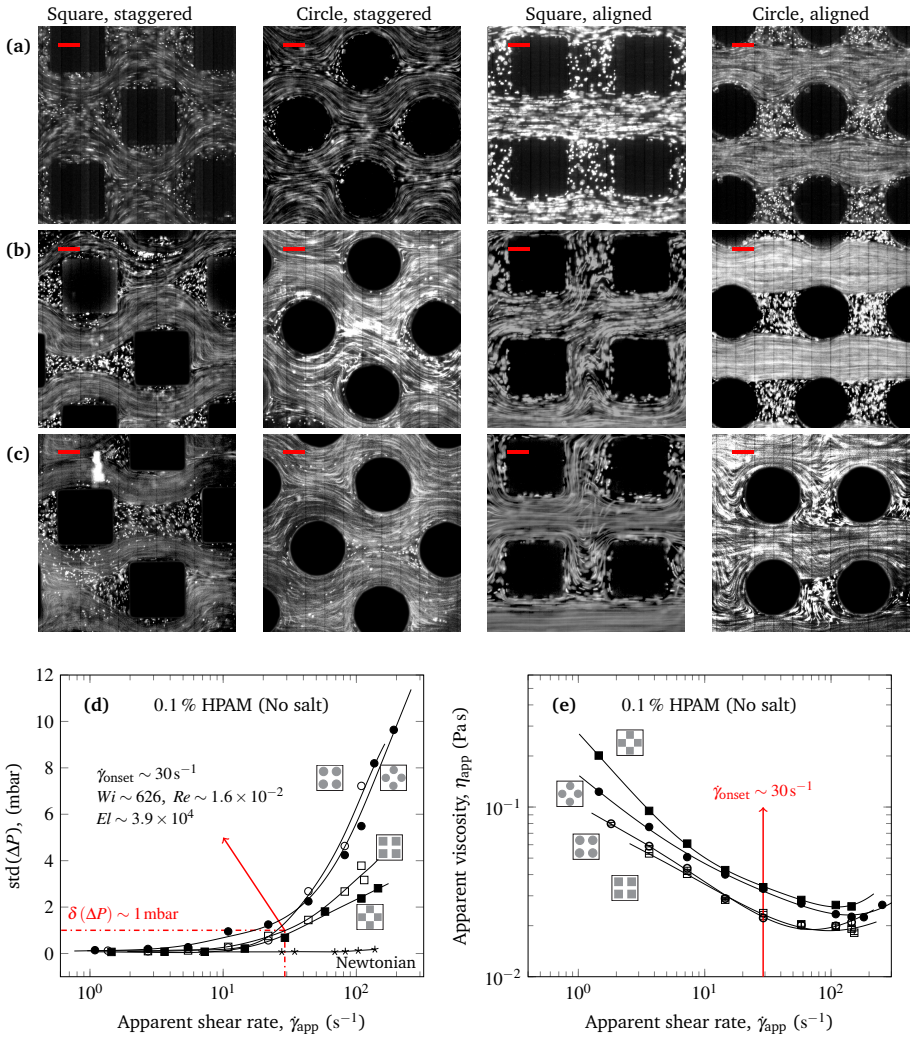


Figure 3.3: Results for 0.1 % HPAM in DI water (without salt). Streamline snapshots of the flow through the four microfluidic geometries showing (a) stationary DZ, $\dot{\gamma}_{app} = 3.63\,s^{-1}$, (b) the onset of elastic instabilities, $\dot{\gamma}_{onset} \sim 30\,s^{-1}$ (c) elastic instabilities at $\dot{\gamma}_{app} = 145.33\,s^{-1}$. Scale bar = 100 µm, flow direction is from left to right. (d) Standard deviation (std) of ΔP fluctuations over apparent shear rate for the four microfluidic devices. Sampling period is 120 s and 600 s for Newtonian and polymer solutions respectively. (e) The apparent viscosity calculated from Darcy's law versus the apparent shear rate. Note that in (d) and (e) the solid lines are spline fit to the data shown solely to guide the reader's eye.

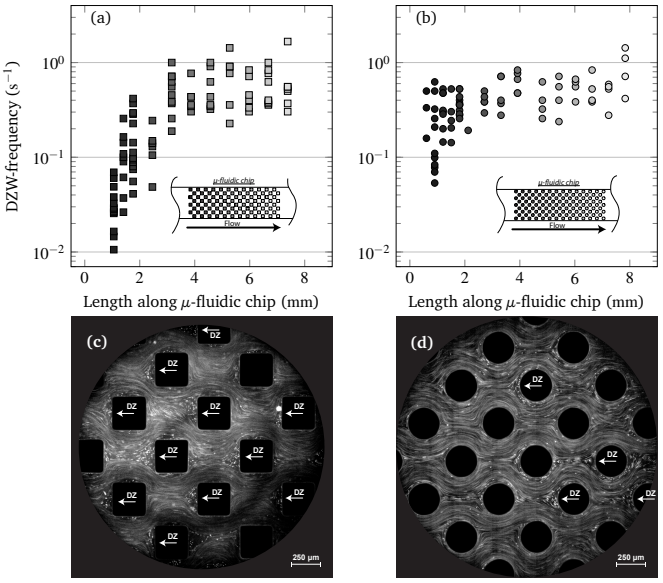


Figure 3.4: (a) and (b) Dead zone washing (DZW) frequency over the pillars from the entrance to the exit of the square and circular-staggered geometry, respectively. The DZW frequency is measured for multiple dead zones at pillars located at a fixed distance from the entrance. We can see that the average frequency near the entrance is lower than that at the exit. The insets in (a) and (b) show a map of the obstacles along L_{pm}. (c) and (d) Snapshots of streamlines, showing the number of dead zones in both geometries. The square-staggered geometry is able to sustain more dead zones than the circular-staggered geometry at $\dot{\gamma}_{\mathrm{app}} = 145.33\,\mathrm{s}^{-1}$.

3.3.1. EFFECT OF PORE-SHAPE

The effect of pore-shape was studied for the four microfluidic geometries shown in figure 3.1b and with 0.1 % HPAM in DI water. The shape of the DZ varies for every geometry that we considered; for instance in the staggered geometries the DZ shape appears like a *prism*. In the aligned geometries, the DZ develops between the pillars, and therefore they conform to the geometry. Refer to streamline snapshots in figure 3.3a for these DZ shapes. DZ-like flow feature was also observed by Khomami and Moreno [18] at a porosity of 0.45, wherein they define it as a transient circular structure. Until $\dot{\gamma}_{\mathrm{app}} \sim 30\,\mathrm{s}^{-1}$, the DZ remains stationary, pinned upstream of the pillar without any wobbling. Streamline images at $\dot{\gamma}_{\mathrm{app}} = 3.63\,\mathrm{s}^{-1}$ showing such a stationary DZ instability are shown in figure 3.3a. The ΔP signal in this range of apparent shear rates is also flat without any amplitude peaks over the corresponding apparent shear rate for a Newtonian fluid. In figure A.5 an example of ΔP signal is shown, and in figure 3.3d the standard deviation of the ΔP fluctuations over apparent shear rates is shown. In the next section we will explain the transition from a stationary DZ to an non-stationary DZ elastic instability.

MECHANISM OF FLOW FIELD FLUCTUATIONS

Beyond $\dot{\gamma}_{app} \sim 30\,s^{-1}$ ($Wi \sim 412$), the flow field undergoes a transition from spatial and temporal steady state to an unsteady state. In the case of the staggered geometries, this unsteady-state flow field consists of periodic *DZ washing* (DZW). These periodic features occur in a sequence as follows: (1) a small DZ is formed upstream of every pillar, (2) the DZ wobbles perpendicular to the flow direction as its size increases, (3) the DZ grows so big that its wobbling motion causes it to be flushed downstream, and (4) the flushed DZ disturbs the wobbling DZ further downstream. This sequence of upstream DZ washing is shown in figure A.6. The disturbed flow field can either lead to small eddies colliding with the walls or cause a change to give rise to cross flows. In the case of aligned geometries, the instabilities start due to wobbling of the DZ that exists between two pillars. As the wobbling motion intensifies, it gets flushed disturbing the downstream DZ. In figure 3.3b we show the streamline snapshots at $\dot{\gamma}_{app} = 29.07\,s^{-1}$, at which the DZW has begun. In figure 3.3c, the streamline snapshots at $\dot{\gamma}_{app} = 145.33\,s^{-1}$ show that the DZW persists.

A single confined cylinder has been used in the past to study flow of Boger fluid[57–59], weakly shear-thinning fluid[60] and worm-like micellar solutions.[61] Kenney *et al.* [58] reported that in flow around a confined cylinder, for $Re \ll 1$, a downstream wake instability is observed, and at $Re > 1$, an upstream instability is observed. Shi *et al.* [59] proposed that the upstream inertio-elastic instability depends on the relative contribution of the local flow speed to the viscoelastic wave speed as quantified by the viscoelastic Mach number, $Ma = \sqrt{Re\,Wi}$.

The flow pattern of the upstream instability in the single-confined-cylinder experiments using PEO-based Boger fluid of Kenney *et al.* [58] starts at $Ma \sim 1$ with the pinching of streamlines at the upstream stagnation point of the cylinder. At $Ma > 10$, the pinch point appears to separate from the cylinder, moving upstream, and a chaotic DZ-like flow feature appears in between the pinch point and the cylinder. In our experiments, we first note that there is an absence of confinement, as the pillar array also extends perpendicular to flow-direction. We do not observe a downstream wake instability. The upstream instability that we report starts with DZ formation at $El \gg 1$. Therefore we hypothesize that the formation of DZ in our strongly shear-thinning polymer solution can be associated to elastic stresses at $Wi > 1$ in the shear-thinning regime at $Re \ll 1$. This instability is reminiscent of shear banding observed in entangled polymer solutions[23, 61–63] or vortex formation/growth in microfluidic geometries[40]. So far in the current chapter, we have not discussed the effect of salt and it will be discussed in the next chapter, but in view of this discussion we highlight a key point. DZ instability ceases

to exist as salt suppresses the fluid shear-thinning. At the $\dot{\gamma}_{\text{onset}} = 29\,\text{s}^{-1}$, $Ma = \mathcal{O}(1)$ we observe DZW instability, suggesting that the transition to the temporal instability occurs when the shear-wave speed is comparable to the flow speed. At the onset point the $Re = \mathcal{O}(10^{-2})$ and the $El \gg 1$, which indicates strong elasticity compared to inertia. The nature of DZW instability seems to be comparable with those at $Ma = \mathcal{O}(1-100)$ in the experiments by Kenney *et al.* [58] Both these instabilities are periodic, following the DZW sequence we listed earlier in this section: DZ formation, growth, wobbling and washing.

APPARENT VISCOSITY

The apparent viscosity η_{app} was calculated from Darcy's law (Eq. 3.2), whereas the apparent shear rate, $\dot{\gamma}_{\text{app}}$ was estimated based on the global average velocity. In all the four porous media geometries, η_{app} continues to decrease beyond $\dot{\gamma}_{\text{onset}}$ even though flow field becomes unsteady. The shear-thinning curve flattens around $\dot{\gamma}_{\text{app}} \sim 100\,\text{s}^{-1}$. As the shear rate increases beyond $\dot{\gamma}_{\text{onset}} \sim 30\,\text{s}^{-1}$, the flow field becomes unsteady (figure 3.3b) and the ΔP fluctuations increase exponentially (figure 3.3d). The onset shear rate, $\dot{\gamma}_{\text{onset}} \sim 30\,\text{s}^{-1}$, was determined from figure 3.3d as the point where std(ΔP) fluctuations increased beyond the pressure-sensor accuracy, $\delta(\Delta P) \sim 1\,\text{mbar}$. We can see in this figure that std(ΔP) for a Newtonian fluid (abs. Ethanol) does not increase beyond $\delta(\Delta P)$ over the entire range of $\dot{\gamma}_{\text{app}}$ probed, validating that the increase in std(ΔP) is due to the elastic instability of polymer solutions. The std(ΔP) is used to calculate error bars in figure 3.3e, but in most cases they are smaller than the marker size. Comparing the η_{app} across the four microfluidic geometries in figure 3.3e, we note that both the aligned geometries have marginally lower η_{app} than both the staggered geometries.

DZW occurs along the entire length of the microfluidic device. We measured the *DZW-frequency* as inverse of the time it takes for a DZ to grow, wobble and eventually wash-away. DZW-frequency was measured for both the staggered geometries at every pillar in the direction of flow. The DZW frequency is lowest near the entrance of the geometry and it increases along the length, until $\sim 4\,\text{mm}$, beyond which the DZW washing frequency stays constant at $\sim 0.5\,\text{s}^{-1}$ (figure 3.4a and 3.4b). Each marker in these figures corresponds to a washing frequency of one DZ upstream of a given pillar. Two pillars close to each of the microfluidic device edges in the y-direction are skipped.

The number of visible DZs in the square-staggered geometry is significantly larger than those in the circle-staggered geometry, as shown in figures 3.4c and 3.4d. The square pillar with its edge perpendicular to the direction of flow seems to support larger DZ-sizes. Since the DZ shedding is responsible for the flow-field disturbance, which eventually leads to small eddies colliding with the walls, we would expect the washing of larger-DZ in square-staggered geometry to have larger pressure loss. Contrary to our

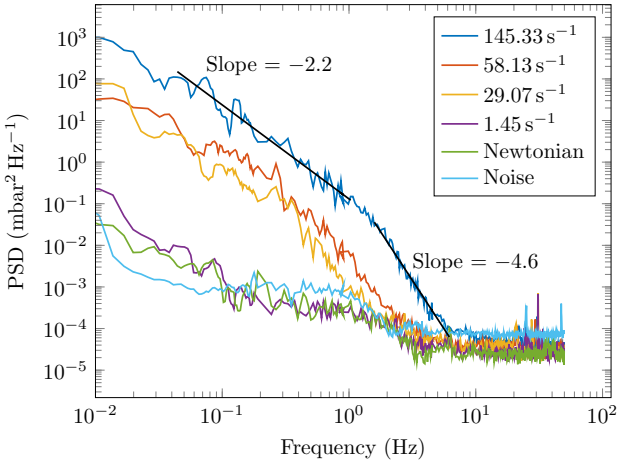


Figure 3.5: Power spectral density at various apparent shear rates for 0.1 % HPAM solution in DI water (without salt) flowing through the square, staggered geometry. The spectral curves for Newtonian fluid flow and when the pressure sensors are disconnected from microfluidic geometry (Noise) give the base-line reference.

expectations, the difference between apparent viscosity across our staggered geometries (figure 3.3e) is insignificant. This suggests that even when the local flow characteristics are different, the global flow resistance between two different realizations of porous media is equivalent.

POWER SPECTRAL DENSITY OF ΔP FLUCTUATIONS

In order to statistically characterize elastic instabilities in porous media, we calculated the spectral density of the pressure-drop fluctuations. Figure 3.5 shows the power spectral density (PSD) curves for the square-staggered geometry and 0.1 % HPAM solution in DI water (no salt). The spectral curves for other geometries (shown in the figure A.7 and A.8) have similar shapes as the square-staggered geometry. Therefore we did not discuss them in this section. As a reference base-line, the spectral curves for the instrumental noise is also shown in figure 3.5. For a Newtonian fluid, there are no significant fluctuations other than the signal noise, indicating that, within experimental accuracy, the flow is entirely steady. The same can be said for the polymer solution at the low shear rates ($\dot{\gamma}_{\text{app}} = 1.45\,\text{s}^{-1}$). For higher shear rates, we observe that the power of the fluctuations, at all frequencies that were sampled experimentally, increases with $\dot{\gamma}_{\text{app}}$. At $\dot{\gamma}_{\text{app}} = 29.07\,\text{s}^{-1}$ which is the onset of flow instabilities, and at higher $\dot{\gamma}_{\text{app}}$, the power decays according to a power-law with an exponent β over three orders of magnitude. We were unable to measure spectral curves at $f \sim> 10\,\text{Hz}$, due to the instrumental noise (signified by the flattening of the spectral curves). The PSD (figure 3.5) exhibits two different exponents,

−2.2 at lower frequencies, and −4.6 at higher frequencies, with an inflection point. The low frequency slope, −2.2 fits equally well to spectral curves for apparent shear rates of 145.33 s^{-1}, 58.13 s^{-1} and 29.07 s^{-1}.

Khomami and Moreno [18] studied the flow of a Boger fluid through an array of circular-aligned geometry. They found that the peak frequencies of the pressure-drop-fluctuation spectral density shifted to higher frequencies as $\dot{\gamma}$ increases (from 0.008 Hz at $Wi = 0.96$ to 0.056 Hz at $Wi = 1.51$). In figure 3.5, we observe that the PSD frequencies also shift to higher values as the apparent shear rate increases. The frequency of DZW varies from 0.01 Hz near the entrance to 1 Hz at the exit (figure 3.4a and 3.4b). This frequency range is coincidentally the same as the power-law decay with an exponent of $\beta \sim -2.2$. This might imply that the dual exponents are due to superposition of two 'types' of instabilities; one due to the DZW, and the other instability that has exponent of $\beta \sim -4.6$. In order to compare the time scales at which the spectral density decays with the polymer relaxation time, we can calculate the product of frequency with the relaxation time, $f\tau$. When $f\tau < 1$, the relaxation time scale is less than the power decay time scale, at $f\tau \sim 1$, these two time scales are comparable whereas when $f\tau > 1$, then the relaxation time scale is faster than the power decay time scale. In figure 3.5, $f\tau \sim 0.22$ to 22 in the low-frequency regime, whereas, $f\tau \sim 22$ to 220 in the high-frequency regime. Note that in our experiments, the pressure fluctuation PSD is same as that of the pressure drop PSD as shown in figure A.9. Jun and Steinberg [64] investigated the pressure fluctuation spectral density over wide range of polymer concentrations in elastic turbulence. They reported $f\tau \sim 1$ to 140. Further investigation is needed to understand the spectral decay at slope of $\beta = -4.6$.

Finally, we review previous works that studied the pressure (or stress) fluctuation spectral density for elastic turbulent flow field for completeness. Beaumont *et al.* [33] studied the flow of elastic worm-like micelles in a Couette geometry. They found that the slope of stress fluctuation spectral density curve remains constant at $\beta \sim -2.0$ over $\dot{\gamma} = 2\,s^{-1}$ to $200\,s^{-1}$. Jun and Steinberg [64] found that the slope of the pressure-fluctuation spectral-density curve in elastic-turbulent flow (in swirling flow between parallel plate) varied between −2.3 in the entangled regime and −3 in semi-dilute and dilute regime. Watanabe and Gotoh [65] also reported similar range of slopes (−2.8 to −3.2) from numerical simulations of elastic turbulence. In both these studies on elastically turbulent flow, the flow is spatially smooth and random in time, whereas the flow field in our microfluidic geometries contains DZW with increasing frequency in the direction of flow.

3.4. CONCLUSIONS

We find that polymer solution flowing through a model porous media ($Wi > 1.0$) shows two distinct elastic instabilities. The first elastic instability exists during an apparent shear-thinning regime at shear rate, $\dot{\gamma}_1 = 3.63\,\mathrm{s}^{-1}$ ($Wi \approx 80$, based on Carreau-Yasuda relaxation time): stationary DZs appear around obstacles with fast flow-zones between them. The second, elastic, instability is at $\dot{\gamma}_2 \sim 30\,\mathrm{s}^{-1}$ ($Wi \approx 626$): DZs become unstable with strong temporal fluctuations in both pressure drop and flow field. In the case of polymer solutions without any added salt, the apparent shear-thinning behaviour corresponds to the second type of elastic instability. A direct comparison of η_{app} was possible by fabricating constant-porosity microfluidic geometries consisting of periodic arrays of square and cylindrical pillars in staggered and aligned layouts. The presence of sharp edges (square-staggered geometry) in realistic porous media can significantly alter the nature of elastic instabilities in porous media. The square-staggered geometry sustains more dead zones than a circle-staggered geometry. These DZs wash along the microfluidic geometry until they disintegrate violently into small eddies. These events cause pressure-drop fluctuations, which are characterized from their spectral density. The spectral density decays via a power law that has two distinct regions separated by an inflection point.

Characterizing pore-scale flow features of polymer solutions in a realistic porous medium is often desired to identify the dominant mechanism of the dramatic increase in pressure loss. DZ washing appears to be a crucial element that feeds the cascade of events responsible for the typically observed dramatic increase in pressure drop. Quantifying the contribution of dead-zone washing to the total pressure drop in porous media, especially considering that a dead zone will eventually dissipate energy as small eddies, could improve the predictability of models for polymeric flow through porous media.

REFERENCES

[1] J. G. Savins, *Non-newtonian flow through porous media,* Industrial & Engineering Chemistry **61**, 18 (1969).

[2] R. P. Chhabra, J. Comiti, and I. Machač, *Flow of non-newtonian fluids in fixed and fluidised beds,* Chemical Engineering Science **56**, 1 (2001).

[3] J. Sheng, *Modern Chemical Enhanced Oil Recovery: Theory and Practice* (Gulf Professional Publishing, 2010).

[4] L. W. Lake, R. Johns, W. Rossen, and G. Pope, *Fundamentals of enhanced oil recovery* (Society of Petroleum Engineers, 2014).

[5] A. E. Peksa, K.-H. A. Wolf, and P. L. Zitha, *Bentheimer sandstone revisited for experimental purposes,* Marine and Petroleum Geology **67**, 701 (2015).

[6] F. Durst, R. Haas, and W. Interthal, *The nature of flows through porous media,* Journal of Non-Newtonian Fluid Mechanics **22**, 169 (1987).

[7] R. Haas and F. Durst, *Viscoelastic flow of dilute polymer solutions in regularly packed beds,* in *Progress and Trends in Rheology* (Springer, 1982) pp. 212–217.

[8] J. Deiber and W. Schowalter, *Flow through tubes with sinusoidal axial variations in diameter,* AIChE Journal **25**, 638 (1979).

[9] R. B. Bird, ed., *Dynamics of polymeric liquids*, 2nd ed. (Wiley, New York, 1987) p. 2.

[10] C. J. S. Petrie, *Extensional viscosity: a critical discussion,* Journal of non-newtonian fluid mechanics **137**, 15 (2006).

[11] A. Magueur, M. MOAN G, and G. Chauveteau, *Effect of successive contractions and expansions on the apparent viscosity of dilute polymer solutions,* Chemical engineering communications **36**, 351 (1985).

[12] G. Chauveteau, M. Moan, and A. Magueur, *Thickening behaviour of dilute polymer solutions in non-inertial elongational flows,* Journal of non-newtonian fluid mechanics **16**, 315 (1984).

[13] J. Odell and S. Haward, *Viscosity enhancement in the flow of hydrolysed poly (acrylamide) saline solutions around spheres: implications for enhanced oil recovery,* Rheologica Acta **47**, 129 (2008).

[14] F. Durst, R. Haas, and B. Kaczmar, *Flows of dilute hydrolyzed polyacrylamide solutions in porous media under various solvent conditions,* Journal of Applied Polymer Science **26**, 3125 (1981).

[15] N. Zamani, I. Bondino, R. Kaufmann, and A. Skauge, *Effect of porous media properties on the onset of polymer extensional viscosity,* Journal of Petroleum Science and Engineering **133**, 483 (2015).

[16] S. Flew and R. Sellin, *Non-newtonian flow in porous media-a laboratory study of polyacrylamide solutions,* Journal of non-newtonian fluid mechanics **47**, 169 (1993).

[17] D. F. James, n_1 *stresses in extensional flows,* Journal of Non-Newtonian Fluid Mechanics **232**, 33 (2016).

[18] B. Khomami and L. D. Moreno, *Stability of viscoelastic flow around periodic arrays of cylinders,* Rheologica acta **36**, 367 (1997).

[19] F. J. Galindo-Rosales, L. Campo-Deaño, F. Pinho, E. Van Bokhorst, P. Hamersma, M. Oliveira, and M. Alves, *Microfluidic systems for the analysis of viscoelastic fluid flow phenomena in porous media,* Microfluidics and nanofluidics **12**, 485 (2012).

[20] A. M. Howe, A. Clarke, and D. Giernalczyk, *Flow of concentrated viscoelastic polymer solutions in porous media: effect of mw and concentration on elastic turbulence onset in various geometries,* Soft matter **11**, 6419 (2015).

[21] A. Machado, H. Bodiguel, J. Beaumont, G. Clisson, and A. Colin, *Extra dissipation and flow uniformization due to elastic instabilities of shear-thinning polymer solutions in model porous media,* Biomicrofluidics **10**, 043507 (2016).

[22] E. S. Shaqfeh, *Purely elastic instabilities in viscometric flows,* Annual Review of Fluid Mechanics **28**, 129 (1996).

[23] S.-Q. Wang, S. Ravindranath, and P. E. Boukany, *Homogeneous shear, wall slip, and shear banding of entangled polymeric liquids in simple-shear rheometry: A roadmap of nonlinear rheology,* Macromolecules **44**, 183 (2011), http://dx.doi.org/10.1021/ma101223q .

[24] R. G. Larson, *Instabilities in viscoelastic flows,* Rheologica Acta **31**, 213 (1992).

[25] R. G. Larson, E. S. Shaqfeh, and S. J. Muller, *A purely elastic instability in taylor–couette flow,* Journal of Fluid Mechanics **218**, 573 (1990).

[26] P. E. Boukany, S.-Q. Wang, S. Ravindranath, and L. J. Lee, *Shear banding in entangled polymers in the micron scale gap: a confocal-rheoscopic study,* Soft Matter **11**, 8058 (2015).

[27] P. E. Arratia, C. C. Thomas, J. Diorio, and J. P. Gollub, *Elastic instabilities of polymer solutions in cross-channel flow,* Physical Review Letters **96**, 144502 (2006).

[28] S. Haward and G. McKinley, *Instabilities in stagnation point flows of polymer solutions,* Physics of Fluids (1994-present) **25**, 083104 (2013).

[29] A. Groisman and V. Steinberg, *Mechanism of elastic instability in couette flow of polymer solutions: experiment,* Physics of Fluids (1994-present) **10**, 2451 (1998).

[30] A. Groisman and V. Steinberg, *Elastic turbulence in a polymer solution flow,* Nature **405**, 53 (2000).

[31] A. Groisman and V. Steinberg, *Efficient mixing at low reynolds numbers using polymer additives,* Nature **410**, 905 (2001).

[32] A. Groisman and V. Steinberg, *Elastic turbulence in curvilinear flows of polymer solutions,* New Journal of Physics **6**, 29 (2004).

[33] J. Beaumont, N. Louvet, T. Divoux, M.-A. Fardin, H. Bodiguel, S. Lerouge, S. Manneville, and A. Colin, *Turbulent flows in highly elastic wormlike micelles,* Soft Matter **9**, 735 (2013).

[34] G. M. Whitesides, *The origins and the future of microfluidics,* Nature **442**, 368 (2006).

[35] X. Hu, P. E. Boukany, O. L. Hemminger, and L. J. Lee, *The use of microfluidics in rheology,* Macromolecular Materials and Engineering **296**, 308 (2011).

[36] D. Sinton, *Microscale flow visualization,* Microfluidics and Nanofluidics **1**, 2 (2004).

[37] L. E. Rodd, T. P. Scott, D. V. Boger, J. J. Cooper-White, and G. H. McKinley, *The inertio-elastic planar entry flow of low-viscosity elastic fluids in micro-fabricated geometries,* Journal of Non-Newtonian Fluid Mechanics **129**, 1 (2005).

[38] Z. Li and S. J. Haward, *Viscoelastic flow development in planar microchannels,* Microfluidics and Nanofluidics **19**, 1123 (2015).

[39] C. J. Pipe and G. H. McKinley, *Microfluidic rheometry,* Mechanics Research Communications **36**, 110 (2009).

[40] O. L. Hemminger, P. E. Boukany, S.-Q. Wang, and L. J. Lee, *Flow pattern and molecular visualization of dna solutions through a 4: 1 planar micro-contraction,* Journal of Non-Newtonian Fluid Mechanics **165**, 1613 (2010).

[41] A. K. Sankaran, D. A. Dros, H. J. Meerman, S. J. Picken, and M. T. Kreutzer, *Increasing the stability of high contraction ratio flow of boger fluids by pre-deformation,* Journal of Non-Newtonian Fluid Mechanics **196**, 27 (2013).

[42] L. Rems, D. Kawale, L. J. Lee, and P. E. Boukany, *Flow of dna in micro/nanofluidics: From fundamentals to applications,* Biomicrofluidics **10**, 043403 (2016).

[43] A. Groisman and S. R. Quake, *A microfluidic rectifier: anisotropic flow resistance at low reynolds numbers,* Physical review letters **92**, 094501 (2004).

[44] L. Pan, A. Morozov, C. Wagner, and P. E. Arratia, *Nonlinear elastic instability in channel flows at low reynolds numbers,* Physical review letters **110**, 174502 (2013).

[45] C. Chmielewski and K. Jayaraman, *Elastic instability in crossflow of polymer solutions through periodic arrays of cylinders,* Journal of non-newtonian fluid mechanics **48**, 285 (1993).

[46] F. P. T. Baaijens, *Mixed finite element methods for viscoelastic flow analysis: a review,* Journal of Non-Newtonian Fluid Mechanics **79**, 361 (1998).

[47] X. Wu, D. Hunkeler, A. Hamielec, R. Pelton, and D. Woods, *Molecular weight characterization of poly (acrylamide-co-sodium acrylate). i. viscometry,* Journal of applied polymer science **42**, 2081 (1991).

[48] A. V. Dobrynin, R. H. Colby, and M. Rubinstein, *Scaling theory of polyelectrolyte solutions,* Macromolecules **28**, 1859 (1995).

[49] C. W. Macosko, ed., *Rheology: principles, measurements, and applications* (VCH, New York, 1994) p. 550.

[50] J. Sukpisan, J. Kanatharana, A. Sirivat, and S. Wang, *The specific viscosity of partially hydrolyzed polyacrylamide solutions: Effects of degree of hydrolysis, molecular weight, solvent quality and temperature,* Journal of Polymer Science Part B: Polymer Physics **36**, 743 (1998).

[51] A. Ait-Kadi, P. J. Carreau, and G. Chauveteau, *Rheological properties of partially hydrolyzed polyacrylamide solutions,* Journal of Rheology **31**, 537 (1987).

[52] K. Y. Yasuda, R. C. Armstrong, and R. E. Cohen, *Shear flow properties of concentrated solutions of linear and star branched polystyrenes,* Rheologica Acta **20**, 163 (1981).

[53] D. C. Duffy, J. C. McDonald, O. J. A. Schueller, and G. M. Whitesides, *Rapid prototyping of microfluidic systems in poly (dimethylsiloxane),* Analytical chemistry **70**, 4974 (1998).

[54] J. C. McDonald and G. M. Whitesides, *Poly (dimethylsiloxane) as a material for fabricating microfluidic devices,* Accounts of chemical research **35**, 491 (2002).

[55] T. Gervais, J. El-Ali, A. Günther, and K. F. Jensen, *Flow-induced deformation of shallow microfluidic channels,* Lab on a Chip **6**, 500 (2006).

[56] C. Meinhart, S. Wereley, and M. Gray, *Volume illumination for two-dimensional particle image velocimetry,* Measurement Science and Technology **11**, 809 (2000).

[57] G. H. McKinley, R. C. Armstrong, and R. A. Brown, *The wake instability in viscoelastic flow past confined circular cylinders,* Philosophical Transactions of the Royal Society of London A: Mathematical, Physical and Engineering Sciences **344**, 265 (1993).

[58] S. Kenney, K. Poper, G. Chapagain, and G. F. Christopher, *Large deborah number flows around confined microfluidic cylinders,* Rheologica Acta **52**, 485 (2013).

[59] X. Shi, S. Kenney, G. Chapagain, and G. F. Christopher, *Mechanisms of onset for moderate mach number instabilities of viscoelastic flows around confined cylinders,* Rheologica Acta **54**, 805 (2015).

[60] K. P. Nolan, A. Agarwal, S. Lei, and R. Shields, *Viscoelastic flow in an obstructed microchannel at high weissenberg number,* Microfluidics and Nanofluidics **20**, 1 (2016).

[61] Y. Zhao, A. Q. Shen, and S. J. Haward, *Flow of wormlike micellar solutions around confined microfluidic cylinders,* Soft Matter **12**, 8666 (2016).

[62] P. E. Boukany, S.-Q. Wang, *et al.*, *Shear banding or not in entangled dna solutions,* Macromolecules **43**, 6950 (2010).

[63] S. Jaradat, M. Harvey, and T. A. Waigh, *Shear-banding in polyacrylamide solutions revealed via optical coherence tomography velocimetry,* Soft Matter **8**, 11677 (2012).

[64] Y. Jun and V. Steinberg, *Power and pressure fluctuations in elastic turbulence over a wide range of polymer concentrations,* Physical review letters **102**, 124503 (2009).

[65] T. Watanabe and T. Gotoh, *Power-law spectra formed by stretching polymers in decaying isotropic turbulence,* Physics of Fluids (1994-present) **26**, 035110 (2014).

4

ELASTIC INSTABILITIES WITH VARYING IONIC STRENGTH

We experimentally investigate the flow of hydrolyzed polyacrylamide (HPAM) solution with salt in model porous media at high Weissenberg numbers ($Wi > 1.0$). To this end, we use microfluidic model porous media containing a periodic array of square pillars in staggered layout. In the apparent shear-thinning regime, we observe stationary dead zones upstream of the pillars. In addition, we confirm that the size of stationary dead zones is correlated with the level of shear thinning, by varying the amount of salt in HPAM solution.

4.1. INTRODUCTION

In the previous chapter, we studied the flow of hydrolyzed polyacrylamide (HPAM) solutions without salt in four different realizations of model porous media. We observed that at $Wi > 1$ the flow field shows several non-Newtonian effects such as *dead zone* (DZ) formation and *Deadzone washing* (DZW). A DZ is a stationary stagnation region upstream of the obstacles that has low local shear-rates inside the stagnation region, compared to the fast flow-zones outside this stagnation region. A DZW refers to a time-dependant instability of the DZ, wherein the DZ wobbles and periodically washes away. Since the

Parts of this chapter have been published in **D. Kawale**, E. Marques, P. L. J. Zitha, M. T. Kreutzer, W. R. Rossen, P. E. Boukany, *Elastic instabilities during the flow of hydrolyzed polyacrylamide solution in porous media: effect of pore-shape and salt*, Soft Matter, **13**, 765 (2017).

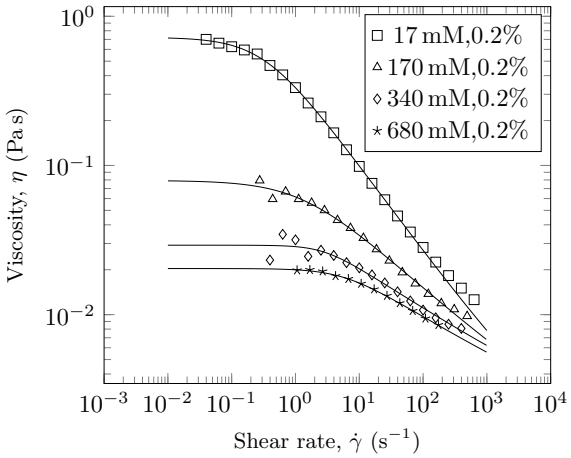


Figure 4.1: Steady-state shear viscosity of 0.2 % HPAM in DI water with addition of salt from 17 mM to 680 mM at 22 °C. The solid line is obtained by fitting the Carreau-Yasuda model shown in Eq. 4.1, and its fitting parameters are tabulated in table A.1.

local velocity inside the DZ is low, compared to outside of the DZ, for a shear-thinning fluid the local viscosity will also differ. Addition of salt in a polyelectrolyte solution (like HPAM) suppresses the shear-thinning behaviour. In this chapter we study the effect of salt on the elastic instabilities during flow of HPAM solutions through microfluidic porous media.

4.2. EXPERIMENTAL DETAILS

0.2 % Aqueous hydrolyzed polyacrylamide, HPAM (MW = 15×10^6 g mol^{-1}, 30% hydrolysis; Flopam 3530s, SNF Floerger, France) was used to study the effect of pore-shape by using the square staggered geometry (see figure 3.1b). In the presence of salt, we expect our polymer solutions to be in the dilute regime. We have studied the effect of salt, NaCl by using 0.2 % of HPAM solution at different NaCl concentrations: 17 mM, 170 mM, 340 mM, 680 mM. The polymer solutions were prepared by using NaCl solution at required concentration in deionised (DI) water. The polymer dispersion procedure is same as described in sec. 3.2.1. The rheological properties of 0.2 % HPAM solution (with NaCl) was characterized in a Couette cell (cup ID = 30.36 mm, bob OD = 28 mm, gap = 1.18 mm) using the AR-G2 rheometer (TA Instruments). All experiments were performed at the room temperature, $T = (22 \pm 2)$ °C as shown in figure 4.1.

Our working polymer solutions are shear-thinning as shown in figure 4.1. The Carreau-Yasuda model[1] shown below (eq. 4.1) is used to fit the steady-shear flow curve. We

could not observe a plateau at high shear rate; therefore we set the $\eta_\infty = 10^{-3}$ Pa s, the viscosity of our solvent for fitting the shear rheology data. Figure 4.1 shows the measured rheology fitted to the Carreau-Yasuda model.

$$\eta - \eta_\infty = (\eta_0 - \eta_\infty)\left[1 + (\tau_{CY}\dot{\gamma})^a\right]^{\frac{n-1}{a}} \tag{4.1}$$

Here, the parameter a allows control over the width of the transition region from the zero-shear-viscosity plateau to the shear-thinning part; n is the power-law slope; and the relaxation time, (1) $\tau_{CY} = 3.03$ s for 0.2 % HPAM in 17 mM NaCl; (2) $\tau_{CY} = 0.75$ s for 0.2 % HPAM in 170 mM NaCl; (3) $\tau_{CY} = 0.35$ s for 0.2 % HPAM in 340 mM NaCl; (4) $\tau_{CY} = 0.17$ s for 0.2 % HPAM in 680 mM NaCl. The results of CY-model fit are summarized in the table A.1.

All other experimental details including microfluidic device fabrication, pressure drop measurement and experiment protocols are same as explained in the chapters 3.

4.3. RESULTS AND DISCUSSION

The effect of salt was studied for 0.2 % HPAM solution in 17 mM, 170 mM, 340 mM and 680 mM NaCl solutions. The concentration of salt needed to fully balance the polyelectrolyte charges in HPAM solution can be found considering 30 % hydrolysis and valency of charges on the hydrolyzed portion of a polymer chain[2]. For 0.2 % HPAM concentration, a NaCl concentration of ~26 mM would introduce counterion concentration that equals the polyelectrolyte charge concentration. When the NaCl concentration is 17 mM, then the number of polyelectrolyte charges is larger than the number of the NaCl counterion charges. At the other NaCl concentrations considered in this chapter, the number of polyelectrolyte charges is less than the number of NaCl counterion charges. Adding NaCl significantly decreases η_0 and τ of the HPAM polymer solutions (figure 4.1 and table A.1). As NaCl concentration increases, the level of Debye length screening increases reducing the polymer intra-molecular interactions. Therefore the equilibrium polymer radius of gyration decreases. Both η_0 and τ decreased by almost three orders of magnitude (table A.1). The square, staggered geometry is used to study the effect of salt.

APPARENT VISCOSITY

The onset shear rate is calculated when $\delta(\Delta P) > 1$ mbar, analogous to our experiments without salt. We show that the onset of the DZW instabilities occurs at a constant $\dot{\gamma}_{app} \sim 35\,s^{-1}$ when the counterion charge concentration is higher than polymer chain concentration (figure 4.2a). In the case of higher polyelectrolyte concentration (NaCl concentration of 17 mM), the $\dot{\gamma}_{onset}$ is roughly half of the onset shear rate for all higher counterion

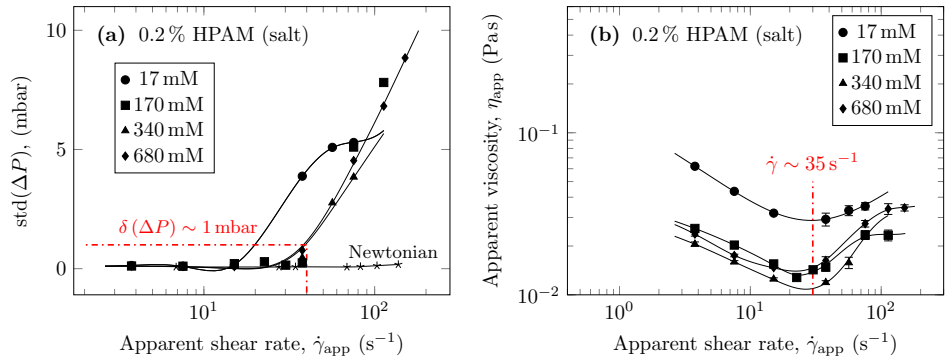


Figure 4.2: All results shown for 0.2 % HPAM with varying NaCl concentration. (a) Standard deviation (std) of ΔP fluctuations over apparent shear rate. Sampling period is 120 s and 1200 s for Newtonian and polymer solutions respectively. (b) The apparent shear rate calculated from Darcy's law versus the apparent shear rate. Note that in (d) and (e) the solid lines are spline fit to the data shown solely to guide the reader's eye.

concentration. Despite these differences in the onset shear rate, the apparent shear-thickening region at all the salt concentrations starts at $\dot{\gamma}_{app} \sim 35\,s^{-1}$ (figure 4.2b). Such a salinity invariance has been typically observed for polymeric flows in model-porous media[3] and consolidated/unconsolidated porous media.[4, 5] Elastic flow instabilities also emerge at the $\dot{\gamma}_{onset}$, suggesting that these flow instabilities are a cause of the apparent shear-thickening region.

We also note that since the relaxation time of all the salt solutions varies over three orders of magnitude, the corresponding Wi number at which the apparent shear-thickening region starts also varies over three orders of magnitude. In comparison with η_{app} without salt, the onset point of DZW ($\dot{\gamma}_{app} \sim 30\,s^{-1}$) corresponds with the shear-thinning regime; whereas, the onset point of DZW with salt ($\dot{\gamma}_{app} \sim 35\,s^{-1}$) corresponds with the apparent shear-thickening region (see figure A.10).

4.3.1. MAXIMUM DEAD-ZONE AREA

The local shear rates in DZ are negligible compared to the local shear rate in fluid flowing around the pillars as described in Ch. 3. Figure 4.3a shows the normalized DZ area (A_{DZ}/A_{pillar}) averaged roughly over ~ 10 DZs at each shear rate versus the ratio $\tilde{\eta} = \eta_0/\eta_\infty$. We estimate A_{DZ}/A_{pillar} by dividing the area of a polygon that encloses a given DZ from our streamline images using ImageJ and normalizing it by the area of the pillar. Examples of the polygons enclosing DZs can be found in figure 4.3b-c. The normalized DZ size increases by 200 % as $\tilde{\eta}$ decreases by two orders of magnitude (from 80 to 8100). Therefore, as the salt concentration increases, the zero-shear viscosity decreases, mak-

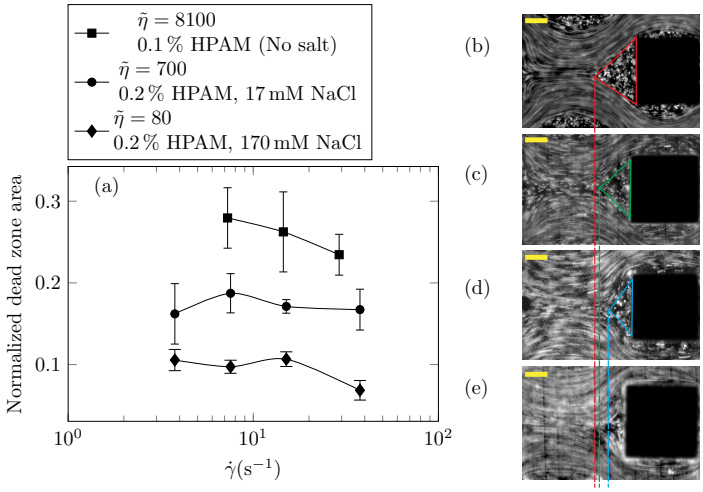


Figure 4.3: (a) Correlation between the normalized DZ size and $\tilde{\eta} = \eta_0/\eta_\infty$ for the square, staggered geometry. The error bars represent standard deviation of dead zone area. Streamline snapshots showing DZ at $\dot{\gamma}_{app} = 14.53\,s^{-1}$ for (b) $\tilde{\eta} = 8100$, (c) $\tilde{\eta} = 700$, (d) $\tilde{\eta} = 80$. (e) Streamline snapshot showing that at $\tilde{\eta} = 30$ (0.2 % HPAM, 340 mM NaCl) a DZ is not visible. Scale bar = 100 µm

ing the polymer solutions less shear-thinning. For 170 mM NaCl, (0.2 % HPAM solution), $A_{DZ}/A_{pillar} \sim 0.1$, and from 340 mM NaCl concentration ($\tilde{\eta} = 30$) onwards, we are unable to clearly identify a DZ by our streamline visualization (see figure 4.3e). In the case of a Boger fluid, $\tilde{\eta} = 1$, and consequently we expect absence of the DZ instability.

4.3.2. *Wi – Re* AND *Ma – El* FLOW PATTERN MAP

In figure 4.4 we summarize the flow transitions in the square, staggered geometry described so far on the *Ma – El* and the *Wi – Re* phase space map. The *Wi* - *Re* map in figure 4.4a covers the *Wi* number over $\mathcal{O}(1 - 10^4)$ and the *Re* number over $\mathcal{O}(10^{-4} - 1)$. Two time-dependant instabilities were observed depending on whether DZ formed or not. Upon formation of DZ, the time-dependant DZW instability (see figure 3.4a and figure A.6) was observed at $Ma \sim 1$. If DZ was not formed (see figure 4.3e and figure A.10), then a time-dependant flow instability at $Ma \sim 1$ did not contain a DZW-like feature. In figure 4.4b, we summarize the flow transitions in the *Ma* - *El* space map, covering the *Ma* number over $\mathcal{O}(10^{-1} - 10^2)$ and the *El* number over $\mathcal{O}(10^2 - 10^5)$. Transition to the DZW and the non-DZW time-dependant flow instabilities occurs along the $Ma = \mathcal{O}(1)$ path.

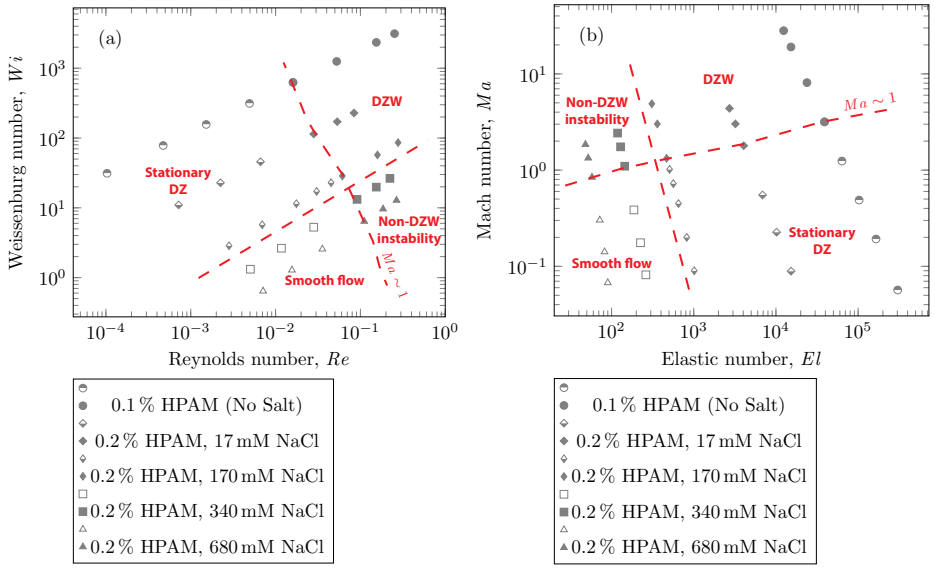


Figure 4.4: Summary of flow transitions in the square, staggered geometry on the (a) $Wi-Re$ and the (b) $Ma-El$ phase space map. The dashed lines are a guide to the reader's eyes, showing the boundaries between the various flow transitions. Half-open symbols indicate formation of stationary DZ, open symbols indicate smooth flow without DZ formation. Solid symbols indicate time-dependant DZW and non-DZW flow instabilities.

4.4. CONCLUSIONS

We find that polymer solution flowing through a model porous media ($Wi > 1.0$) shows two distinct elastic instabilities. The first elastic instability exists during an apparent shear-thinning regime at shear rate, $\dot{\gamma}_1 = 3.63\,\mathrm{s}^{-1}$ ($Wi \approx 80$, based on Carreau-Yasuda relaxation time): stationary DZs appear around obstacles with fast flow-zones between them. The size of these DZs increases with the ratio η_0/η_∞, suggesting that the first type of elastic instability ceases to exist for weakly shear-thinning polymer solution. The second, elastic instability is at $\dot{\gamma}_2 \sim 30\,\mathrm{s}^{-1}$ ($Wi \approx 626$): DZs become unstable with strong temporal fluctuations in both pressure drop and flow field. In the case of polymer solutions without any added salt, the apparent shear-thinning behaviour corresponds with the second type of elastic instability. In the case of polymer solutions with added salt, the onset of apparent shear-thickening corresponds with the second type of elastic instability.

REFERENCES

[1] C. W. Macosko, ed., *Rheology: principles, measurements, and applications* (VCH, New York, 1994) p. 550.

[2] A. V. Dobrynin, R. H. Colby, and M. Rubinstein, *Scaling theory of polyelectrolyte solutions,* Macromolecules **28**, 1859 (1995).

[3] R. Haas and F. Durst, *Viscoelastic flow of dilute polymer solutions in regularly packed beds,* in *Progress and Trends in Rheology* (Springer, 1982) pp. 212–217.

[4] F. Durst, R. Haas, and B. Kaczmar, *Flows of dilute hydrolyzed polyacrylamide solutions in porous media under various solvent conditions,* Journal of Applied Polymer Science **26**, 3125 (1981).

[5] S. Flew and R. Sellin, *Non-newtonian flow in porous media-a laboratory study of polyacrylamide solutions,* Journal of non-newtonian fluid mechanics **47**, 169 (1993).

5

POLYMER CHAIN DYNAMICS DURING ELASTIC INSTABILITIES IN POROUS MEDIA

Molecular conformations of individual polymers during flow through porous media is directly observed by single-DNA imaging in microfluidics. As the Weissenberg number increases during flow ($Wi > 1$), we observe two types of elastic instabilities: (a) stationary dead-zone and (b) time-dependant dead-zone washing. When stretched polymer chains enter a dead-zone, they first re-coil and, once inside the dead-zone, they rotate and re-stretch again. The probability distribution of DNA chains under the stretched condition inside the dead-zone is found to be heterogeneous with a broad distribution.

5.1. INTRODUCTION

Flow of polymer solutions through porous media play a crucial role in various applications such as injection molding, textile coating, inkjet printing, turbulent drag reduction and enhanced oil recovery.[1] As polymer solutions flow through a porous medium it shows several non-Newtonian behaviours such as dramatic increase in pressure drop

This chapter is currently under review as a research article in Soft Matter as **D. Kawale**, G. Bouwman, S. Sachdev, P. L. J. Zitha, M. T. Kreutzer, W. R. Rossen, P. E. Boukany, *Polymer conformation during flow in porous media.*

and flow instabilities at high Weissenberg number, $Wi > 1$ ($Wi = \tau\dot{\gamma}$, where τ is the polymer relaxation time and $\dot{\gamma}$ is the deformation rate of the imposed flow).[2–4] Often these non-Newtonian behaviours are characterized by flow visualization and by measuring the pressure drop, or stresses due to flow. For instance, elastic instabilities are observed during the flow through porous media increases beyond $Wi > 1$.[5–7] The corresponding molecular conformation beyond $Wi > 1$ is unknown for flow of polymer solutions through porous media.

Traditionally, flow through packed beds of spheres or particles was used to investigate the resistance to flow of polymeric fluids through porous media and determine the constitutive parameters that describe the rheological properties of polymeric fluids.[8–10] When the Wi is larger than a critical value at low Reynold number, Re, ($Re = \rho v l/\eta(\dot{\gamma})$, where ρ is density, v is velocity, l is a characteristic length scale and η is viscosity) there is a sudden increase in the pressure drop across the porous medium.[11–14] Direct visualization of flow in two-dimensional (2D) models of porous media (such as a periodic array of cylinder), was a first step towards understanding of pore-scale flow phenomena related to polymer flows (from Boger fluids to shear-thinning systems) in porous media.[5–7, 15–19].

In recent years, planar microfluidic devices have been widely used to investigate the strong viscoelastic features of polymer flow over a very wide range of Wi under non-inertial conditions ($Re \ll 1$).[20, 21] By using microfluidic analogues of a porous medium, elastic instabilities were shown to cause the dramatic pressure drop increase during flow of Boger and shear-thinning fluids.[6, 7, 22] In particular, Kawale *et al.* [6] studied the flow of a shear-thinning system, hydrolyzed polyacrylamide with and without salt, through a microfluidic device containing periodic array of obstacles. At very low flow rates ($Wi \ll 1$, $Re \ll 1$), as expected, creeping flow was obtained. As the flow rate was increased ($Wi > 1$, $Re \ll 1$), the non-Newtonian effects emerged. Stationary *dead zones* (DZ) appeared to be pinned upstream of the obstacles. The local shear rate in a DZ is negligible compared to that outside the DZ. As the flow rates increased further ($Wi \gg 1$, $Re < 1$), the stationary DZ starts wobbling and washing away periodically. This time-dependant elastic instability, *dead zone washing* (DZW), was found to start when the viscoelastic Mach number, $Ma \sim 1$ ($Ma = \sqrt{Wi\,Re}$). DZW-like instabilities were also observed during flow of Boger fluids[23, 24] and worm-like micellar solutions[25] around a single cylinder. Not only is the local velocity magnitude inside a DZ close to zero,[6, 24, 25] but there is also a stagnation point upstream of the pillar where the local velocity magnitude is zero. The flow inside a DZ is a combination of steady shear flow and extensional flow.[6] In a $Wi < 1$ steady shear flow, the polymer chains will be

coiled.[26] At the same time, the polymer chains in an extensional flow field can be stretched beyond $Wi \sim 0.5$.[27] Given a combination of steady shear and extensional flow inside a DZ, the corresponding dynamics of polymer chain is unclear as a polymer chain approaches and enters a DZ.

Rheo-optical methods have been used to complement bulk rheometric measurements with the aim of the direct measurement of stresses, deformations and alignment of polymer chains in the flow of viscoelastic fluids.[21, 28–30] Specifically, flow-induced birefringence (FIB) imaging has been employed to determine the localized deformation and alignment of worm-like micelles at high Wi during flow through a micro-channel, containing either a single cylinder or a periodic array of cylinders.[31–33] Zhao *et al.* [25]investigated vortex formation and growth in micellar solution flow around a cylinder with increasing Wi near the upstream stagnation point of the cylinder by using a combination of FIB and velocimetry measurements. In such FIB measurements, the molecular parameters are extracted based on an ensemble average, which does not necessarily reflect the molecular individualism of polymer during flow. Direct visualization of fluorescently labeled DNA provides a unique opportunity for polymer scientists to reveal polymer chain conformation and address molecular processes behind the macroscopic flow phenomena under strong flow conditions ($Wi \gg 1$).[27, 34, 35] For instance, Perkins *et al.* [35] used these techniques to directly observe the tube-like motion of polymer molecules assumed in the reptation model[36, 37] for an entangled polymer-solution dynamics. Fluorescent DNA molecules that act as a molecular tracers have also often been employed to confirm various phenomena such as (1) coil-stretch (C-S) transition in extensional flows,[27, 38, 39] (2) C-S transition with periodic tumbling in shear flows,[26, 40] (3) C-S transition in free surface flow,[41–43] and (4) interfacial disentanglement of DNA chains as the cause for wall-slip[44] and transient stress overshoot in startup shear flows.[45–47] All these studies successfully link polymer conformation to the macroscopic behaviour of flow.

To date, experimental studies on pressure driven flow of polymer solutions in microfluidic geometries consisting of contractions and obstacles were focussed on size-based separation of DNA chains.[48–50] For instance, for a cylindrical obstacle, the diameter would be small (order of few tens of nanometers or about a micrometer) such that a DNA chain can 'hook' on the post. Understanding the hooking and unhooking process is crucial for separating DNA chain based on their size. Little attention was given to high-Wi number flows around larger diameter obstacles wherein the flow field becomes unstable. In the field of single-molecule sequencing, the flow of DNA across single/array of obstacles with electric-field[51] or pressure-drop[48, 50] is often studied

with an intention of DNA chain stretching or size-based DNA chain separation. The length scales of obstacles in these studies is much smaller than the DNA chain length. During DNA flow due to an electric-field, the resulting local velocity-field near an insulating obstacle (like PDMS) is purely elongational.[52] On the other hand, DNA flow due to pressure-gradient results in shear flow across the entire channel. In the current chapter, we will focus on polymer conformation in microfluidic geometries during elastic instabilities due to pressure-driven flow.

Corner vortex formation during polymeric flow through a planar, sharp or gradual contraction geometry is typically observed around $Wi = \mathcal{O}(1) - \mathcal{O}(10)$.[53, 54] For an entangled shear-thinning polymer solution, Hemminger *et al.* [53] showed that the DNA molecules located in the corner vortex disentangle from the molecules in the center of the channel. This observation is reminiscent of shear banding in entangled polymer solutions [55]. Francois *et al.* [56] studied drag enhancement during Boger fluid flow around a single cylindrical obstacle. They also observed shear-banding at $Wi \sim 1$ near the vicinity of the obstacle. The DNA extension distribution in both shear-bands was positively skewed, with the mean extension in the high shear-rate band (closer to the obstacle) being twice that in the low shear-rate band (further away from the obstacle). As Wi increases in shear flow, the DNA extension distribution shifted from positively skewed to a broad probability distribution.[26] Such a broad distribution of DNA extensions in a shear flow is caused by the tumbling motion of DNA chains. Liu and Steinberg [57] studied DNA chain dynamics in elastic turbulence and found that the DNA extension distribution is negatively skewed with mean fractional extension reaching value of 0.8 asymptotically. Such a high mean fractional extension has also been observed in an extensional flow field.[27, 58] In this paper, we report the molecular processes leading to DZ formation during flow of shear-thinning polymer solutions through a periodic array of obstacles. We probe conformation of single chains by visualizing fluorescently labelled DNA molecules in polyacrylamide (PAA) solutions with and without addition of salt. In addition, we use a combination of pressure-drop measurement and streamline visualization to map elastic instabilities and the corresponding pressure losses.

5.2. EXPERIMENTAL DETAILS

5.2.1. MICROFLUIDIC DEVICE AND PRESSURE MEASUREMENTS

A microfluidic device was combined with an inverted fluorescence microscope as shown in fig. 5.1 to enable visualization of streamlines and single DNA molecules. The microfluidic device consisted of a periodic array of cylinders in a hexagonal layout. The

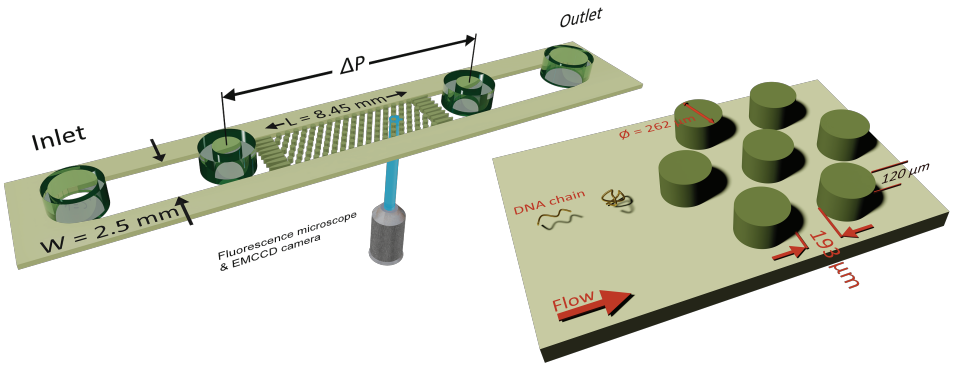


Figure 5.1: Schematic of the microfluidic device combined with an inverted microscope for streamline and single-molecule visualization. The position where the laser from objective falls on the periodic array indicates the streamline and the DNA visualization location. Microfluidic device height, H is 120 µm; width, W, is 2.5 mm and length of the periodic array, L is 8.45 mm. Diameter of the cylindrical pillar, D is 262 µm and spacing between the pillars is 193 µm.

cylinder diameter was 262 µm, with a spacing of 193 µm from the surrounding cylinders. The height of the cylinders was 120 µm. The cylinder diameter was chosen to maintain consistency with the Ch. 3 on elastic instabilities in porous media.[6] Spacing between the pillars was indirectly determined as a conscious decision of maintaining a porosity of 0.7 to match our previous chapter with a hexagonal layout of cylinder placement. The microfluidic geometry was fabricated out of PDMS (Polydimethylsiloxane; Sylgard® 184, Dow Corning Corporation) using standard soft-lithography techniques.[59] Pressure drop (ΔP) across the periodic array was measured via two pressure taps, to which two piezoresistive silicon pressure sensors (HSCMRNT005PGAA5, Honeywell Sensing and Control) were attached. Pressures were monitored using an in-house-developed LabVIEW data acquisition program sampling at 100 Hz. Pressure sensors were accurate to within 0.25 % of the full-scale-span. After calibrating the sensors using a pressure pump (MFCS™, Fluigent GmbH) the instantaneous signal fluctuated with a standard deviation of 0.1 mbar around the mean value. The permeability of our microfluidic porous media was $k = 6 \times 10^{-11}\,\mathrm{m}^2$ according to the Darcy's law, $k = \left(v\eta L_{\mathrm{PM}}/\Delta P\right)$, where v is the superficial velocity; η is the viscosity; $L_{\mathrm{PM}} = 8.5 \times 10^{-3}\,\mathrm{m}$ is the length of periodic array and ΔP is the pressure-drop across the periodic array of cylinders. To probe the flow behaviour of polymer solutions in porous media, we measured pressure drop for 600 s and simultaneously visualized the streamlines. The pressure drop measurements from flow of polymer solutions were also used to calculate an apparent viscosity from Darcy's law. All experiments were performed at room temperature, $T = (22 \pm 2)\,^{\circ}\mathrm{C}$.

Table 5.1: Carreau model fitted parameters for experimentally measured polymer solution shear-viscosity shown in fig. B.1 in the Appendix B.

Polymer & NaCl concentration	η_0 (Pa s)	η_∞ (Pa s)	n (-)	τ (s)
0.2 g L^{-1} PAA, 0 mM NaCl	2.71	0.001	0.24	88.17
0.2 g L^{-1} PAA, 6 mM NaCl	0.01	0.001	0.70	0.48

5.2.2. POLYMER SOLUTIONS

Polymer solutions used in the experiments were prepared by dissolving the required amount of polyacrylamide, PAA (Catalog No. 18522-100, Polyacrylamide/sodium acrylate - 70:30, Molecular Weight, MW = 18×10^6 g mol^{-1}, Polysciences, Inc.) in either brine or deionized (DI) water. Two PAA solutions at a concentration of $C = 0.2$ g L^{-1} in presence or absence of salt were prepared. The first polymer solution was prepared by using deionized (DI) water as a solvent, whereas the second polymer solution was prepared using a 6 mM NaCl solution in DI water as solvent. Adding salt fixes the ionic strength of the polymer solution, reduces the relaxation time and also suppresses the shear-thinning effect. We chose to limit salt concentration to 6 mM such that the shear rheology is still shear-thinning, since at higher salt concentrations the shear-viscosity became nearly independent of the shear-rate. In the earlier chapter, we found that DZ forms in shear-thinning polymer solutions and that the DZ ceases to exist when shear-viscosity is independent of the shear-rate.[6]

After adding the polymer granules to the solvent, the bottle was covered with an opaque material such as aluminium foil to minimize photo-degradation.[60, 61] The approximate radius of gyration for PAA in DI water was estimated from the scaling relation, $R_g = 0.0749 \times \text{MW}^{0.64}$ Å,[56] as 330 nm. The critical overlap concentration for PAA in DI water was estimated as 200 µg mL^{-1} according to the formula, $C^* = (3 \cdot \text{MW}) / \left(4\pi N_A R_g^3\right)$. Here, C^* is the overlap concentration; N_A is the Avogadro's number; and R_g is the radius of gyration. Therefore, our polymer solutions are close to the semi-dilute regime. The shear viscosity of our polymer solution was measured in a Couette geometry (cup ID = 28.92 mm, bob OD = 26.668 mm, gap = 1.626 mm) using a commercial rheometer, (MCR-302, Anton Paar GmBH) and is plotted in fig. B.1. Both the polymer solutions showed shear-thinning behaviour which is correlated to the DZ size.[6] The relaxation time was estimated by fitting the shear rheology to the Carreau model,

$$\eta - \eta_\infty = (\eta_0 - \eta_\infty)\left[1 + (\tau\dot{\gamma})^2\right]^{\frac{n-1}{2}} \tag{5.1}$$

Here, η (Pa s) is the viscosity; η_0 is the zero-shear viscosity; η_∞ is the infinite shear viscosity; n is the power-law index; and τ is the estimated relaxation time. We could not measure η_∞, and therefore it was set to the viscosity of our solvent (DI water and aq. 6 mM NaCl), $\eta_\infty = 10^{-3}$ Pa s. For shear-thinning polymer solutions, the η_∞ is equal to the viscosity of the solvent in which the polymer chains are dispersed.[10]

The Carreau model was fitted to the shear-viscosity experimental data by non-linear least-square regression. Table 5.1 lists the fitting parameters of the Carreau model. The Weissenberg number, Wi, was then calculated as $Wi = \tau\dot{\gamma}_{\text{app}}$, where $\dot{\gamma}_{\text{app}} = v/(D/2)$ is the apparent shear rate in the microfluidic geometry; D is the diameter of the cylinder. Note that Wi number is calculated based on the relaxation time of PAA. All experiments were done at the room temperature, $T = (22 \pm 2)\,^{\circ}$C.

5.2.3. FLOW VISUALIZATION

To push the working solutions through the microfluidic devices, a syringe pump (PHD 2000, Havard Instruments) fitted with Hamilton Gastight syringes was used. The connection from the syringe to the microfluidic device was made by using a PTFE tubing (ID = 0.5 mm, OD = 1.6 mm). In order to visualize the streamlines, the polymer solutions were seeded with 1 − µm-dyed-red aqueous fluorescent particles (emission 542 nm/excitation 612 nm wavelength, Catalog # R0100, Thermo Scientific$^{\text{TM}}$) at ~0.1 % (w/w) concentration. The entire microfluidic device assembly was installed on top of an inverted fluorescent microscope (Axiovert 100M, Carl Zeiss AG) fitted with a 10X (N.A. = 0.5) magnification objective and a high-speed camera (Phantom v9.1, Vision Research Inc.) to record videos. All streamlines were visualized near the exit of the periodic array of pillars within the microfluidic device, with the focal plane adjusted at the center along the vertical axis to minimize contribution from top/bottom wall effects.

5.2.4. DNA VISUALIZATION

To visualize polymer conformation during flow, we used fluorescently stained T4-DNA molecules which were purchased from Nippon Gene Co. Ltd. at concentration of 440 µg mL^{-1} in 10 mM Tris (pH = 8.0) and 1 mM EDTA, 165 600 base-pairs. The contour length L_c of T4-DNA was 56 µm, which is close to the contour length of PAA (53 µm). YOYO-1 dye (Molecular Probes Inc.) was used to stain T4-DNA solution at a base-pair to dye ratio of 5:1. Finally, in order to prevent photo-degradation, 20 % (v/v) of β-mercaptanol was added to the T4-DNA solution. The resulting solution of stained DNA molecules in the buffer solution and β-mercaptanol was labelled as the DNA mother stock solution. For DNA-imaging, we dissolved 10 µL of the DNA mother stock solution in 5 mL of the

polymer solutions. Eventually, the working polymer solutions for DNA visualization contain around 0.01 parts per million (PPM) of DNA molecules. DNA was imaged on an inverted fluorescence microscope (Zeiss AxioObserver-Z1, Carl Zeiss AG) fitted with an EMCCD camera (ANDOR ixon3, Andor Technology Ltd.). The recorded DNA images had a resolution of 512×512 pixels (px) at the frame acquisition rate of 34 (fps). The frame acquisition rate could be increased up to 127 fps, with 4×4 image binning. These frame-acquisition rates are sufficiently high to capture DNA motion inside the DZ without blur for flow rates reported in this chapter. We increased the frame acquisition rate upto the maximum achievable (127 fps) for flow rates between $5\,\mu m\,min^{-1}$ and $50\,\mu m\,min^{-1}$ to ensure motion blur does not introduce artefacts during DNA visualization experiments. DNA conformation near multiple pillars was imaged. We choose pillars close to the exit of the array of pillars.

DNA imaging was performed upstream of the pillar such that the conformation within a DZ can be captured. Using ImageJ, we extracted the end-to-end vector of the DNA chain, $\vec{R}$. The fluorescent microscopy technique employed in current work visualizes along an xy-plane, where x is along the length and y is the along the width of the microfluidic device. The depth of field is around 5 to 10 µm depending on the objective lenses. Therefore, the extracted end-to-end vector would be a projection of the true 3D DNA chain conformation on the xy-plane. The magnitude of this vector is termed as the DNA length, and its direction is the orientation angle, θ (see a schematic in fig. B.4). Two objective lenses were used during imaging, namely 40X (N.A. = 1.3) or 63X (N.A. = 1.0) giving a single pixel resolution of 0.4 (µm/px) or 0.25 (µm/px) respectively. The corresponding field of view with the 40X objective was $205 \times 205\,\mu m^2$ and with the 63X objective it was $128 \times 128\,\mu m^2$. All the DNA lengths and orientations angles are plotted as a probability distribution, with a bin width of 5.5 µm and 18° respectively.

PAA molecules can not be visualized natively, and hence we used T4-DNA molecules as a molecular probe. Using T4 or λ-DNA molecules as molecular probes in a solution of PAA or PEO solutions has been fruitful in linking the molecular conformation with the macroscopic flow phenomena, such as (1) drag enhancement, [62, 63] (2) droplet pinch-off,[42, 43] (3) elastic turbulence, [57, 64] (4) impacting droplets,[65] and (5) unstable polymeric flows in a straight channel due to an initial perturbation.[66] In order to ensure that the DNA stretching is representative of the PAA conformation, we performed DNA-imaging at $Wi < 1$ and at $Wi > 1$ (see fig. 5.2a,b). The coil-stretch transition is observed in the range of $Wi = 0.5$ to $Wi = 1$.[10, 34] If the DNA molecules also undergo C-S transition in the vicinity of the Wi number based on the relaxation time of (PAA) polymer solution, then we can conclude that the C-S transition of the DNA molecules

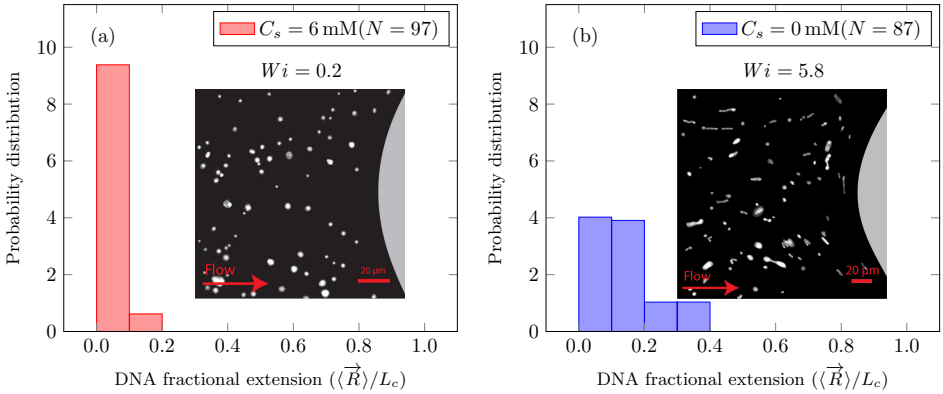


Figure 5.2: DNA fractional extension probability distribution at $\dot{\gamma}_{\text{app}} = 0.07\,\text{s}^{-1}$ upstream a pillar at (a) $Wi = 0.2$, $C_s = 6\,\text{mM}$ and (b) $Wi = 5.8$, $C_s = 0\,\text{mM}$. Inset shows the fluorescent image of DNA molecules and also the imaging location with respect to the pillar. N is the number of DNA molecules measured.

5

also occurs at comparable time scales. Such a sanity check can validate utility of using fluorescent DNA molecules as a tracer for PAA molecule conformation. Furthermore, recently Liu *et al.* [67] suggested that the relaxation time of T4-DNA and PAA are comparable in dilute and semi-dilute regime. Therefore, we expect that at $Wi < 0.5$, the DNA would be predominantly in the coiled conformation. Indeed, in fig. 5.2a we show that when $Wi = 0.2$ the DNA remains in the coiled conformation (mean fractional extension, $\mu = 0.06$). Furthermore, we also confirm that at $Wi = 0.2$, flow of saline polymer solution was uniform (referred as creeping flow). Similarly, we expect that at $Wi > 1$, the DNA would exist in the stretched conformations. Indeed, in fig. 5.2b we show that for $Wi = 5.8$ the DNA molecules have began to stretch with a fractional extension of up to 0.4 (mean fractional extension, $\mu = 0.15$). At $Wi = 5.8$, DZ formation was observed. DZ formation was the onset of non-Newtonian effects, which emerged at $Wi \sim 1$. While, the DNA-extension probability distribution shown in the fig. 5.2b for $Wi = 5.8$ are in polymer solutions prepared with DI water ($C_s = 0\,\text{mM}$, where C_s is the NaCl concentration), we also note that the DNA begins to stretch at $Wi > 1$ in the presence of salt as shown later in the manuscript. This shows that the DNA undergoes coil-stretch transition at a comparable time-scale to that of our polymer solutions during flow through the periodic array of pillars.

5.3. RESULTS AND DISCUSSION

5.3.1. APPARENT VISCOSITY AND STREAMLINE VISUALIZATION

The standard deviation of pressure drop fluctuations, std(ΔP) $\sim$ 0.1 mbar when DZ formation is observed during flow of PAA solutions with and without salt, and also for Newtonian fluid flow (fig. B.2a). At a certain $\dot{\gamma}_{app}$, the pressure fluctuations increased over those for Newtonian fluid, and simultaneously the flow-field transitioned to DZW. The onset apparent shear rate, $\dot{\gamma}_{onset}$ was determined as the intersection of two curves: first one obtained by fitting a power-law in the DZW region and the second one obtained by fitting a power-law to the Newtonian fluid std(ΔP) as shown in fig. B.2a. In absence of salt, the onset apparent shear rate was $\dot{\gamma}_{onset}^{C_s=0\,mM} = 9.5\,s^{-1}$ ($Ma \sim 1$, $Wi \sim 842$), whereas in presence of 6 mM NaCl, the onset apparent shear rate is $\dot{\gamma}_{onset}^{C_s=6\,mM} = 15.8\,s^{-1}$ ($Ma \sim 1$, $Wi \sim 8$).

The apparent viscosity for salt-free polymer solutions is three times higher than that for saline polymer solutions at the $\dot{\gamma}_{onset}$ (fig. B.2b). In the absence of salt, the apparent shear-viscosity is in the apparent shear-thinning region over $\dot{\gamma}_{app} = 0.1$ to $300\,s^{-1}$. However, in the case of saline polymer solutions, the apparent shear-viscosity is shear-thinning up to the $\dot{\gamma}_{onset} = 15.8\,s^{-1}$, beyond which apparent shear-thickening is observed. Fig. B.6 shows the ratio of the apparent viscosity to the steady shear viscosity at the apparent shear rate versus the Wi number. We can see that such a viscosity ratio shows a dramatic increase for both the polymer solutions. For $C_s = 0$ mM, such an increase in the viscosity ratio occurs at $Wi \sim 1$ whereas for $C_s = 6$ mM, it occurs at $Wi \sim 1000$. The increase in viscosity ratio appears to correlate with the onset of DZW-instability and consequently with the apparent shear-thickening region. An apparent shear-thickening region has been commonly observed for flow of polymer solutions in porous media.[5, 6, 68–71]

Using streamline visualization, we mapped how the flow-field changes with respect to the flow rate. In fig. 5.3a we represent this on a $Wi - Re$ flow space map. The DZ formation for flow of shear-thinning polymer solutions in periodic array of pillars occurs at $Ma \leq 1$.[6] In the case of Boger fluid, no DZ formation was observed.[6] However, for Boger fluid flow around a single cylinder, DZ-like flow field was observed upstream the cylinder at $Ma \sim 10$.[23, 24] In our previous chapter, we discussed the local flow field kinetics in DZ. For the specific experimental conditions of the current manuscript, the velocity field measurement using Particle Image Velocimetry (PIV) can be found in fig. B.5 In fig. B.5a we show the specific streamlines for 0.2 g L^{-1} PAA in DI water and in fig. B.5b the corresponding velocity field calculated by PIV is shown. Fig. B.5c shows a zoomed-in image of the velocity field inside a DZ. The velocity inside the DZ is close to zero whereas the velocity outside the DZ is $\sim 3 \times 10^{-4}$ m s^{-1}. Downstream a pillar,

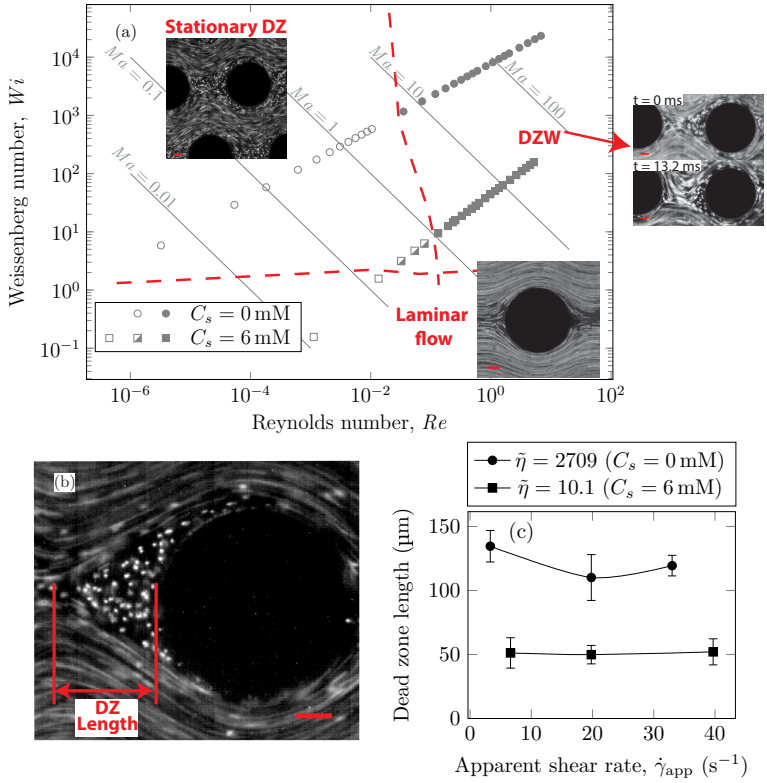


Figure 5.3: (a) Wi - Re flow space map showing that the transition from DZ (open symbols) to DZW instability (closed symbols) occurs at $Ma \sim 1$. Below $Wi \sim 1$ laminar flow (half open symbols) is obtained. The streamline snapshots show laminar flow at $\dot{\gamma}_{app} = 0.07\,s^{-1}$, $Wi = 0.03$ ($C_s = 6$ mM); stationary DZ at $\dot{\gamma}_{app} = 3.3\,s^{-1}$, $Wi \sim 291$ ($C_s = 0$ mM); wobble of DZ in the DZW regime at $\dot{\gamma}_{app} = 20\,s^{-1}$, $Wi \sim 1164$ ($C_s = 0$ mM) (b) Streamline snapshot showing DZ location and definition of DZ length. (c) Plot showing DZ length remains roughly constant over $\dot{\gamma}_{app}$. Error bars indicate standard deviation of DZ length measured over 15 DZs at multiple pillars. $\tilde{\eta} = \eta_0/\eta_\infty$. All scale bars = 50 μm; flow direction is from left to right.

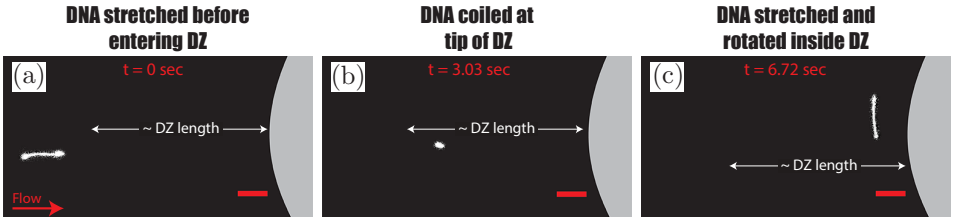


Figure 5.4: Sequence of images showing (a) stretched DNA chain approaching a pillar before entering DZ, (b) re-coiled DNA chain at roughly the tip of DZ and (c) re-stretched again and rotated inside the DZ. DZ length refers to the data shown in fig. 5.3c. $C_s = 0$ mM, $\dot{\gamma}_{app} = 3.3\,s^{-1}$, $Wi \sim 291$. Scale bar = 20 µm.

the velocity field converges at the tip of the DZ. Inside a DZ, the flow appears to be almost stationary. Close to the stagnation point upstream the pillar, we can observe an extensional flow field. A detailed report on steady-state and unstable velocity fields of polymer solution flow through periodic arrays of cylinder has been reported earlier.[72] In this work, we focus on the DZ formation in shear-thinning solutions. With increasing flow rate, the stationary DZs started wobbling in a direction perpendicular to the average flow direction and eventually got washed away. Dead zone washing (DZW) refers to this time-dependent instability and was observed at $Ma > 1$ for both polymer solutions as shown in fig. 5.3a. We measured the DZ length, defined as the shortest distance between the tip of DZ and the pillar (see fig. 5.3b for a schematic). Fig. 5.3c shows DZ length, l_{DZ}, versus the apparent shear rate, $\dot{\gamma}_{app}$. For a given polymer system, l_{app} is practically independent of $\dot{\gamma}_{app}$.

5.3.2. DNA CONFORMATIONS

As the DNA chains approach the pillar, they undergo the coil-stretch transition. In our microfluidic device, the DNA chains undergo coil-stretch transition at the upstream of every pillar. We choose to visualize the DNA chain near the exit of the array of pillars. Our choice was motivated based on our previous chapter, in which we studied the dynamics of the DZW instability in a periodic array of pillars.[6] We observed that the DZW washing frequency (which is the inverse of the time that a DZ takes to form, grow and wash) reaches a pseudo-steady state after roughly the 4^{th} pillar column. Based on this, we decided to visualize DNA chain dynamics at a location where the DZ dynamics have certainly reached the pseudo-steady state. The prior deformation history of DNA chains near the exit of pillared array (visualization region) is then assumed to have reached a certain pseudo-steady state similar to DZW washing frequency. Further research is necessary to understand the effect of DNA chain dynamics at varying deformation histories

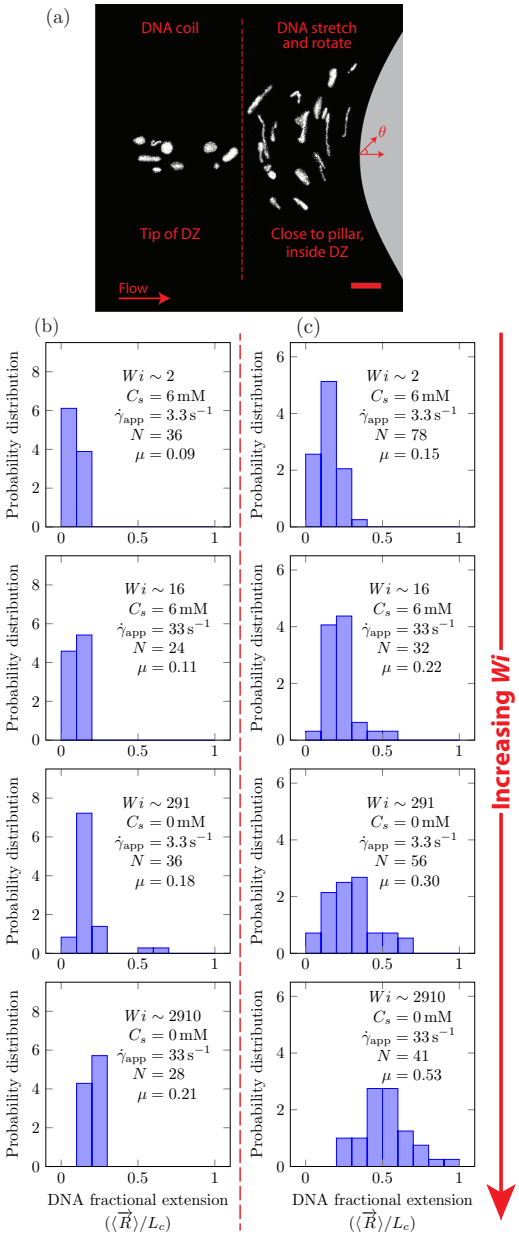


Figure 5.5: (a) DNA molecules visualized at $\dot{\gamma}_{app} = 3.3\,s^{-1}$ upstream the pillar for $C_s = 0$ mM NaCl. At the tip of the DZ, the DNA is coiled (to the left of dashed line) whereas within the DZ the DNA is stretched and rotated (to the right of dashed line). Probability distribution of DNA fraction extensional as Wi number increases at the (b) tip of DZ and (c) inside the DZ. N is the number of DNA molecules measured. In (a) the scale bar is 20 µm.

in a periodic array of pillars.

The coil-stretch transition occurs in both the polymer solutions. In fig. 5.4 (a-c) we the DNA conformation at $\dot{\gamma}_{app} = 3.3\,s^{-1}$, $C_s = 0\,mM$ as an example. The DNA chain is stretched and oriented in the average flow direction (see fig. 5.4a) before entering a DZ. This stretched conformation is likely because of the converging-diverging nature of flow in staggered array of pillars. As the DNA chain moves closer to the pillar, it re-coils (see fig. 5.4b). By comparing the position of the DNA-coiling region from the DNA-imaging experiments with the DZ size from streamline visualization experiment, we note that the DNA re-coiling process occurs roughly at the tip of the DZ. After re-coiling, as the DNA chain traverses closer to the pillar, inside the DZ, it unravels to stretch and rotate in a direction perpendicular to the average flow direction (see fig. 5.4c). Therefore, the DNA chains appear to align along the local flow-field upstream of the pillars inside the DZs. The Large Amplitude Oscillatory Extension experiments (LAOE) represent realistic flows better than the idealized stead-state or elongational flow fields that are typically used to characterize polymer rheology. LAOE flow field can be obtained using the Stokes trap with a model predictive control,[73] allowing for precise positioning and manipulating particles in flow. Recently, the Stokes trap was used to impose a LAOE flow and investigate single polymer dynamics. Polymer chain LAOE dynamics, under varying flow strength, like re-stretch–re-coil–re-stretch were studied to obtain the single-molecule Lissajous plots showing molecular stretch-strain rate curves.[74] In a followup study, the transient response during LAOE was investigated.[75] Understanding these molecular processes are crucial for studying time-dependent flow of polymer solutions such as the instabilities reported in this chapter.

In fig. 5.5, we quantify the DNA chain coil-stretch transition inside DZ by measuring the probability distribution of DNA fractional extensions as the apparent Wi increases. In fig. 5.5a, we superimpose conformation of multiple DNA chains as it enters the DZ at $\dot{\gamma}_{app} = 3.3\,s^{-1}$, $Wi = 291$, $C_s = 0\,mM$. The DNA chains at the tip of DZ are in coiled conformation, whereas inside the DZ they are stretched and rotated by $\theta \sim 90°$. Fig. 5.5b shows the probability distribution of DNA fractional extension in the coiled-state (tip of DZ) for both salt-free and saline polymer solutions. The mean fractional extension, μ varies from 0.09 to 0.21 as the apparent Wi number increases from 1.6 to 2910 respectively. On the other hand, fig. 5.5c shows the probability distribution of DNA fractional extension in the stretched-state (inside DZ) for both salt-free and saline polymer solutions. As Wi increases, the probability distribution shifts to higher fractional extensions. The mean fractional extension μ increases from 0.15 to 0.53 as the Wi increases from 1.6 to 2910 respectively. The mean and skewness of the probability distribution are summarized in

table B.1, whereas the probability distribution of the DNA orientation angle, θ, inside the DZ is shown in fig. B.3.

The shape of distribution (for example uniform or positively/negatively skewed) of DNA fractional extensions depends on the flow-field and the Wi number. In steady-shear flow of dilute DNA solutions, Smith *et al.* [26] found that as Wi increases from $\mathcal{O}(1)$ to $\mathcal{O}(100)$, the distribution moves from positively skewed to uniform, respectively. Later, Teixeira *et al.* [45] reported similar changes in distribution shape in semi-dilute and entangled DNA solutions. François *et al.* [62] studied the flow of Boger fluid around a single cylinder. Using DNA-imaging near the vicinity of cylinder ($\theta = 90°$ according to fig. 5.5a) they showed that at $Wi = \mathcal{O}(1)$, the DNA close to cylinder is stretched with $\mu = 0.33$, with a positively skewed distribution. In fig. 5.5b-c ($Wi \sim 2$), we also find that the distribution is positively skewed (also see table B.1 for skewness values); however, the mean fractional extension, $\mu = 0.15$. Few polymer chains at $Wi \sim 2910$ are fully stretched, however, the distribution of polymer conformations is still heterogenous with the mean fractional extension of roughly half.

Maximum polymer chain extension in an extension flow-field has been reported for dilute solutions[27] and semi-dilute solutions.[76] In semi-dilute solutions, broader distribution of chain extensions are observed in transient extensional flow compared to dilute solutions.[76] Intermolecular interactions between polymer chains in the semi-dilute region are suggested as a cause for the broad distribution of chain extensions. Upon reaching steady-state extension, the polymer chain fractional extension in dilute-solutions was found to be higher than in semi-dilute solutions. A closer examination of the Wi number at which the coil-stretch transition occurs in both dilute and semi-dilute solutions revealed that this Wi number depends on the concentration.[76] Polymer chain extension in an *random-flow* has also been reported for dilute and semi-dilute solutions.[57] A polymer chain's extension increases with the accumulated fluid strain at the stagnation point of the extension flow-field.[27, 76] In our microfluidic experiments, the flow field upstream of the pillar is a planar-extensional flow, similar to the flow in a microfluidic T-junction. The flow-field upstream the pillar diverges creating a region with extensional flow-field.

The fact that we measured the DNA orientation-angle of $\sim 90°$ within the DZ indicates that the DNA chains are aligned along the extensional flow component of the mixed flow-field upstream of the pillar. To study the effect of local Weissenberg number, Wi_{loc}, on the DNA fractional extension inside DZ, we calculated the DNA velocity inside DZ, v_{DNA}. The v_{DNA} was calculated by averaging the velocity of 20 DNA chains by DNA tracking velocimetry ($v_{\mathrm{DNA}} \sim 19$ - $575\,\mu\mathrm{m\,s}^{-1}$). In particular, we tracked the mid-point

Table 5.2: Summary of DNA fractional extension inside DZ, local Wi and DNA velocity inside DZ. The standard deviation of Wi_{loc} and v_{DNA} values is based on the ensemble of 20 individual DNA tracking velocimetry measurements, whereas the standard deviation of DNA fractional extension is based on the number of DNA molecules measured as shown in fig. 5.5c.

DNA fractional extension (-)	Wi_{loc} (-)	v_{DNA} ($\mu m\,s^{-1}$)
0.15 ± 0.07	0.72 ± 0.31	78.48 ± 27.43
0.22 ± 0.10	4.78 ± 1.81	497.19 ± 174.17
0.30 ± 0.15	12.63 ± 3.62	19.28 ± 5.24
0.53 ± 0.18	458.89 ± 178.13	573.29 ± 202.09

of the DNA end-to-end vector. The distance between the midpoint of a DNA in the coiled state (at the tip of DZ) to the midpoint of the same DNA when it reaches the stagnation point upstream the obstacle divided by the time this particular DNA chain takes is defined as the velocity of DNA chains. v_{DNA}. In this way, v_{DNA} accounts for the transient residence time of DNA chains inside the DZ in the calculation of the Wi_{loc} number. Additionally, we also used the DNA residence time in the DZ to calculate a local Deborah number, De_{loc}. The De_{loc} values are reported in tab. B.2. Note that the average velocity outside the DZ has a value of $\sim 430\,\mu m\,s^{-1}$ at both salt concentrations. Then, $Wi_{loc} = \tau \cdot (v_{DNA}/L_{DZ})$, where L_{DZ} is DZ length as shown in fig. 5.3c. This Wi_{loc} quantifies the transient time scale of flow inside the DZ. As the Wi_{loc} increases from 0.72 ± 0.31 until 458.89 ± 178.13, the DNA fractional extension increases from 0.15 ± 0.07 to 0.53 ± 0.18 inside DZ (see table 5.2).

5.4. CONCLUSIONS

We investigated the stationary dead-zone (DZ) and dead-zone washing (DZW) elastic instabilities of polymer solutions in porous media at the molecular scale. The DNA chain is coiled at the tip of the DZ. Close to the stagnation point upstream the pillar inside the DZ, the DNA chain stretches and rotates in a direction perpendicular to the average flow direction. The mean fractional extension of DNA chain at the DZ-tip is roughly the same in the DZ and the DZW instability for a given polymer solution. Inside the DZ, the DNA chains appear as if they are in a planar-extensional flow-field, with a positively skewed distribution of fractional extension. The fractional extension distribution for DNA chains inside the DZ shifts to higher extensions as the apparent Wi increases. The mean fractional extension in the DZ instability at constant apparent shear-rate ($3.3\,s^{-1}$) is 0.3 and 0.15 for salt-free and saline polymer solutions respectively. The difference is attributed to the higher local Weissenberg number inside DZ, as calculated by DNA

tracking velocimetry.

We believe that microfluidics combined with single molecule experiments can provide a unique opportunity to study the dynamics of single chains in pore-scale flow features of various polymer solutions (ranging from dilute to well-entangled solutions with different architectures) in a realistic porous medium. These single molecule experiments can aid in developing a realistic theoretical picture of polymer solutions during flow in porous media.

REFERENCES

[1] J. Dealy and R. Larson, *Structure and Rheology of Molten Polymers* (Hanser Publications, 2006).

[2] R. B. Bird, ed., *Dynamics of polymeric liquids*, 2nd ed. (Wiley, New York, 1987) p. 2.

[3] M. Rubinstein and R. H. Colby, *Polymer physics*, Vol. 23 (Oxford University Press New York, 2003).

[4] J. D. Ferry, *Viscoelastic properties of polymers* (John Wiley & Sons, 1980).

[5] A. M. Howe, A. Clarke, and D. Giernalczyk, *Flow of concentrated viscoelastic polymer solutions in porous media: effect of mw and concentration on elastic turbulence onset in various geometries,* Soft matter **11**, 6419 (2015).

[6] D. Kawale, E. Marques, P. L. J. Zitha, M. T. Kreutzer, W. R. Rossen, and P. E. Boukany, *Elastic instabilities during the flow of hydrolyzed polyacrylamide solution in porous media: effect of pore-shape and salt,* Soft Matter **13**, 765 (2017).

[7] A. Machado, H. Bodiguel, J. Beaumont, G. Clisson, and A. Colin, *Extra dissipation and flow uniformization due to elastic instabilities of shear-thinning polymer solutions in model porous media,* Biomicrofluidics **10**, 043507 (2016).

[8] C. Chmielewski and K. Jayaraman, *The effect of polymer extensibility on crossflow of polymer solutions through cylinder arrays,* Journal of Rheology **36**, 1105 (1992).

[9] D. F. James and A. J. Acosta, *The laminar flow of dilute polymer solutions around circular cylinders,* Journal of Fluid Mechanics **42**, 269 (1970).

[10] C. W. Macosko, ed., *Rheology: principles, measurements, and applications* (VCH, New York, 1994) p. 550.

[11] J. G. Savins, *Non-newtonian flow through porous media,* Industrial & Engineering Chemistry **61**, 18 (1969).

[12] R. P. Chhabra, J. Comiti, and I. Machač, *Flow of non-newtonian fluids in fixed and fluidised beds,* Chemical Engineering Science **56**, 1 (2001).

[13] S. Flew and R. Sellin, *Non-newtonian flow in porous media-a laboratory study of polyacrylamide solutions,* Journal of non-newtonian fluid mechanics **47**, 169 (1993).

[14] T. Sochi, *Flow of non-newtonian fluids in porous media,* Journal of Polymer Science Part B: Polymer Physics **48**, 2437 (2010).

[15] F. J. Galindo-Rosales, L. Campo-Deaño, F. Pinho, E. Van Bokhorst, P. Hamersma, M. Oliveira, and M. Alves, *Microfluidic systems for the analysis of viscoelastic fluid flow phenomena in porous media,* Microfluidics and nanofluidics **12**, 485 (2012).

[16] M. Grilli, A. Vázquez-Quesada, and M. Ellero, *Transition to turbulence and mixing in a viscoelastic fluid flowing inside a channel with a periodic array of cylindrical obstacles,* Physical review letters **110**, 174501 (2013).

[17] B. Khomami and L. D. Moreno, *Stability of viscoelastic flow around periodic arrays of cylinders,* Rheologica acta **36**, 367 (1997).

[18] C. Chmielewski and K. Jayaraman, *Elastic instability in crossflow of polymer solutions through periodic arrays of cylinders,* Journal of non-newtonian fluid mechanics **48**, 285 (1993).

[19] A. Clarke, A. M. Howe, J. Mitchell, J. Staniland, L. Hawkes, and K. Leeper, *Mechanism of anomalously increased oil displacement with aqueous viscoelastic polymer solutions,* Soft matter **11**, 3536 (2015).

[20] X. Hu, P. E. Boukany, O. L. Hemminger, and L. J. Lee, *The use of microfluidics in rheology,* Macromolecular Materials and Engineering **296**, 308 (2011).

[21] L. Rems, D. Kawale, L. J. Lee, and P. E. Boukany, *Flow of dna in micro/nanofluidics: From fundamentals to applications,* Biomicrofluidics **10**, 043403 (2016).

[22] C. Scholz, F. Wirner, J. R. Gomez-Solano, and C. Bechinger, *Enhanced dispersion by elastic turbulence in porous media,* EPL (Europhysics Letters) **107**, 54003 (2014).

[23] S. Kenney, K. Poper, G. Chapagain, and G. F. Christopher, *Large deborah number flows around confined microfluidic cylinders,* Rheologica Acta **52**, 485 (2013).

[24] X. Shi, S. Kenney, G. Chapagain, and G. F. Christopher, *Mechanisms of onset for moderate mach number instabilities of viscoelastic flows around confined cylinders,* Rheologica Acta **54**, 805 (2015).

[25] Y. Zhao, A. Q. Shen, and S. J. Haward, *Flow of wormlike micellar solutions around confined microfluidic cylinders,* Soft Matter **12**, 8666 (2016).

[26] D. E. Smith, H. P. Babcock, and S. Chu, *Single-polymer dynamics in steady shear flow,* Science **283**, 1724 (1999).

[27] T. T. Perkins, D. E. Smith, and S. Chu, *Single polymer dynamics in an elongational flow,* Science **276**, 2016 (1997).

[28] P. Van Puyvelde, C. Clasen, P. Moldenaers, and J. Vermant, *Rheo-physical and imaging techniques,* Rheology-Volume I , 359 (2010).

[29] G. G. Fuller, *Optical rheometry,* Annual Review of Fluid Mechanics **22**, 387 (1990).

[30] A. B. Marciel and C. M. Schroeder, *New directions in single polymer dynamics,* Journal of Polymer Science Part B: Polymer Physics **51**, 556 (2013).

[31] G. R. Moss and J. P. Rothstein, *Flow of wormlike micelle solutions past a confined circular cylinder,* Journal of Non-Newtonian Fluid Mechanics **165**, 1505 (2010).

[32] G. R. Moss and J. P. Rothstein, *Flow of wormlike micelle solutions through a periodic array of cylinders,* Journal of Non-Newtonian Fluid Mechanics **165**, 1 (2010).

[33] C.-l. Sun and H.-Y. Huang, *Measurements of flow-induced birefringence in microfluidics,* Biomicrofluidics **10**, 011903 (2016).

[34] T. T. Perkins, Quake, D. E. Smith, and S. Chu, *Relaxation of a single dna molecule observed by optical microscopy,* Science **264**, 822 (1994).

[35] T. T. Perkins, D. E. Smith, and S. Chu, *Direct observation of tube-like motion of a single polymer chain,* Science **264**, 819 (1994).

[36] P. G. De Gennes, *Scaling concepts in polymer physics* (Cornell university press, 1979).

[37] M. Doi and S. Edwards, *The theory of polymer dynamics clarendon,* (1986).

[38] C. M. Schroeder, H. P. Babcock, E. S. G. Shaqfeh, and S. Chu, *Observation of polymer conformation hysteresis in extensional flow,* Science **301**, 1515 (2003).

[39] C. M. Schroeder, E. S. G. Shaqfeh, and S. Chu, *Effect of hydrodynamic interactions on dna dynamics in extensional flow:: Simulation and single molecule experiment,* Macromolecules **37**, 9242 (2004).

[40] C. M. Schroeder, R. E. Teixeira, E. S. G. Shaqfeh, and S. Chu, *Characteristic periodic motion of polymers in shear flow,* Physical Review Letters **95**, 018301 (2005).

[41] G. Juarez and P. E. Arratia, *Extensional rheology of dna suspensions in microfluidic devices,* Soft Matter **7**, 9444 (2011).

[42] F. Ingremeau and H. Kellay, *Stretching polymers in droplet-pinch-off experiments,* Physical Review X **3**, 041002 (2013).

[43] S. Sachdev, A. Muralidharan, and P. E. Boukany, *Molecular processes leading to "necking" in extensional flow of polymer solutions: Using microfluidics and single dna imaging,* Macromolecules (2016).

[44] P. E. Boukany, O. Hemminger, S.-Q. Wang, and L. J. Lee, *Molecular imaging of slip in entangled dna solution,* Physical review letters **105**, 027802 (2010).

[45] R. E. Teixeira, A. K. Dambal, D. H. Richter, E. S. G. Shaqfeh, and S. Chu, *The individualistic dynamics of entangled dna in solution,* Macromolecules **40**, 2461 (2007).

[46] H. P. Babcock, D. E. Smith, J. S. Hur, E. S. Shaqfeh, and S. Chu, *Relating the microscopic and macroscopic response of a polymeric fluid in a shearing flow,* Physical review letters **85**, 2018 (2000).

[47] J. S. Hur, E. S. G. Shaqfeh, H. P. Babcock, D. E. Smith, and S. Chu, *Dynamics of dilute and semidilute dna solutions in the start-up of shear flow,* Journal of Rheology (1978-present) **45**, 421 (2001).

[48] N. P. Teclemariam, V. A. Beck, E. S. Shaqfeh, and S. J. Muller, *Dynamics of dna polymers in post arrays: Comparison of single molecule experiments and simulations,* Macromolecules **40**, 3848 (2007).

[49] K. D. Dorfman, S. B. King, D. W. Olson, J. D. Thomas, and D. R. Tree, *Beyond gel electrophoresis: Microfluidic separations, fluorescence burst analysis, and dna stretching,* Chemical reviews **113**, 2584 (2012).

[50] C. D. DeLong and D. A. Hoagland, *Imaging of individual polymers undergoing flow in a bed of small spheres,* Macromolecules **41**, 4887 (2008).

[51] K. D. Dorfman, *Dna electrophoresis in microfabricated devices,* Reviews of Modern Physics **82**, 2903 (2010).

[52] G. C. Randall and P. S. Doyle, *Dna deformation in electric fields: Dna driven past a cylindrical obstruction,* Macromolecules **38**, 2410 (2005).

[53] O. L. Hemminger, P. E. Boukany, S.-Q. Wang, and L. J. Lee, *Flow pattern and molecular visualization of dna solutions through a 4: 1 planar micro-contraction,* Journal of Non-Newtonian Fluid Mechanics **165**, 1613 (2010).

[54] S. Gulati, S. J. Muller, and D. Liepmann, *Flow of dna solutions in a microfluidic gradual contraction,* Biomicrofluidics **9**, 054102 (2015).

[55] P. E. Boukany, S.-Q. Wang, S. Ravindranath, and L. J. Lee, *Shear banding in entangled polymers in the micron scale gap: a confocal-rheoscopic study,* Soft Matter **11**, 8058 (2015).

[56] J. Francois, D. Sarazin, T. Schwartz, and G. Weill, *Polyacrylamide in water: molecular weight dependence of< r 2> and [η] and the problem of the excluded volume exponent,* Polymer **20**, 969 (1979).

[57] Y. Liu and V. Steinberg, *Single polymer dynamics in a random flow,* in *Macromolecular Symposia*, Vol. 337, Wiley Online Library (Wiley Online Library, 2014) pp. 34–43.

[58] D. E. Smith and S. Chu, *Response of flexible polymers to a sudden elongational flow,* Science **281**, 1335 (1998).

[59] D. C. Duffy, J. C. McDonald, O. J. A. Schueller, and G. M. Whitesides, *Rapid prototyping of microfluidic systems in poly (dimethylsiloxane),* Analytical chemistry **70**, 4974 (1998).

[60] M. J. Caulfield, G. G. Qiao, and D. H. Solomon, *Some aspects of the properties and degradation of polyacrylamides,* Chemical reviews **102**, 3067 (2002).

[61] S. Vijayalakshmi and G. Madras, *Photocatalytic degradation of poly (ethylene oxide) and polyacrylamide,* Journal of applied polymer science **100**, 3997 (2006).

[62] N. François, D. Lasne, Y. Amarouchene, B. Lounis, and H. Kellay, *Drag enhancement with polymers,* Physical review letters **100**, 018302 (2008).

[63] N. François, Y. Amarouchene, B. Lounis, and H. Kellay, *Polymer conformations and hysteretic stresses in nonstationary flows of polymer solutions,* EPL (Europhysics Letters) **86**, 34002 (2009).

[64] S. Gerashchenko, C. Chevallard, and V. Steinberg, *Single-polymer dynamics: Coil-stretch transition in a random flow,* EPL (Europhysics Letters) **71**, 221 (2005).

[65] M. Smith and V. Bertola, *Effect of polymer additives on the wetting of impacting droplets,* Physical review letters **104**, 154502 (2010).

[66] D. Bonn, F. Ingremeau, Y. Amarouchene, and H. Kellay, *Large velocity fluctuations in small-reynolds-number pipe flow of polymer solutions,* Physical Review E **84**, 045301 (2011).

[67] Y. Liu, Y. Jun, and V. Steinberg, *Concentration dependence of the longest relaxation times of dilute and semi-dilute polymer solutions,* Journal of Rheology **53**, 1069 (2009).

[68] P. L. Zitha, G. Chauveteau, and L. Léger, *Unsteady-state flow of flexible polymers in porous media,* Journal of colloid and interface science **234**, 269 (2001).

[69] G. Chauveteau, M. Moan, and A. Magueur, *Thickening behaviour of dilute polymer solutions in non-inertial elongational flows,* Journal of non-newtonian fluid mechanics **16**, 315 (1984).

[70] F. Durst, R. Haas, and B. Kaczmar, *Flows of dilute hydrolyzed polyacrylamide solutions in porous media under various solvent conditions,* Journal of Applied Polymer Science **26**, 3125 (1981).

[71] R. Haas and F. Durst, *Viscoelastic flow of dilute polymer solutions in regularly packed beds,* in *Progress and Trends in Rheology* (Springer, 1982) pp. 212–217.

[72] S. De, J. van der Schaaf, N. Deen, J. Kuipers, E. Peters, and J. Padding, *Elastic instabilities in flows through pillared micro channels,* arXiv preprint arXiv:1607.03672 (2016).

[73] A. Shenoy, C. V. Rao, and C. M. Schroeder, *Stokes trap for multiplexed particle manipulation and assembly using fluidics,* Proceedings of the National Academy of Sciences **113**, 3976 (2016).

[74] Y. Zhou and C. M. Schroeder, *Single polymer dynamics under large amplitude oscillatory extension,* Physical Review Fluids **1**, 053301 (2016).

[75] Y. Zhou and C. M. Schroeder, *Transient and average unsteady dynamics of single polymers in large-amplitude oscillatory extension,* Macromolecules **49**, 8018 (2016).

[76] K.-W. Hsiao, C. Sasmal, J. R. Prakash, and C. M. Schroeder, *Direct observation of dna dynamics in semidilute solutions in extensional flow,* Journal of Rheology **61**, 151 (2017), http://dx.doi.org/10.1122/1.4972236 .

6

CONCLUSIONS AND OUTLOOK

6.1. CONCLUSIONS

This thesis was focussed on the fundamental understanding of polymer flows through porous media at $Wi > 1$. As polymer solutions flow through the complex pore-space within a porous medium, the flow behaviour markedly deviates from Newtonian fluids above $Wi \sim 1$. Conventionally, the polymer steady-shear viscosity was attributed to the apparent shear-thinning region, whereas the polymer extensional viscosity was attributed to the apparent shear-thickening behaviour. The total apparent viscosity curve could then be constructed as a superposition of polymer steady-shear and extensional viscosities. Such a phenomenological approach lacked predictive capabilities.

In this thesis, we identified the mechanism causing the apparent shear-thickening behaviour. By direct flow visualization through a microfluidic model of porous media we showed that both, the apparent shear-thinning as well as the apparent shear-thickening region of the apparent viscosity curve, contains non-Newtonian flow behaviour. Depending on the level of polymer shear-thinning, stationary dead zones are formed in the apparent shear-thinning region. As the apparent shear-rate is increased, if dead zones are formed, then a time-dependent elastic instability comprising of periodic washing of the dead zones causes the apparent shear-thinning behaviour. In case the polymer solution is not shear-thinning (also known as Boger fluid), a time-dependent elastic instability comprising of rapid bursts of flow-field fluctuations causes the apparent shear-thickening behaviour. Although the exact pore-shape determines the individual flow

features during elastic instability, the shape of the apparent viscosity curves does not significantly differ.

We then focussed on the molecular processes that occur during flow of polymer-solution through porous media. By using novel single-DNA visualization experiments we studied the polymeric conformation during flows through porous media, particularly during the dead zone formation and dead zone washing elastic instabilities. We found that when a stretched polymer chain enters a dead zone, it recoils. As the polymer chains approach an obstacle, it reorients and restretches upstream of the obstacle.

The following subsections contains the individual chapter conclusions.

6.1.1. POLYMER CHAIN DYNAMICS DURING SIMPLE AND COMPLEX FLOWS

Microfluidic systems have been utilized to probe, manipulate, and to visualize DNA molecules for various biomedical applications as well as fundamental studies concerning polymer rheology and physics. Recent progress and advances in fabrication of microfluidics have facilitated the study of polymer rheology at the single-molecule level. We have reviewed a selection of fundamental concepts in the flow of DNA inside microfluidics, which allows us to create a conceptual framework for nonlinear polymer rheology. This field is undergoing unprecedented changes, because DNA with different architecture and topology can be made and can serve as a new model for polymer scientists and engineers. We anticipate that future studies will focus on relating the polymer microstructure to bulk flow properties in flow fields relevant to the industry. In addition, new molecular-level experiments would be highly desirable in the flow of well-entangled polymer solution, to improve our theoretical understanding in nonlinear flow regimes.[1] Still, nonlinear rheological responses of well-entangled polymer such as shear banding and stress overshoot are not understood and under debate, therefore in-depth single-molecule studies of DNA are necessary to resolve the remaining issues in polymer rheology.[2] These examinations at the single-molecule level will allow us to create new models, by unraveling the detailed molecular mechanisms behind various nonlinear rheology phenomena.

6.1.2. ELASTIC INSTABILITIES DURING POLYMER SOLUTION FLOW THROUGH POROUS MEDIA

We find that polymer solution flowing through a model porous media ($Wi > 1.0$) shows two distinct elastic instabilities. The first elastic instability exists during an apparent shear-thinning regime at shear rate, $\dot{\gamma}_1 = 3.63\,\mathrm{s}^{-1}$ ($Wi \approx 80$, based on Carreau-Yasuda

relaxation time): stationary DZs appear around obstacles with fast flow-zones between them. The size of these DZs increases with the ratio of the zero-shear viscosity and the infinity-shear viscosity, η_0/η_∞, suggesting that the first type of elastic instability ceases to exist for weakly shear-thinning polymer solution. The second, elastic instability is at $\dot{\gamma}_2 \sim 30\,\mathrm{s}^{-1}$ ($Wi \approx 626$): DZs become unstable with strong temporal fluctuations in both pressure drop and flow field. In the case of polymer solutions without any added salt, the apparent shear-thinning behaviour corresponds with the second type of elastic instability. In the case of polymer solutions with salt, the onset of apparent shear-thickening corresponds with the second type of elastic instability. A direct comparison of η_{app} was possible by fabricating constant-porosity microfluidic geometries consisting of periodic arrays of square and cylindrical pillars in staggered and aligned layouts. The presence of sharp edges (square-staggered geometry) in realistic porous media can significantly alter the nature of elastic instabilities in porous media. The square-staggered geometry sustains more dead zones than a circle-staggered geometry. These DZs wash along the microfluidic geometry until they disintegrate violently into small eddies. These events cause pressure-drop fluctuations, which are characterized from their spectral density. The spectral density decays via a power law that has two distinct regions separated by an inflection point. The DZ and DZW flow instabilities were mapped on a $Wi-Re$ space-map. The transition from time-independent instability (such as the DZ) to time-dependent instability (such as the DZW or the non-DZW instability) occurs when the viscoelastic Mach number, $Ma \sim 1$.

Characterizing pore-scale flow features of polymer solutions in a realistic porous medium is often desired to identify the dominant mechanism of the dramatic increase in pressure loss. DZ washing appears to be a crucial element that feeds the cascade of events responsible for the typically observed dramatic increase in pressure drop. Quantifying the contribution of dead-zone washing to the total pressure drop in porous media, especially considering that a dead zone will eventually dissipate energy as small eddies, could improve the predictability of models for polymeric flow through porous media.

6.1.3. POLYMER CHAIN DYNAMICS DURING ELASTIC INSTABILITIES IN POROUS MEDIA

We investigated the stationary dead-zone (DZ) and dead-zone washing (DZW) elastic instabilities of polymer solutions in porous media at the molecular scale. The DNA chain is coiled at the tip of the DZ. Close to the stagnation point upstream the pillar inside the DZ, the DNA chain stretches and rotates in a direction perpendicular to the average flow direction. The mean fractional extension of DNA chain at the DZ-tip is roughly same in

the DZ and the DZW instability for a given polymer solution. Inside the DZ, the DNA chains appear as if they are in a planar-extensional flow-field, with a positively skewed distribution of fractional extension. The fractional extension distribution for DNA chains inside the DZ shifts to higher extensions as the apparent Wi increases. The mean fractional extension in DZ instability at constant apparent shear-rate ($3.3\,s^{-1}$) is 0.3 and 0.15 for salt-free and saline polymer solutions respectively. The difference is attributed to the higher local Weissenberg number inside DZ, as calculated by DNA tracking velocimetry.

We believe that microfluidics combined with single molecule experiments can provide a unique opportunity to study the dynamics of single chains in pore-scale flow features of various polymer solutions (ranging from dilute to well-entangled solutions with different architectures) in a realistic porous medium. These single molecule experiments can aid in developing a realistic theoretical picture of polymer solutions during flow in porous media.

6.2. OUTLOOK

In this thesis we investigated high Wi flow of polymer solutions through porous media. The results from this thesis can be used to identify several opportunities to advance the field of polymer EOR, as well as developing polymer structure-performance predictive capabilities. The following subsections are devoted to highlight some of these opportunities.

6.2.1. 2D POROUS MEDIA *versus* 3D POROUS MEDIA

In this thesis, we investigated flow in a planar (2D) microfluidic device. In a realistic geological porous media, the pore-space varies in 3D that can give rise to spatially heterogenous flow behaviour. Understanding the flow in 3D pore-space can be achieved by various techniques such as X-Ray computed tomography,[3] nuclear magnetic resonance imaging,[4] or by optical techniques. Optical techniques include matching refractive index of fluids with that of the porous material (for instance glass beads).[5, 6] Utilizing such an optical technique to probe 3D flows of polymer solutions in porous media is a suitable method to investigate the elastic instabilities in a realistic porous medium.

6.2.2. EFFECT OF OIL ON ELASTIC INSTABILITIES

All the results shown in this thesis are based on single-phase flow of polymer solutions through porous media. In order to utilize our findings for polymer EOR processes, it is

essential to study the effect elastic instabilities have on the oil recovery. Recently, Clarke *et al.* [4] suggested that the time-dependent elastic instabilities increase the displacement efficiency of a polymer flood. This implies that the residual oil saturation can be decreased for a water-swept region in an oil reservoir if locally the polymer solution flow is unstable. Additional research on the effect of oil on elastic instabilities can be useful for optimizing polymer EOR processes that improves sweep efficiency and displacement efficiency.

6.2.3. APPARENT VISCOSITY MODEL WITH ELASTIC INSTABILITIES

A common practice for including non-Newtonian effects in a reservoir simulator is to implement an aqueous-phase apparent viscosity model.[7–10] The apparent viscosity, η_{app} as obtained from Darcy's law is correlated to an apparent shear rate in porous media. According to this practice, η_{app} is typically expressed as a superposition of a viscous, shear-thinning part, η_{sh} and an extensional, shear-thickening part, η_{ext} as follows,

$$\eta_{\text{app}} = \eta_{\text{sh}} + \eta_{\text{ext}} \tag{6.1}$$

The shear-thinning and shear-thickening part is then modelled with a Carreau-Yasuda model such as,

$$\frac{\eta_{\text{sh}} - \eta_s}{\eta_{\text{sh0}} - \eta_s} = \left(1 + \left(\lambda_1 \dot{\gamma}_{\text{app}}\right)^{a_1}\right)^{\frac{n_1 - 1}{a_1}} \tag{6.2}$$

$$\eta_{\text{ext}} = \left(1 + \left(\lambda_2 \dot{\gamma}_{\text{app}}\right)^{a_2}\right)^{\frac{n_2 - 1}{a_2}} \tag{6.3}$$

where η_{sh0} is apparent zero-shear viscosity, η_s is solvent viscosity. λ_1 and λ_2 are time constants that determine the transition to an apparent shear-thinning region and to an apparent shear-thickening region respectively. The other parameters, a_1, n_1, a_2 and n_2 are fitting parameters to match the apparent viscosity curves. According to such an approach, the existing apparent viscosity models are largely phenomenological based on an assumption that the coil-stretch transition occurs at the onset of apparent shear-thickening region. In chapter 5, we showed that the coil-stretch transition occurs even in the apparent shear-thinning region. In order to improve predictability of an apparent viscosity model, future efforts to improve model predictability would benefit from the mechanism presented in this thesis. Particularly, the pressure drop measured during single-phase core floods experiments is known to fluctuate. We showed that pressure drop fluctuations could be related to flow field fluctuations and even to dead zone washing via power spectral density. Macroscopic data on pressure drop fluctuations obtained

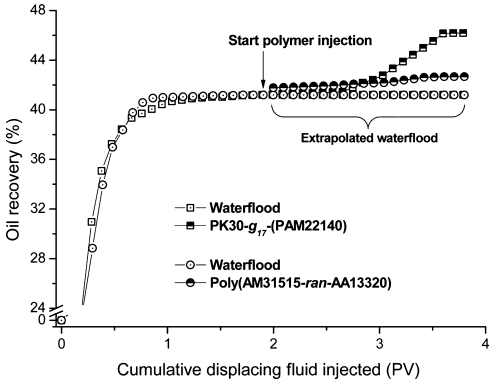


Figure 6.1: Oil recovery from low permeable Berea sandstone cores due to polymer flood from 17-arm branched PAM (PK30-g_{17}-(PAM22170)) and linear HPAM (Poly(AM31515-*ran*-AA13320)). Both polymer solutions have identical steady-shear viscosity at $10\,s^{-1}$. Additional details can be found in the original research article.[12]

from core flood experiments such as the standard deviation might be correlated to η_{ext}.

6

6.2.4. INVESTIGATE EFFECT OF HPAM ARCHITECTURE

In this thesis, we established a protocol to study the mechanism of apparent shear-thickening behaviour in porous media for solutions containing linear HPAM molecules. Recently, polymer solutions of branched polyacrylamide chains (PAM) were shown to recover more crude oil in core flood experiments compared to linear HPAM at same shear-viscosity and relaxation time.[11, 12] In figure 6.1 we show the oil recovery as two polymer solutions (17-arm branched PAM and linear HPAM) are injected in low permeability Berea ($k \sim 300\,D$) sandstone cores. Such an effect of branched HPAM to recover more oil can then be correlated to their ability to develop elastic instabilities. This study would allow us to investigate the correlation between crude oil recovery, and the nature of elastic instabilities.

6.2.5. RELATE HPAM MOLECULAR CONFORMATION TO MACROSCOPIC BEHAVIOUR

In chapter 2 and 5 we showed that fluorescent DNA could be used as a molecular probe to relate molecular conformation to macroscopic flow behaviour such as elastic instabilities. One of the key assumptions in this approach is that the molecular conformation of fluorescently stained DNA chains is representative of the conformation of non-fluorescent PAM chains. We validated the applicability of this assumption by showing that, both DNA chains as well as PAM chains undergo coil-stretch transition at simi-

lar time scales under flowing conditions. Recently, Tai *et al.* [13] reported a method to natively attach fluorescent chemical groups to HPAM chains. This approach allows visualization of molecular conformation by maintaining the inter- and intra-molecular interactions of PAM chains under flowing conditions. Furthermore, natively-fluorescent HPAM chains can also allow for direct visualization of branched polymer chains under flowing conditions. Possibilities are not only limited to investigating the flow behaviour, but also include the study of different phenomenon such as adsorption and mechanical degradation.

REFERENCES

[1] P. E. Boukany, S.-Q. Wang, S. Ravindranath, and L. J. Lee, *Shear banding in entangled polymers in the micron scale gap: a confocal-rheoscopic study,* Soft Matter **11**, 8058 (2015).

[2] S.-Q. Wang, *Nonlinear rheology of entangled polymers at turning point,* Soft Matter **11**, 1454 (2015).

[3] S. L. Wellington, H. J. Vinegar, *et al., X-ray computerized tomography,* Journal of Petroleum Technology **39**, 885 (1987).

[4] A. Clarke, A. M. Howe, J. Mitchell, J. Staniland, L. Hawkes, and K. Leeper, *Mechanism of anomalously increased oil displacement with aqueous viscoelastic polymer solutions,* Soft matter **11**, 3536 (2015).

[5] S. S. Datta, H. Chiang, T. Ramakrishnan, and D. A. Weitz, *Spatial fluctuations of fluid velocities in flow through a three-dimensional porous medium,* Physical review letters **111**, 064501 (2013).

[6] S. S. Datta, J.-B. Dupin, and D. A. Weitz, *Fluid breakup during simultaneous two-phase flow through a three-dimensional porous medium,* Physics of Fluids **26**, 062004 (2014).

[7] J. Heemskerk, R. Rosmalen, R. Janssen-van, R. Holtslag, D. Teeuw, *et al., Quantification of viscoelastic effects of polyacrylamide solutions,* in *SPE Enhanced Oil Recovery Symposium* (Society of Petroleum Engineers, 1984).

[8] A. Stavland, H. Jonsbraten, A. Lohne, A. Moen, and N. Giske, *Polymer flooding-flow properties in porous media versus rheological parameters,* in *SPE EUROPEC/EAGE Annual Conference and Exhibition* (2010).

[9] D. G. Hatzignatiou, U. L. Norris, and A. Stavland, *Core-scale simulation of polymer flow through porous media,* Journal of Petroleum Science and Engineering **108**, 137 (2013).

[10] M. Delshad, D. Kim, O. Magbagbeola, C. Huh, G. Pope, and F. Tarahhom, *Mechanistic interpretation and utilization of viscoelastic behavior of polymer solutions for improved polymer-flood efficiency,* in *SPE/DOE Symposium on Improved Oil Recovery* (2008).

[11] D. Wever, F. Picchioni, and A. Broekhuis, *Polymers for enhanced oil recovery: a paradigm for structure–property relationship in aqueous solution,* Progress in Polymer Science **36**, 1558 (2011).

[12] D. A. Wever, F. Picchioni, and A. A. Broekhuis, *Comblike polyacrylamides as flooding agent in enhanced oil recovery,* Industrial & Engineering Chemistry Research **52**, 16352 (2013).

[13] J. Tai, C. P. Lim, and Y. C. Lam, *Visualization of polymer relaxation in viscoelastic turbulent micro-channel flow,* Scientific Reports **5**, 16633 (2015).

SUMMARY

Crude oil has been an important source of energy for several decades now. Upon discovery of a crude oil reservoir until its abandonment, typically the oil recovery process can be classified in three stages. The primary and the secondary stage involve utilizing and maintaining reservoir pressure to recover oil respectively. The tertiary, or the Enhanced Oil Recovery (EOR) stage relates to employing various chemical or thermal methods to recover oil. Polymer flooding is the most promising enhanced oil recovery method that has shown potential to increase the oil recovery. Considering all the proven oil reserves from which mankind has recovered oil until now and average the oil recovery, it is less than 40%. EOR technologies have the potential to tap into the ~ 60% crude oil that is still present in the oil reservoirs. One of the biggest technical challenges in perfecting a polymer EOR process is predicting the polymer injectivity. The viscoelastic behaviour of polymer solutions coupled with the complex pore-scale flow geometry of geological porous media gives rise to non-linear resistance to flow. Consequently, during injection of polymer solutions in an oil reservoir, the pressure-drop can increase dramatically beyond certain flow rates. This behaviour is known as *apparent shear-thickening*. In this thesis, we focus on understanding the apparent shear-thickening behaviour of polymer solutions as they flow through porous media. We identify the mechanism causing the non-linear resistance to flow of polymer solutions through porous media. Our experiments reveal the mechanisms at the pore-scale and also at the molecular-scale.

In the second chapter, we review the state-of-art on the polymer chain dynamics in simple and complex flows. We also explain the typical dimensionless numbers that are useful in studying polymer solution flows in porous media and motivate the choice for using microfluidic devices. We show that a fluorescent labelled DNA chain can be used as a molecular probe to visualize polymer conformation in various flow fields. Direct visualization of a polymer chain under static and dynamic conditions was able to validate several polymer physics scaling laws. The approach also led to the discovery of the fascinating molecular *individualism*. When identical chains of long, flexible polymer chains have been prepared and exposed to the same conditions, they stretch (or unfold) in a variety of different ways.

In the third and the fourth chapter we investigate the flow of hydrolyzed polyacry-

lamide solutions through various realisations of microfluidic porous media. In the third chapter, we focus on the effect of pore-shape whereas in the fourth chapter we focus on the effect of salt on the flow behaviour. We fabricate microfluidic devices containing a periodic array of (cubic and cylindrical) obstacles in a staggered and an aligned layout. By visualizing flow streamlines and measuring pressure-drop simultaneously, we then mapped the relation of pressure-drop with the flow field. We found that the flow of shear-thinning polymer solutions in the apparent shear-thinning region contains the *dead-zone* elastic instability upstream of every obstacle. As the apparent shear-rate increases, these dead-zones become unstable leading to the *dead-zone washing* elastic instability. The presence of elastic instabilities is accompanied by pressure-drop fluctuations. In this thesis, we are able to unambiguously demonstrate that the apparent shear-thickening behaviour of polymer-solutions containing flexible polymer chains (such as hydrolyzed polyacrylamide) is due to time-dependent elastic instability.

In the fifth chapter, we develop novel single-DNA experiments to directly visualize polymer conformation during the polymer-solution flow instabilities in microfluidic porous media. In particular, we focus on understanding the polymer conformation in the dead-zone and the dead-zone washing instability. We show that the polymer chains undergo re-coil and re-orient/re-stretch events as the polymer chain enters a dead-zone and moves closer to the obstacle. We characterize the probability distribution of polymer chain fractional extension and compare it with the local Wi number. Our results demonstrate the molecular individualism in porous media. We also show that the polymer coil-stretch transition occurs even in the apparent shear-thinning region. As a polymer chain enters the dead zone, it first re-coils, then it re-orients and re-stretches in a direction perpendicular to the average flow.

The results from this thesis can be crucial for perfecting a polymer EOR process and help in predicting the polymer injectivity. We demonstrate that the apparent shear-thickening behaviour of polymer solutions is caused by elastic instabilities. We also show that the transition between apparent shear-thinning to the apparent shear-thickening behaviour is accompanied by transition from time-independent elastic instabilities to time-dependent elastic instabilities. Finally, the single-molecule experiments relate the pore-scale flow of polymer solutions to the molecule-scale phenomena.

SAMENVATTING

Ruwe olie is al tientallen jaren een belangrijke bron van energie. Vanaf de ontdekking van het olieveld tot het is uitgeput, doorloopt het winningsproces ruwweg 3 fases. In de eerste en tweede fase wordt respectievelijk de initiële druk en extern opgelegde druk gebruikt voor de winning. De derde fase, de zogenaamde 'Enhanced Oil Recovery' (EOR) fase behelst het toepassen van chemische en thermische methodes voor de winning. Het gebruik van polymeren, 'polymer flooding', lijkt de meest belovende tertiaire methode die olie opbrengst kan vergroten. Als wij van alle bekende olie reserves waaruit men tot nu toe olie heeft gewonnen de gemiddelde opbrengst bekijken is dat minder dan 40%. EOR technologie biedt de mogelijkheid om de ongeveer 60% die nog in olie reservoirs aanwezig is aan te boren. Eén van de grootste technische uitdagingen in het optimaliseren van een polymeer EOR proces is het voorspellen van de polymeer injectiviteit. Het visco-elastische gedrag van polymeeroplossingen samen met de complexe stromingsgeometrie op porieschaal in geologische poreuze media veroorzaakt niet-lineaire stromingsweerstand. Hieruit vloeit voort dat gedurende de injectie van polymeeroplossingen in een oliereservoir de drukval dramatisch kan toenemen bij bepaalde stroomsnelheden. Dit stromingsgedrag staat bekend als 'apparent shear-thickening'. In dit proefschrift richten wij ons op het 'apparent shear-thickening' gedrag van polymeeroplossingen als ze door poreuze media stromen. Wij beschrijven de mechanismen die de niet-lineaire stromingsweerstand van polymeeroplossingen in poreuze media veroorzaken. Onze experimenten tonen de mechanismen op porieschaal en ook op moleculaire schaal.

In het tweede hoofdstuk beschouwen wij de laatste stand van zaken met betrekking tot de dynamica van polymeerketens in eenvoudige en complexe stromingen. Ook leggen wij het gebruik van karakteristieke dimensieloze getallen uit die nuttig zijn bij de bestudering van de stroming van polymeeroplossingen in poreuze media en motiveren wij het gebruik van microfluïdische cellen. Wij laten zien dat een fluorescerend gelabelde DNA keten gebruikt kan worden als een moleculaire probe om het polymeer zichtbaar te maken in stromingsvelden. Het zichtbaar maken van polymeerketens onder statische en dynamische omstandigheden maakte het mogelijk om enkele fysische schaalregels voor polymeren te valideren. Deze aanpak leidde ook tot de ontdekking van het fascine-

rende individueel gedrag van moleculen. Wanneer identieke ketens van lange flexibele polymeerketens geprepareerd worden en blootgesteld aan dezelfde omstandigheden, strekken (of ontvouwen) ze zich op een aantal verschillende manieren.

In het derde en vierde hoofdstuk onderzoeken wij de stroming van gehydroliseerde polyacrylamide oplossingen in verschillende uitvoeringen van microfluïdische poreuze media. In het derde hoofdstuk richten wij ons op de invloed van de vorm van de poriën terwijl wij in het vierde hoofdstuk de invloed van zout op het stromingsgedrag bekijken. Er zijn microfluïdische cellen gemaakt die bestaan uit periodieke rijen van (vierkante en cilindrische) obstakels in een afwisselende of uitgelijnde lay-out. Door stroomlijnen zichtbaar te maken en tegelijkertijd de drukvallen te meten verbinden wij de drukval met het stromingsveld. Wij vonden dat bij stroming van 'shear-thinning' polymeer oplossingen in het 'apparent shear-thinning' gebied het een 'dead-zone' elastische instabiliteit bevat in de bovenstrooms van elk obstakel. Wanneer de 'apparent shear-rate' toeneemt worden deze 'dead-zones' onstabiel wat leidt tot de 'dead-zone washing' elastische instabiliteit. De aanwezigheid van elastische instabiliteit wordt vergezeld door drukval variaties. In dit proefschrift hebben wij onomstotelijk aangetoond dat het 'apparent shear-thickening' gedrag van polymeer oplossingen die flexibele polymeerketens bevatten (zoals gehydroliseerde polyacrylamide) komt door tijdsafhankelijke elastische instabiliteit.

In hoofdstuk vijf beschrijven wij de ontwikkeling van nieuwe 'single-DNA' experimenten om hiermee direct visueel het gedrag van polymeren te kunnen aantonen bij instabiliteit in stroming van polymeeroplossingen in microfluïdische poreuze media. In het bijzonder richten wij ons op het begrip van het aantonen van polymeer aanpassingen in de 'dead-zone' en de 'dead-zone washing' instabiliteit. Wij laten zien dat de polymeerketens zich opnieuw oprollen, heroriënteren/her-strekken als de polymeerketen een 'dead-zone' betreedt en een obstakel nadert. Wij karakteriseren de waarschijnlijkheidsverdeling van de polymeerketens 'fractional extension' en vergelijken het met het lokale Wi nummer. Onze resultaten laten het individuele gedrag van moleculen zien in poreuze media. Ook laten wij zien dat de oprol-strek overgang van het polymeer ook in het 'apparent shear-thinning' optreedt. Als een polymeerketen de 'dead-zone' betreedt zal het zich eerst opnieuw opwinden dan heroriënteren en opnieuw strekken, in een richting loodrecht op de gemiddeld stroming.

De resultaten uit dit proefschrift kunnen cruciaal zijn bij het optimaliseren van een polymeer 'EOR' proces en helpen bij het voorspellen van de polymeer injectiviteit. Wij tonen aan dat het 'apparent shear-thickening' gedrag van polymeeroplossingen wordt veroorzaakt door elastische instabiliteiten. Evenzo wordt duidelijk dat de overgang tus-

sen ‘apparent shear-thinning’ en ‘apparent shear-thickening’ gedrag samen gaat met de overgang van tijdsonafhankelijke elastische stabiliteit naar tijdsafhankelijke elastische stabiliteit. Tenslotte verbinden de één-molecuul experimenten de stroming op porie-schaal van polymeeroplossingen met de fenomenen op molecuul schaal.

ACKNOWLEDGEMENTS

"As we express our gratitude, we must never forget that the highest appreciation is not to utter words, but to live by them."
- John F. Kennedy

Words cannot express the surge of emotions I am feeling as my PhD journey is coming to an end. The highs, the lows and the in-betweens of my past years all supposed to be contained in these 150 pages or so. This thesis would have been impossible without the support, guidance, belief, encouragement, love and friendship of numerous people. With great excitement I want to express my gratitude to all the people who made it happen.

I want to thank Prof. Bill Rossen, Prof. Michiel Kreutzer and Prof. Pacelli Zitha for giving me the opportunity to pursue a PhD under their guidance. I appreciate your supervision, constant support and motivation during my PhD. I am grateful for all our valuable discussions and your relentless dedication to improve my critical thinking. Thank you for pushing me to grow professionally and personally. Thank you for providing all opportunities that helped me to improve my efficiency, scientific output and communication skills.

Prof. Rossen, thank you for your supervision and support. I admire your prompt and polite composure, and your efforts to teach me the correct use of hyphens in written English. Prof. Kreutzer, thank you for your supervision and support. Thank you for inculcating critical/analytical thinking and communication skills in me. I have learnt a lot about structuring scientific ideas and making clear presentations from you. Prof. Zitha, thank you for the support, supervision and freedom you have provided. Thank you for always encouraging me to develop my ideas, for your advice and support in matters concerning both PhD and life.

In my second year, Dr. Pouyan Boukany, became part of my PhD project as my daily supervisor. I am truly honoured and fortunate to have had your support and motivation over the past years. Thank you for all the valuable discussions, the meetings and the

brain-storming sessions. I learnt many concepts in polymer rheology and microfluidics from you. Your enthusiasm for all matters, scientific or not, is contagious. Thank you for giving me the opportunity to be part of the invited manuscripts, challenging me to find scientific explanations and your relentless dedication to see me grow me grow as a scientist and to develop my personality. Thank you for pushing me to make clear presentations, write high-quality scientific papers and for pointing out my blind-spots.

I want to thank the Dutch Polymer Institute (DPI) and its industrial partners - Shell Global Solutions and the SNF-Group for not only sponsoring this PhD project, but also to be actively involved throughout it. The half-yearly DPI cluster meetings have been crucial for shaping the research project, and I always learnt many things at these meetings. Over the years, several people have provided valuable suggestions such as Jan Stamhuis, Gerard Glasbergen, Marco Welling, Diego Wever, Nicolas Gaillard, Thierry Leblanc, Frank van Mastrigt, Francesco Picchioni and all other participants from SNF, Shell and DPI.

To my doctoral defence committee, Prof. Stephen Picken, Prof. Jan-Dirk Jansen, Prof. Francesco Picchioni and Dr. Steffen Berg, thank you for taking the time to be part of the committee, reviewing and providing feedback on the thesis.

A special thanks to Dr. Luis Portela, Dr. Dries van Nimwegen, Dr. Menno van Dijk and Prof. Ruud Henkes for their encouragement during my MSc thesis. They made research exciting and had it not been due to their support I would have never considered pursuing a PhD. I also thank Prof. Ruud van Ommen for his advice when I was searching for a PhD project after my MSc thesis. Prof. Van Ommen, had you not advised me to approach Prof. Kreutzer about a potential PhD project, this thesis would not have materialized.

During my PhD, I also had the opportunity to assist in teaching the 'Properties of Hydrocarbon Fluids' course together with some great teachers. Thanks to the teachers from whom I have had the privilege to learn - Dr. Hadi Hajibeygi, Dr. Renato Markovinovic and Dr. Denis Voskov. Thank you all for giving me freedom to take more responsibility during the course, develop new assignment questions and sometimes give lectures. I enjoyed all our valuable discussions, and learnt a great deal about the art and responsibilities of teaching.

I performed many experiments during my PhD at the microfluidics- & the Kramers-lab in the Chemical Engineering department, Dietz laboratory in the Geosciences and Engineering department, Water-lab in the Water Management department and the Kavli Nanolab at the Applied Physics department. The help of many technical experts at these labs have been absolutely paramount for my experiments. I want to thank Wim van Oordt, Mojgan Talebi, Evert Wagner, Ben Norder and Armand Middeldorp for their help

with microfluidic and rheology experiments. I thank Marc Friebel, Michiel Slob, Wim Verwaal, Karel Heller, Jolanda van Haagen, Jens van den Berg, Ellen Meijvogel-de Koning, Joost van Meel, Jan Etienne, Arno Mulder and Henk van Asten for their help with experiments at the Dietz lab. I am also thankful to Roel Mattern and Eugene Straver at the Kavli Nanolab for their help with fabricating patterned silicon-wafers. In particular, Marc - your jovial and lively personality made working at the Dietz lab a great fun! Thanks for teaching me how to build setups and for the fishing evenings at the Rotterdam harbour. Karel, thanks for helping me with the LabVIEW programming and for translating my thesis summary. Apart from the technical support I am thankful for the administrative support for getting things done at a rapid pace. Thank you Marlijn Ammerlaan, Margot Bosselaar-Perk, Lydia Broekhuijsen-Bentvelzen, Anke Dählmann, Marja Roep-Van der Klis, Marijke Schillemans-Van Tuijl, Hannie Zwiers, Ralf Haak, Claudia Baltussen, Elly Hilkhuijsen, Caroline Monna, Els Arkesteijn, Astrid Barrow, Marian de Bruijn, and Karin Wilhelm.

Over the years, I also had the opportunity and privilege to work with a number of BSc and MSc students. I want to thank Bart, Esteban, Gelmer, Jishnu, Hassam and Nienke for their contribution. Working with you all has been a rewarding experience from which I have learnt a lot. Bart, you were my first student and your work laid the foundation for the future research. Esteban, you performed very meticulous experiments which we could use in a publication immediately. And of course, thanks for introducing *PAYDAY 2* to me, I enjoyed playing the game for many hours. Gelmer, you were my first MSc student and we achieved great results from the many complicated experiments that you did. Jishnu, you were my last MSc student and I always admired how diligently you performed experiments. In the end we made some fascinating and interesting discoveries. Hassam, you worked on some rather tricky microCT experiments and I am thankful for your contribution. Nienke, I am happy to contribute to your MSc project on the novel biopolymer flooding experiments.

An advantage of being part of two faculties is to get access to the best of both faculties. At CiTG, I was fortunate to serve on the SPE Delft Student Chapter Board and to be part of the MV. Thank you - to all the fellow SPE board members. It was my pleasure. At TNW, I was fortunate to become part of a rich group culture that included the journal club and the PPE Days. Being part of all activities and events at both the faculties has been sometimes exhausting, but always rewarding. Most importantly, I thoroughly enjoyed the very many events, activities and societies from both faculties.

My old friends from Delft - Puja, Jeroen, Vipul, Neha, Digda, Joan, Shikha and Harshad, thank you for your friendship. Vipul, thank you for hosting me in Haarlem for a

few months at the start of the PhD while I found a house in Delft. Digda...Digdins, it has been super fun living in the same house with you. All the cooking evenings, guitar hero sessions, movie nights and chatting about all things fun and tough made the PhD-life enjoyable.

There are few people who have gone the extra mile to support me. Thank you Shaurya, Dayinta, Rahul and Suus for proof reading part of this thesis. I also want to thank Janice Rossen for her enthusiastic kind words and encouragement over the years, and especially for her advice on cover designs and printing dissertations. I am humbled by your appreciation and love of my now-famous chicken curry. Manali, thank you for your support, confidence, trust and love in my capabilities over the many years.

To all my friends and colleagues at the PPE-family whose friendship and support is hard to summarize in words, thank you! Dayinta, your positivity is fascinating and I could always count on your genuine support, interest and crazy story-making abilities. Yogesh, the one friend with whom I could speak about anything (in Marathi), I admire your apparently amazing fitness routine, the Oreo-milkshakes that followed it and the confidence that six-pack-abs are always 6 months away. David, the only person I know who is always up for beers, thank you for setting the reference of 'chilled-out'. Andrea, I admire how organized and what an excellent planner you are, thanks for organizing all the dinners, drinks, road trips, Halloween parties, etc. It was fun. Fabio, my rowing buddy, it is still fascinating how everything you touch breaks, surprisingly DDS is still standing strong - thank you for the fun-on-water, the pizza nights and the Diablo 3 marathons. We have many more to come in the future. Samir-the-schnuffilein, you are one energetic and enthusiastic fellow, it was always fun to learn your (sometimes) strange German ways like the Kohlfahrt. Shaurya, thanks for helping with the DNA experiments and the many discussions we had about polymer physics. All the VriMiBo's, Fun Fridays, events, parties and brewing attempts were a lot of fun. Thanks to all the friends and colleagues of the PPE-family - Volkert, Gabrie, Ruud, Pouyan, Michiel K, Peter, Elly, Mojgan, Wim, Henk, Duong, Barbara, Aris, Michiel M, Rajat, Venky, Hrushi, Piotr, Josette, Daoyin, Yujie, Hao, Jillian, Zhi Zhou, Kartik, Melvin, Floris, Lea, Jesús, Fatemeh, Wenjie, Jing, Liang, Dominik, Maulik, Damiano, Sharath and Aswin.

To all my friends and colleagues at the Petroleum engineering group whose support, friendship and company I could always count on, thank you! Rahul, you are a true friend, my go-to person for all happy, sad and angry times, thank you for calling out on my faults and providing solutions. Nikita, the most colourful and positive person I have ever met, we have been in some of the funniest, happiest times together and I will always cherish your happy and calm demeanor. Christian, every time you stayed with me in Delft was

like a holiday for me during which we had fantastic fishing evenings, reibekuchen and German bread/beer. Rahul, Nikita and Christian, I always look forward to our Monschau tradition and I hope we continue with it for the rest of our lives. All the barbeques, MV activies, Barbaraborrels, Tuesday dinner, etc over the past years were enjoyable and I will always fondly remember the company of everyone in the Petro-family - Saskia, Jiakun, Daniel, Matteo, Ehsan, Elisa, Grigori, Negar, Jakolien, Leon, Amin, Maryam, Anna, Amin F., Matei, Mojtaba, Tianqi, Jinyu, Bander, Rodrigo, Ahmed, Mohammed, Siavash, Rafael, Karl-Heinz, Faisal, Martijn, Mark, Chris, Yang, Mohsen, Longlong, Swej, Sian, Brandon and all my other colleagues and friends.

To all my Wacken friends who kept the student alive in me - thank you. It has been fun to learn the very many Delft student traditions and Kings from you all! Thank you Jeroen, Dzware, Inez, Victor, Sjoerd, Jurriaan, Thim, Patrick, Kas and Camiel.

To the special person in my life, Suus, thank you! In the happiest and the darkest of times I can always count on your bright smile, support, love, kindness, trust and motivation. Thank you for all the hard kilometers you drove to Delft; your unreserved affection was pivotal for this thesis.

Finally, my deepest gratitude goes to my family - my mother, father and my sister. Their love, support and encouragement to study led me to do my MSc first and then a PhD. Without their support and sacrifices, I could not have achieved any of this. To my grand mother, who supported me unconditionally through all of my endeavours so far - thank you for being my hero. I regrettably could not be present to say my proper goodbyes. To my grandmother, I dedicate this thesis.

Durgesh Kawale,
September 2017.

A

APPENDIX A

1. Table A.1 shows the shear rheology fit results to the Carreau-Yasuda model for all the HPAM solutions used in the current study.

2. Figure A.1 shows the small amplitude oscillatory strain measurements of all the HPAM solutions used in the current study.

3. Comparison between global shear rate calculation and local shear rate calculation was performed using PIV for a circle, staggered geometry having diameter of 195 µm and height of 85 µm. From PIV, the calculated shear rate was 5.22 s^{-1}, whereas the global shear rate calculation yields 4.6 s^{-1}. In figure A.2 we show these results.

4. Figure A.3 shows mechanical degradation of 0.2 % HPAM solution with 17 mM NaCl. This solution relaxation time is ~3 s, and our test shows that the shear viscosity of fresh solution is same as a solution that was pre-sheared for 120 s at 500 s^{-1} in a Couette geometry. There is no visible decrease in the shear viscosity for both these solution showing that this HPAM solution does not degrade upto shear rate of 500 s^{-1} (or upto $Wi \sim 1500$).

5. Figure A.4 shows stable creeping flow of polymer solutions through the square, staggered geometry at $\dot{\gamma}_{app} = 0.007\,s^{-1}$ ($Wi = 0.1$).

A

Table A.1: Fit results from Carreau-Yasuda model. The infinite shear viscosity, η_∞ is set to 0.001 Pa s for all polymer solutions.

Polymer, NaCl concentration	η_0 (Pa s)	n (-)	τ (s)	a (-)
0.1 % HPAM, 0 mM NaCl	6.65	0.28	21.55	0.62
0.2 % HPAM, 17 mM NaCl	0.72	0.42	3.03	1.11
0.2 % HPAM, 170 mM NaCl	0.08	0.61	0.76	0.88
0.2 % HPAM, 340 mM NaCl	0.03	0.71	0.35	1.8
0.2 % HPAM, 680 mM NaCl	0.02	0.72	0.17	1.30

6. Figure A.5 shows unprocessed ΔP measurements in the square staggered geometry for the flow of 0.1 % HPAM in DI water (no salt) at $\dot{\gamma}_{app} = 3.63\,s^{-1}$ and at $\dot{\gamma}_{app} = 145.33\,s^{-1}$.

7. Figure A.6 shows dead zone washing steps at $\dot{\gamma}_{app} = 29.07\,s^{-1}$ for 0.1 % HPAM solution (without salt)

8. Figure A.7 shows the power spectral density curves for flow of 0.1 % HPAM solution (without salt) in all the four geometries. In figure A.8 power spectral density curves for all geometries at same apparent shear rate are plotted together, showing the the general shape of curve is same in all the geometries.

9. Figure A.9 compares power spectral density of point-pressure fluctuations at the inlet pressure sensor (P_{inlet}) with that of the pressure drop fluctuations. The shape of the spectral density curves is same. Results for 0.2 % HPAM solution in 680 mM NaCl flowing through the square staggered geometry at apparent shear rate of $60\,s^{-1}$.

10. Figure A.10 shows that the onset of apparent shear-thickening region for 0.2 % HPAM solution with 680 mM NaCl starts with the elastic flow instabilities, which in turn is also marked by increase in the std(ΔP) fluctuations.

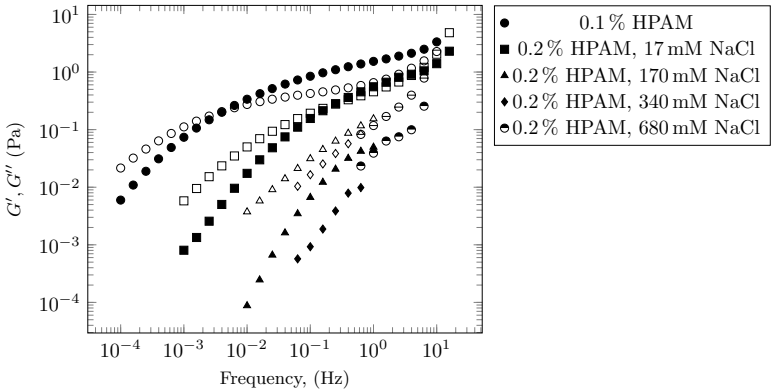


Figure A.1: Small amplitude oscillatory strain measurements of all HPAM solutions used in the experiments shown in the chapters 3 and 4.

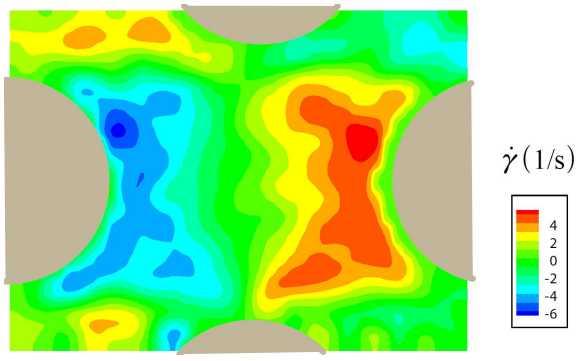


Figure A.2: Local shear rate map for 0.1 % HPAM in DI water flowing through a circle, staggered geometry with volumetric flow of $Q = 4\,\mu L\,min^{-1}$. The circle diameter is 195 µm, height of microfluidic device is 85 µm, porosity is 0.7. Flow direction is left to right. $\dot{\gamma}_{app}^{PIV} = 5.22\,s^{-1}$ and $\dot{\gamma}_{app}^{global} = 4.6\,s^{-1}$.

A

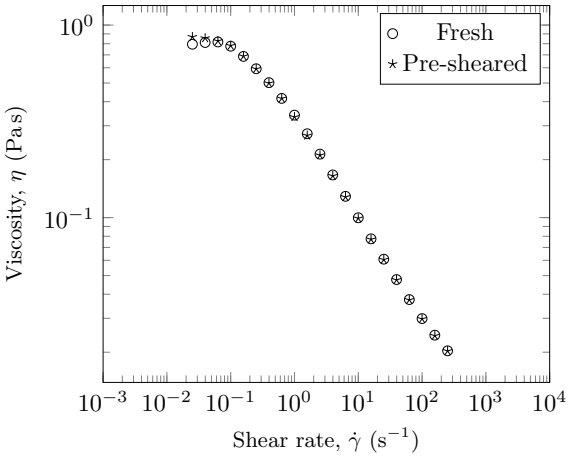


Figure A.3: Mechanical degradation test for 0.2 % HPAM, 17 mM NaCl solution. Pre-shear solution was sheared at 500 s^{-1} for 120 s. Measurement performed in a Couette geometry at $T = 22\,°C$.

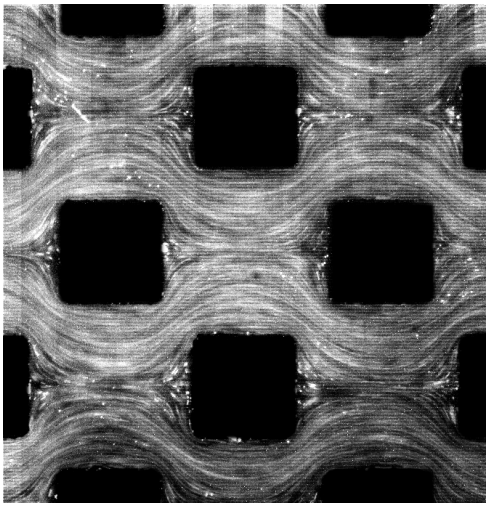


Figure A.4: Streamlines showing creeping flow of polymer solutions in the square staggered geometry at $Wi = 0.1$. Flow direction is from left to right. Side of the square is 262 µm

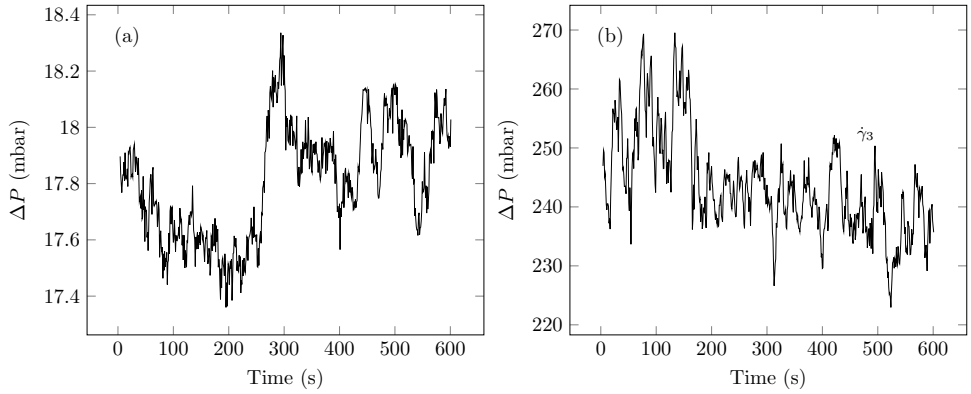


Figure A.5: ΔP measurements in the square staggered for flow of 0.1 % HPAM in DI water (no salt). (a) $\dot{\gamma}_{app} = 3.63\,s^{-1}$, (b) $\dot{\gamma}_{app} = 145.33\,s^{-1}$.

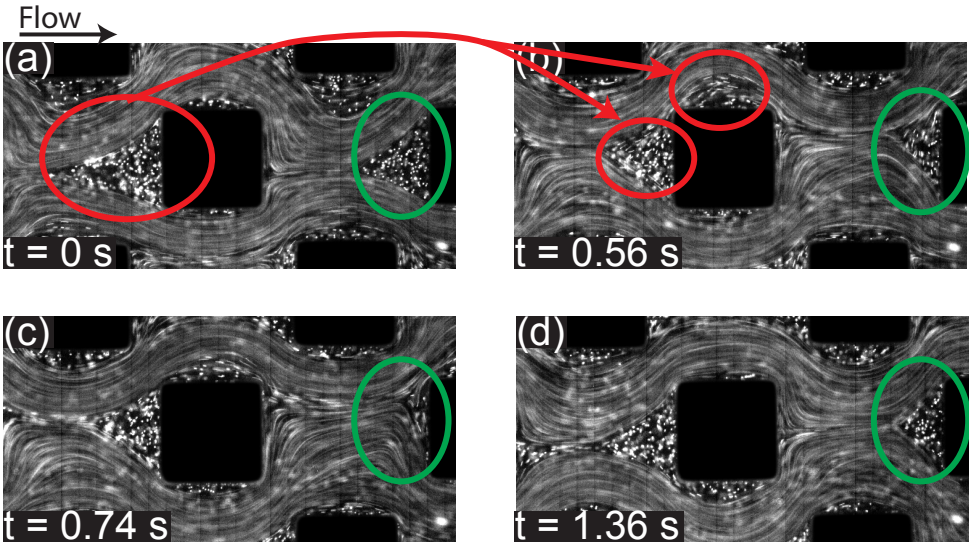


Figure A.6: Dead zone washing can occur in one or two steps. In the single-step washing process, the complete dead zone is washed away. However, in the two-step process, it can wash a part of its mass, such that the (usually smaller) downstream dead zone can shed completely. (a) A fully grown dead zone wobbles perpendicular to the flow direction. (b) A part of the dead zone's mass (in red) is shed causing the downstream dead zone to start shedding (in green) and it rapidly sheds entirely. Notice the time stamps from (a) to (b) and then to (c). In (d) the vortex has grown to roughly half it's full-grown size, for which it took $1.36 - 0.74 = 0.62\,s$.

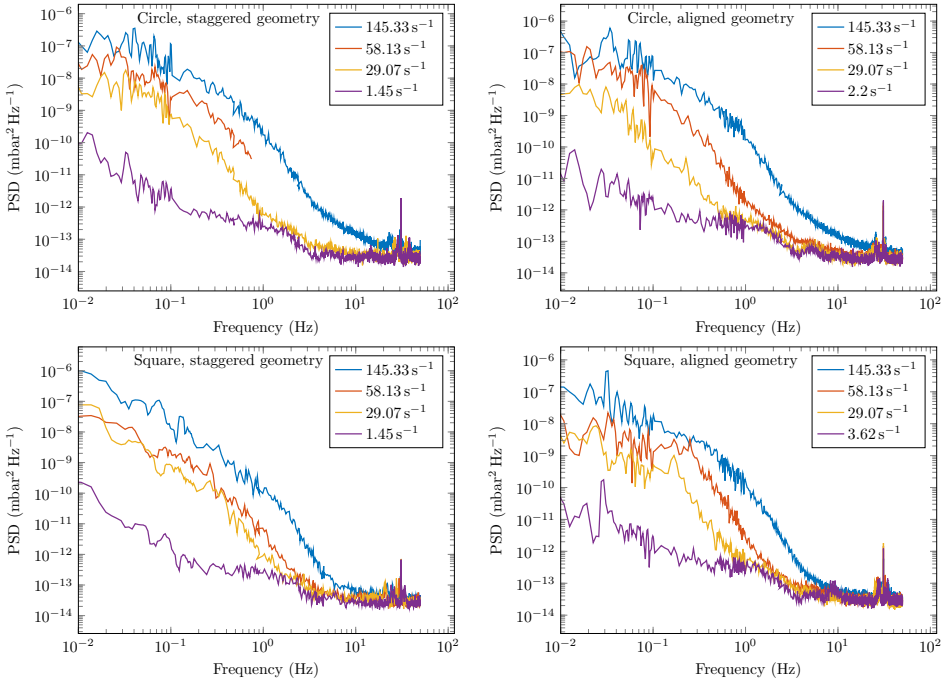


Figure A.7: Power spectral density at various apparent shear rates for 0.1 % HPAM solution (without salt) flowing through all the four geometries.

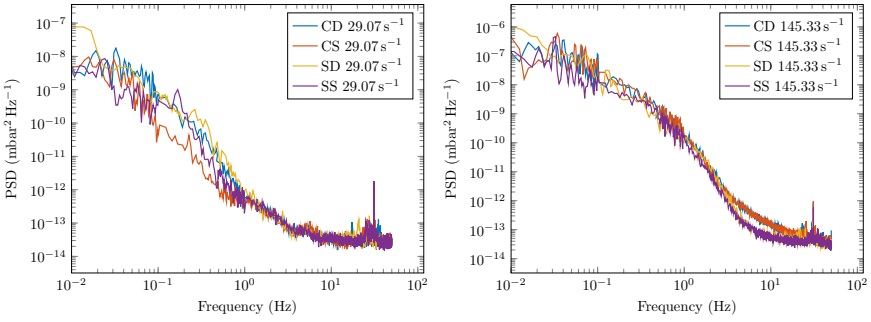


Figure A.8: Left: Power spectral density curves at $\dot{\gamma}_{onset} = 29.07\,s^{-1}$ for all geometries. Right: Power spectral density curves at $\dot{\gamma}_{app} = 145.33\,s^{-1}$ for all geometries. CD = circle staggered, CS = circle aligned, SD = square staggered, SS = square aligned.

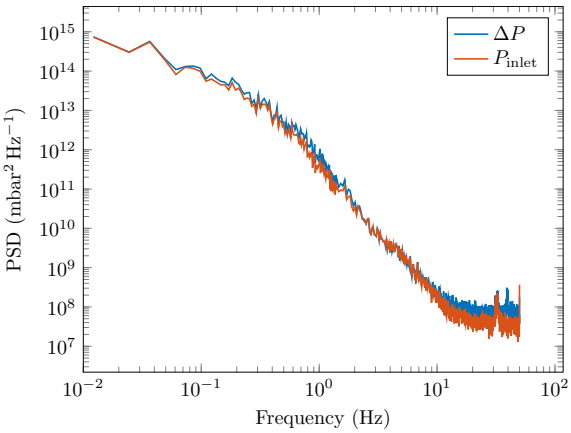


Figure A.9: Power spectral density of ΔP fluctuations and P_{inlet} fluctuations for 0.2 % HPAM in 680 mM NACl, $\dot{\gamma}_{\text{app}} = 60\,\text{s}^{-1}$.

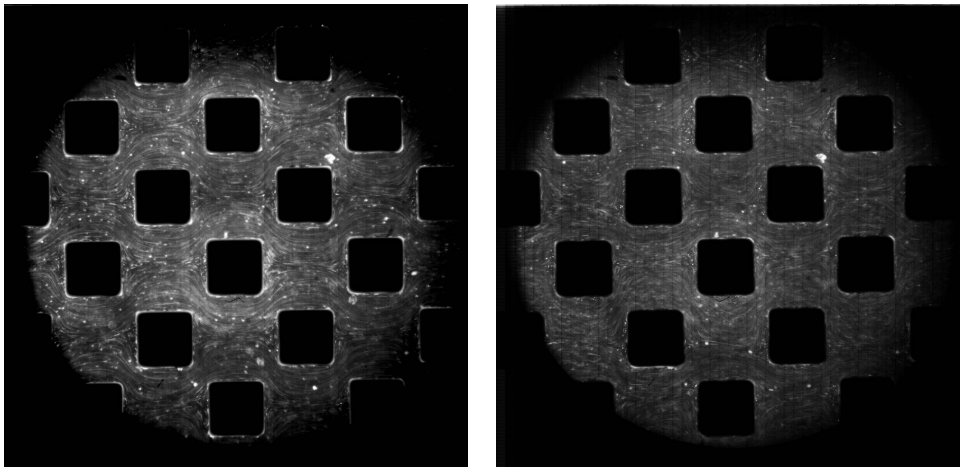


Figure A.10: Streamlines showing that the elastic flow instabilities in HPAM solution with 680 mM NaCl start at the onset shear rate for apparent shear-thickening region. Streamline snapshots at $\dot{\gamma}_{\text{app}} = 15\,\text{s}^{-1}$ (left) and $\dot{\gamma}_{\text{app}} = 37.7\,\text{s}^{-1}$ (right). Flow direction is left to right.

B

APPENDIX B

1. Two movies, SM-1 and SM-2 are included in the supplementary information. Both these movies show one instance of DNA chain (marked with dotted circle) approaching the pillar. The DNA chains coil at the tip of DZ and as it enters the DZ it stretches and rotates in a direction perpendicular to the flow. $\dot{\gamma}_{\text{app}} = 3.3\,\text{s}^{-1}$, $C_s = 0\,\text{mM}$ NaCl, $Wi = 290.98$, $Ma = 0.95$, $Re \ll 1$.

2. Table B.1, we summarize the mean DNA fractional extension, μ and skewness, s.

3. In fig. B.1 we show the stead-shear rheology of $0.2\,\text{g}\,\text{L}^{-1}$ PAA solutions at 22 °C in DI water ($C_s = 0\,\text{mM}$) and in presence of salt ($C_s = 6\,\text{mM}$).

4. In fig. B.2 we show the results from pressure drop measurement across the periodic array. In fig. B.2a the standard deviation (std) of the ΔP fluctuations in the microfluidic device. The sampling period for Newtonian fluid flow is 120 s and for polymer solution flow is 600 s. All three solid are obtained by fitting power law equation of type $y = ax^b$ through experimental data. For Newtonian data, regression is performed over all data points. For polymer solution data, regression is performed for data beyond $\dot{\gamma}_{\text{app}} = 10\,\text{s}^{-1}$. The onset point is obtained as the intersection of polymer solution lines with the Newtonian data lines. In fig. B.2b, the apparent viscosity as calculated by Darcy's law is shown. Error bars are calculated based on std(ΔP).

5. In fig. B.3 we show the probability distribution of DNA orientation angle, θ as Wi number increases. The DNA samples were located inside the DZ.

6. Fig. B.4 shows schematic explaining the molecular parameters extracted from DNA-imaging. The end-to-end vector, $\vec{R}$ is measured manually using ImageJ. The DNA extension, $\langle \vec{R} \rangle$ is the magnitude of $\vec{R}$, whereas the DNA orientation angle, θ is the angle of $\vec{R}$. θ is 0° in the direction of flow (x-axis), whereas it is 90° in the direction perpendicular to the flow (along the microfluidic device width, y-axis).

7. Fig. B.5 shows the velocity field for flow of the 200 ppm PAA solution (in DI Water) through pillared array at $\dot{\gamma}_{app} = 0.07\,s^{-1}$ ($Wi = 5.8$). We can see the dead zone formation in the left figure. The velocity field appears not to be time dependent. Details of the PIV calculations are - the PIV vector calculation was performed using LaVision DaVis 8.4.0 (LaVision inc, England). The background noise was subtracted by subtracting the average intensity of the raw images (in time) from each raw image. The pillars were then masked out using geometric masks. Vector were obtained using multipass FFT based cross correlation with window sizes from 64x64 px (50%, 2 pass) to 16x16 px (50%, 3 pass). Spurious vectors were removed using a median filter. Sub-pixel interpolation was done using a 3 point Gaussian estimator. Final presented results are average of 100 instantaneous vector fields (average in time). The peak standard deviation in velocity is around $5.25 \times 10^{-5}\,m\,s^{-1}$ (at zones with high velocity). Calibration was done with pillar diameter. The other derived parameters were based on the average velocity field using in built functions.

8. Fig.B.6 shows the ratio of the polymer apparent viscosity to the steady shear viscosity calculated at the apparent shear rate, η_{app} plotted against the Wi number.

9. Table B.2 shows the DNA fractional extension inside DZ, local Deborah number, De_{loc} and the DNA velocity, v_{DNA} inside the DZ.

Table B.1: DNA fractional extension mean, μ and skewness, s at the DZ tip (coil) and close to pillar (stretch).

	$C_s = 0\,\text{mM}$		$C_s = 6\,\text{mM}$	
	Coil	Stretch	Coil	Stretch
$\dot{\gamma}_{\text{app}} = 3.3\,\text{s}^{-1}$	$\mu = 0.18 \pm 0.12$ $s = 3.08$	$\mu = 0.30 \pm 0.15$ $s = 0.69$	$\mu = 0.09 \pm 0.02$ $s = 0.84$	$\mu = 0.15 \pm 0.07$ $s = 1.00$
$\dot{\gamma}_{\text{app}} = 33\,\text{s}^{-1}$	$\mu = 0.21 \pm 0.04$ $s = 0.14$	$\mu = 0.53 \pm 0.18$ $s = 1.04$	$\mu = 0.11 \pm 0.03$ $s = 0.38$	$\mu = 0.22 \pm 0.1$ $s = 1.21$

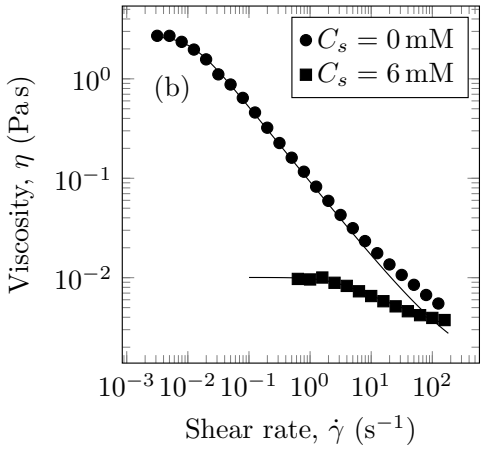


Figure B.1: (b) Steady-state shear rheology of $0.2\,\text{g L}^{-1}$ PAA solutions at 22 °C in DI water (C_s = 0 mM NaCl, filled-circle symbol) and in presence of salt (C_s = 6 mM NaCl, filled-square symbol). The solid line is a Carreau model fit (eqn. 5.1) to the shear rheology.

Table B.2: Summary of DNA fractional extension inside DZ, local *De* and DNA velocity inside DZ. The standard deviation of De_{loc} and v_{DNA} values is based on an ensemble of 20 individual DNA tracking velocimetry measurements, whereas the standard deviation of DNA fractional extension is based on the number of DNA molecules measured as shown in fig. 5.5c

DNA fractional extension (-)	De_{loc} (-)	v_{DNA} ($\mu\text{m s}^{-1}$)
0.15 ± 0.07	0.59 ± 0.28	78.48 ± 27.43
0.22 ± 0.10	4.76 ± 1.45	497.19 ± 174.17
0.30 ± 0.15	15.55 ± 5.00	19.28 ± 5.24
0.53 ± 0.18	735.60 ± 250.20	573.29 ± 202.09

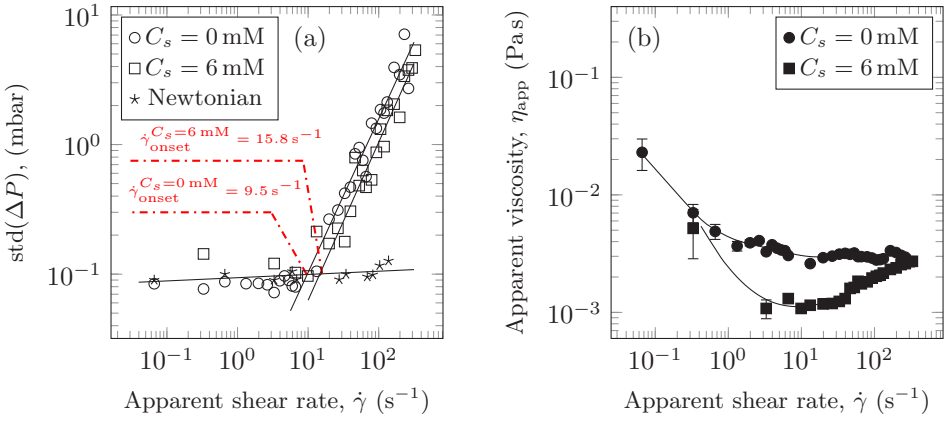


Figure B.2: (a) Standard deviation (std) of the ΔP fluctuations. The dotted curve is fitted to the data. (b) The apparent viscosity as calculated from Darcy's law. The solid lines are spline fit to the data, shown as a guide to the reader's eye. Error bars are based on std(ΔP).

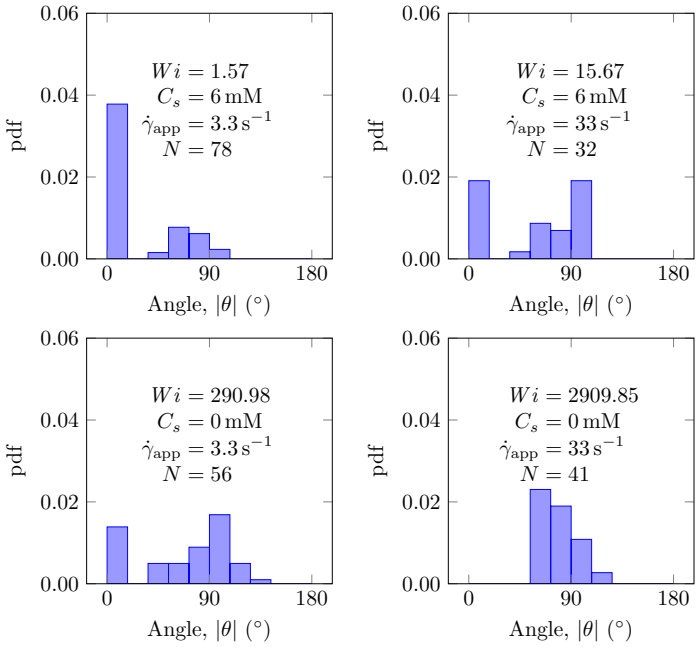


Figure B.3: Probability distribution of DNA orientation angle, θ as Wi number increases. N is the number of samples measured and all the samples are located inside the DZ.

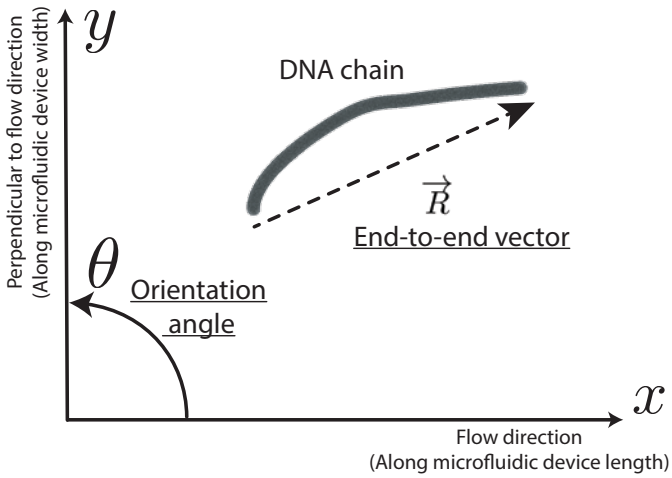


Figure B.4: Schematic showing DNA chain end-to-end vector, $\vec{R}$ and the orientation angle, θ.

B

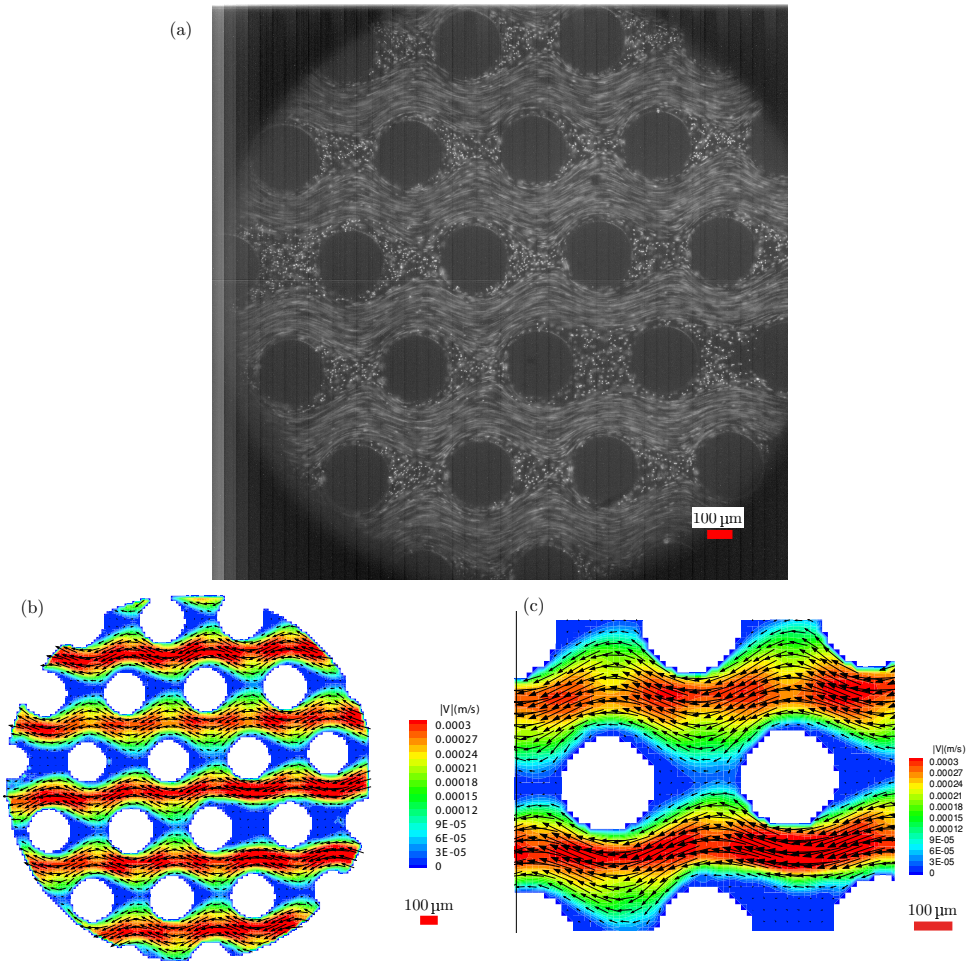


Figure B.5: (a) Streamline snapshots and the (b-c) the velocity field calculated by PIV at $Wi = 5.8$ or $\dot{\gamma}_{app} = 0.07\,s^{-1}$. The fluid is 200 ppm PAA in DI water. Flow direction is from right to left. (c) shows a zoomed-in image of the velocity field in the DZ.

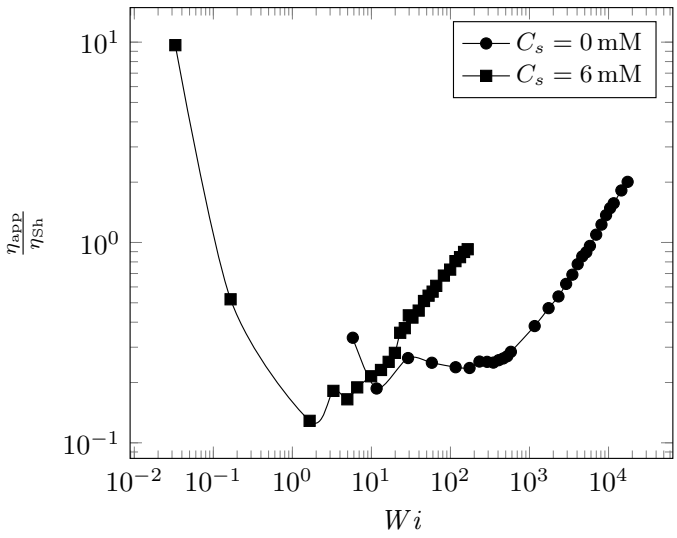


Figure B.6: Figure showing ratio of the apparent viscosity, η_{app} and the steady-shear viscosity, η_{Sh} at the apparent shear rate, $\dot{\gamma}_{\mathrm{app}}$ as a function of the Wi number.

CURRICULUM VITÆ

Durgesh Kawale was born on the 19th of September 1986 in Mumbai, India. In 2008, he obtained a Bachelor degree in Chemical Engineering from the University of Mumbai. After obtaining the Bachelor degree, Durgesh worked as a Process Engineer at Kongsberg Oil & Gas Technologies until 2010. In 2010, he headed to the Netherlands to pursue a Masters in Chemical Engineering with a specialization in process engineering at the Delft University of Technology. During his masters he spent nine months at the Shell Technology Centre in Amsterdam for his masters research project and three months at the Norwegian University of Science and Technology as a visiting scientist.

Upon completing his masters in 2012, he pursued his doctoral studies at the Delft University of Technology under the supervision of Prof. dr. ir. Michiel T. Kreutzer, Prof. dr. William R. Rossen, Prof. dr. Pacelli L. J. Zitha and Dr. Pouyan E. Boukany. During his PhD, he has served as the Vice-President of the SPE Delft Student Chapter. Since July 2017, he is working at the Delft University of Technology as a Research Associate and will continue as a Postdoctoral Researcher at the same university from October 2017.

List of Publications

Journal Publications

D. Kawale, J. Jayaraman, P. L. J. Zitha, M. T. Kreutzer, W. R. Rossen, P. E. Boukany, *Fluidic rectification achieved by polymer solution flow through anisotropic permeability porous media*, Manuscript under preparation.

D. Kawale, G. Bouwman, S. Sachdev, P. L. J. Zitha, M. T. Kreutzer, W. R. Rossen, P. E. Boukany, *Polymer conformation during flow in porous media*, Under review @ Soft Matter.

D. Kawale, E. Marques, P. L. J. Zitha, M. T. Kreutzer, W. R. Rossen, P. E. Boukany, *Elastic instabilities during the flow of hydrolyzed polyacrylamide solution in porous media: effect of pore-shape and salt*, Soft Matter, **13**, 765 (2017).

L. Rems, **D. Kawale**, L. J. Lee, P. E. Boukany, *Flow of DNA in micro/nanofluidics: From fundamentals to applications*, Biomicrofluidics **10**, 043403 (2016).

D. Kawale, A. T. van Nimwegen, L. M. Portela, M. A. van Dijk, R. A. W. M. Henkes, *The relation between the dynamic surface tension and the foaming behaviour in a sparger setup*, Colloids and Surfaces A: Physicochemical and Engineering Aspects **481**, 328 (2015).

Conference Proceedings/Presentations

D. Kawale, P. E. Boukany, M. T. Kreutzer, W. R. Rossen, and P. L. J. Zitha, Contribution of pore-shape to the polymer apparent viscosity. In SPE Asia Pacific Enhanced Oil Recovery Conference. Society of Petroleum Engineers, 2015. Kuala Lumpur, Malaysia.

D. Kawale, P. E. Boukany, M. T. Kreutzer, W. R. Rossen, and P. L. J. Zitha, Dynamics of polymer rheology through different pore-shapes in microfluidic channels. DARSim Seminar on Porous Media Flow Modeling & Simulation, 2015. Delft, Netherlands.

D. Kawale, P. E. Boukany, M. T. Kreutzer, W. R. Rossen, and P. L. J. Zitha, How does pore shape influence the flow of polymer solutions through porous media? Annual European Rheology Conference, 2015. Nantes, France.

P. E. Boukany, **D. Kawale** and S. Sachdev, Microscopic origin of elastic instability in flow of polymer solutions through porous media : Using micro-fluidics and DNA imaging. In 88^{th} Society of Rheology Annual Meeting, 2017. Florida, US.